Fate and Transport of Phosphorus, Colloids, and Biochar in Soils

by Wei Zhang

FATE AND TRANSPORT OF PHOSPHORUS, COLLOIDS, AND BIOCHAR IN SOILS

A Dissertation

Presented to the Faculty of the Graduate School

of Cornell University

In Partial Fulfillment of the Requirements for the Degree of

Doctor of Philosophy

by

Wei Zhang

August 2010

FATE AND TRANSPORT OF PHOSPHORUS, COLLOIDS, AND BIOCHAR IN SOILS

Wei Zhang, Ph. D.

Cornell University 2010

Fate and transport of phosphorus (P) and colloidal particles in soils constitutes two major areas of inquires in contaminant hydrology. The P transport in the northeastern U.S. depends largely on P sorption of soils in variable source areas (VSAs) and land treatment systems (e.g., vegetative treatment areas [VTAs]) that receive large P applications. In this study P sorption of soils from VTAs receiving dairy farm wastewaters in New York was studied using batch P sorption experiments. A modified P sorption model that uses only Langmuir sorption isotherm was compared with a conventional model that needs both linear and Langmuir isotherms for sixteen VTA soil samples of Langford, Volusia, and Mardin channery silt loam soils. The two methods agreed well in describing P sorption, thus proving the modified model a valid tool for P sorption study. Then, the modified model was employed to study the effect of soil redox change on P sorption of an organic-rich Langford silt loam. The findings suggest that with soil redox fluctuation, invoked by alternating saturated and unsaturated soil moisture regimes, soil P sorption was enhanced by formation of freshly precipitated amorphous iron hydroxides.

Colloid transport was investigated using a model colloid (carboxylated polystyrene microsphere) and a non-ideal colloid (biochar particles) in sand columns. For the model colloid, greater input concentrations lead to increased colloid retention at neutral pH in unsaturated sand, and this concentration effect was enhanced by ionic

strength. This has a direct consequence for predicting the transport of colloids where the concentration decreases with depth and thus become more mobile with depth.

It is expected that large quantities of biochar might be produced in the future for carbon sequestration. Therefore, the transport of biochar particles was investigated under three pH and two ionic strength levels in saturated and unsaturated sand. Biochar particles exhibited greater mobility under higher pH and lower ionic strength, and more biochar was transported by saturated flow. The biochar particles larger than 5.4% of median grain diameter were filtered out of suspension during passage through the media, whereas the retention of smaller particles was clearly dependent on solution chemistry.

BIOGRAPHICAL SKETCH

Wei Zhang was born in Zhongxiang, Hubei Province, China on September 27, 1977, the son of Sichuan Zhang and Yuqing Li. He received the Bachelor of Science with distinction in Environmental Chemistry from Nanjing University on 2000. He then worked as an assistant engineer in Shanghai Research Institute of Petrochemical Technology from 2000 to 2004. To pursue a higher education in environmental science and engineering, he went to Oklahoma State University and obtained the Master of Science in Biosystems Engineering on 2006. He is now working toward a Ph.D. degree in Environmental Engineering at Cornell University.

ACKNOWLEDGMENTS

I cannot express my gratitude enough to my major advisor Dr. Tammo S. Steenhuis and other committee members, Mr. Larry D. Geohring, Dr. Jean-Yves Parlange, and Dr. Anthony G. Hay, for inspiration, encouragement, and guidance that they have provided throughout my study.

I am also indebted to the Soil and Water Lab at Cornell University. The lab is diverse and dynamic with a great supporting and caring atmosphere among its members, which has made my Ph.D. journey enjoyable. I would like to particularly thank Joshua Faulkner, Verónica Morales, and Anthony Salvucci for their friendship and research collaboration. The fellowship and help from other lab members, including Brian Richards, Todd Walter, Shree Giri, M. Ekrem Cakmak, Helen Dahlke, Francisco Flores-Lopez, Yuni Zevi, and many others, are also greatly appreciated.

Finally, I would like to thank my fiancée Ms. Xing Chen for her enduring support, and my parents, Sichuan Zhang and Yuqing Li, for their unreserved love.

TABLE OF CONTENTS

Biographical Sketch……...iii

Acknowledgements……....iv

List of Figures……....vi

List of Tables……...viii

Chapter 1 Introduction……....1

Chapter 2 Evaluation of Two Langmuir Models for Phosphorus Sorption of P-enriched Soils in New York for Environmental Applications……..…6

Chapter 3 Effect of Soil Reduction on Phosphorus Sorption of an Organic-rich Silt Loam……..……...32

Chapter 4 Colloid Transport and Retention in Unsaturated Porous Media: Effect of Colloid Input Concentration…….……65

Chapter 5 Transport and Retention of Biochar Particles in Porous Media: Effect of pH, Ionic Strength, and Particle Size……..……...107

Chapter 6 Conclusions and Future Work……146

Appendix A Phosphorus Sorption Data.…….148

Appendix B Column Breakthrough Experiments Data……...151

LIST OF FIGURES

Figure 2.1. Typical observed and fitted Langmuir sorption isotherms of surface and subsurface soils……..…….18

Figure 2.2. Comparison between sorption parameters estimated by the one-step method and the two-step method for surface soils……..23

Figure 2.3. Comparison between sorption parameters estimated by the one-step method and the two-step method for subsurface soils……24

Figure 3.1. Comparison of estimated sorption parameters between the air-dried and reduced soils……45

Figure 3.2. Comparison of estimated sorption parameters between the air-dried and field-wet soils……..46

Figure 3.3. Effect of wastewater sorption matrices on P sorption of the air-dried and reduced soils……47

Figure 3.4. Dissolved organic carbon (DOC) concentrations in the final sorption solutions for air-dried or reduced soils……...52

Figure 3.5. Dissolved Ca concentrations in the final sorption solutions for air-dried or reduced soils……53

Figure 3.6. Solubility diagram of Ca phosphates compared to strengite and variscite.54

Figure 4.1. Colloid deposition rate coefficients in unsaturated media……..73

Figure 4.2. Total DLVO interaction energy (ΔG^{TOT}) for a colloid interacting with the solid-water interface (SWI) and another colloid……75

Figure 4.3. Observed retention sites of colloids in unsaturated and saturated experiments…….……....76

Figure 4.4. Schematic of colloid retention sites in unsaturated media…….77

Figure 4.5. Simulated flow velocity field at the wedge-shaped air-water-solid (AWS) interface……...79

Figure 4.S1. Colloid breakthrough curves for unsaturated and saturated column experiments……89
Figure 4.S2. Observed and fitted bromide breakthrough curves in unsaturated experiments……90
Figure 4.S3. . Total DLVO interaction energy (ΔG^{TOT}) for colloid interacting with the air-water interface (AWI)……94
Figure 4.S4. Image taken on the 110th min at the end of experiment with IS = 0.1 mM and C_0 = 0.1%.....96
Figure 4.S5. Images collected in the experiments at 0.5 mM ionic strength……....97
Figure 4.S6. Images recorded at the end of the experiment with IS = 1.0 mM and C_0 = 0.01%.....98
Figure 5.1. Measured and fitted breakthrough curves for bromide and biochar…….121
Figure 5.2. Deposition rate coefficients (k_d and k_{im}) and biochar mass transfer coefficients (α) between the mobile and immobile regions……..122
Figure 5.3. Microscopic images of biochar particles in the column influent and effluent……..126
Figure 5.4. Particle size distribution in the column influents and effluents……127
Figure 5.S1. Comparison among the kinetic and equilibrium deposition model (KEDM), the kinetic deposition model (KDM), and the kinetic deposition and release model (KDRM)……..134
Figure 5S2. DLVO interaction energy (Φ) of a 1 μm biochar colloid……137

LIST OF TABLES

Table 2.1. Selected chemical properties of soils from three vegetative treatment areas sites……...15

Table 2.2. Estimated sorption parameters by the one-step method and the two-step method in the Langmuir models……...19

Table 3.1. Physicochemical properties of soils…….37

Table 3.2. Batch P sorption isotherm experiments on soil samples conducted in duplicate……38

Table 3.3. Chemical conditions of sorption experiments……..40

Table 3.4. Selected chemical composition of farm wastewater……43

Table 4.1. Properties of background influents and electrophoretic mobility (EM) and ζ-potential of the quartz sand and carboxylated polystyrene colloids……..68

Table 4.2. Column experiment properties, effluent mass recoveries, and colloid deposition rate coefficients in unsaturated and saturated media……..71

Table 4.S1. Typical chemical composition and sieve analysis of the quartz sand.....85

Table 4.S2. Electrophoretic mobility and ζ-potential of acid-cleaned quartz sand…...86

Table 4.S3. Modeling results of bromide tracer experiments in unsaturated columns.88

Table 4.S4. DLVO primary energy barrier and second energy minimum……94

Table 4.S5. Summary of videos and images collected in column experiments……97

Table 5.1. Properties of the biochar used in this study……...112

Table 5.2. Summary of bromide and biochar particle breakthrough experiments..…114

Table 5.3. Properties of background influents and electrophoretic mobility (EM) and ζ-potentials of quartz sand and biochar colloids…….120

Table 5.4. Total DLVO interaction energy parameters for 1 μm biochar colloid…..124

Table 5.5. Summary of biochar particle size in the influent and effluent……...125

CHAPTER 1

INTRODUCTION

Brief Overview

Water scarcity exacerbated by pollution from anthropogenic contaminants is a fundamental challenge of our society, because water is essential to agriculture, industry, ecosystem, and human consumption (Postel, 2000). Understanding the fate and transport of soluble and particulate contaminants (e.g., phosphorus and colloids) is important to safeguarding the quality of surface water and groundwater.

Among many environmentally-significant solutes, the fate and transport of phosphorus (P) in soils have been extensively studied because of its imminent role in agricultural production and water quality (Carpenter et al., 1998; Correll, 1998). Phosphorus is an essential mineral nutrient for all life forms, including agricultural crops and livestock, thus P is applied to crop land as inorganic fertilizer and manure and fed to livestock as dietary supplement (Carpenter et al., 1998; Maguire et al., 2007). The P input into soils is usually greater than the P output by crop production, resulting in a net P accumulation in soils in the United States and elsewhere in the world and a loss of the accumulated P to water bodies (Carpenter et al., 1998; Hens and Merckx, 2001). Thus, P export from agriculture contributes significantly to the P loading of surface waters. Over-enrichment of P in surface waters including freshwater lakes, reservoirs, streams, and headwaters of estuarine systems usually leads to eutrophication, and subsequently algal blooms, anoxia, and fish kills. In the northeastern U.S., P transport largely depends on P sorption of soils in some critical areas including variable source areas and land treatment systems (e.g., vegetative treatment areas). This has prompted the first part of my research, which specifically

studied P sorption of New York's agricultural soils that have received the large loadings of P, organics, and other nutrients from dairy farm wastewaters.

Additionally, colloids defined as fine particles between 10 nm to 10 μm (e.g., soil mineral fragments, microorganisms, and natural organic matter) can be contaminants by themselves (e.g., pathogenic microorganisms) or facilitate the transport of other contaminants (e.g., phosphorus, heavy metals, pesticides, and radionuclides) that otherwise remain immobile in soil (McDowell-Boyer et al., 1986; McCarthy and Zachara, 1989; Hens and Merckx, 2001; Heathwaite et al., 2005; de Jonge et al., 2004; DeNovio et al., 2004; McCarthy and McKay, 2004; Turner et al., 2004). Accurate prediction of colloid transport and retention in the subsurface environment is needed for many applications, including protection of groundwater from pathogenic microorganisms and other colloid associated-contaminants, quantification of soil genesis, erosion, and aquifer and oil reservoir production, as well as development of engineered in-situ remediation strategies (DeNovio et al., 2004; McCarthy and McKay, 2004; Bradford et al., 2009). The majority of the past studies have focused on colloid transport in saturated porous media, although the unsaturated subsurface (i.e., the vadose zone) that connects soil surface and migrating groundwater is important for protecting groundwater (Nielsen et al., 1986; McCarthy and McKay, 2004; DeNovio et al., 2004). Moreover, it is expected that large quantities of biochar (i.e., black carbon powder produced from pyrolysis of biomass) may be produced in the future for carbon sequestration (Lehmann et al., 2006; Lehmann, 2007a, b). However, the knowledge on the transport of biochar in the landscape is still limited (Lehmann et al., 2006). Therefore, the lack of knowledge on colloid transport in the vadose zone and biochar transport has driven the second part of my research, which studied the transport of both ideal and non-ideal colloids in porous media.

Study Objectives

In light of the above overview, the objectives of this work were to:

I. Compare a modified P sorption model that uses only Langmuir P sorption isotherm with a conventional model that needs both linear and Langmuir isotherms for New York soils that heavily receive P applications;

II. Use the modified model to study how soil redox fluctuation affects soil P sorption of an organic-rich silt loam collected from a vegetative treatment area receiving dairy farm wastewaters;

III. Investigate the transport and retention of model colloids in unsaturated sand as influenced by colloid input concentrations, and the coupling of concentration effect and ionic strength;

IV. Study the transport of non-ideal colloids (biochar particles) under the influence of solution pH and ionic strength and biochar particle size.

The following chapters address the four objectives of my research. The Objective I is addressed in Chapter 2, Objective II in Chapter 3, Objective III in Chapter 4, and Objective IV in Chapter 5. The dissertation ends with Chapter 6 that summarizes the findings of the studies that have been conducted and identifies future research directions.

REFERENCES

Bradford, S.A., S. Torkzaban, F. Leij, J. Šimůnek, T.M. van Genuchten. 2009. Modeling the coupled effects of pore space geometry and velocity on colloid transport and retention. *Water Resour. Res.*, 45: W02414.

Carpenter, S.R., N.F. Caraco, D.L. Correll, R.W. Howarth, A.N. Sharpley, and V.H. Smith. 1998. Nonpoint pollution of surface waters with phosphorus and nitrogen. *Ecol. Appl.* 8: 559–568.

Correll, D.L. 1998. The role of phosphorus in the eutrophication of receiving waters: A review. *J. Environ. Qual.* 27: 261–266.

de Jonge, L.W., C. Kjaergaard, P. Moldrup. 2004. Colloids and colloid-facilitated transport of contaminants in soils: An introduction. *Vadose Zone J.* 3: 321–325.

DeNovio, N.M., J.E. Saiers, and J.N. Ryan. 2004. Colloid movement in unsaturated porous media: Recent advances and future directions. *Vadose Zone J.* 3: 338–351.

Hens, M, and R. Merckx. 2001. Functional characterization of colloidal phosphorus species in the soil solution of sandy soils. *Environ. Sci. Technol.* 35(3): 493–500.

Heathwaite, L., P. Haygarth, R. Matthews, N. Preedy, and P. Butler. 2005. Evaluating colloidal phosphorus delivery to surface waters from diffuse agricultural sources. *J. Environ. Qual.* 34: 287–298.

Lehmann, J., J. Gaunt, and M. Rondon. 2006. Bio-char sequestration in terrestrial ecosystems – A review. *Mitigation and Adaptation Strategies for Global Change* 11: 403–427.

Lehmann, J. 2007a. A handful of carbon. *Nature* 447: 143–144.

Lehmann, J. 2007b. Bio-energy in the black. *Front. Ecol. Environ.* 5(7): 381–387.

Maguire, R.O., D.A. Crouse, and S.C. Hodges. 2007. Diet modification to reduce phosphorus surpluses: A mass balance approach. *J. Environ. Qual.* 36: 1235–1240.

McCarthy, J.F., and J.M. Zachara. 1989. Subsurface transport of contaminants. *Environ. Sci. Technol.* 23(5): 496–502.

McDowell-Boyer, L.M., J.R. Hunt, and N. Sitar. 1986. Particle transport through porous media. *Water Resour. Res.* 22(13): 1901–1921.

McCarthy, J.F., and L.D. McKay. 2004. Colloid transport in the subsurface: Past, present, and future challenges. *Vadose Zone J.* 3: 326–337.

Nielsen, D.R., M.Th. van Genuchten, and J.W. Biggar. 1986. Water flow and solute transport processes in the unsaturated zone. *Water Resour. Res.* 22(9): 89S–108S.

Postel, S.L. 2000. Entering an era of water scarcity: The challenges ahead. *Ecological Applications.* 10(4): 941–948.

Turner, B.L., M.A. Kay, and D.T. Westermann. 2004. Colloidal phosphorus in surface runoff and water extracts from semiarid soils of the western United States. *J. Environ. Qual.* 33: 1464–1472.

CHAPTER 2

EVALUATION OF TWO LANGMUIR MODELS FOR PHOSPHORUS SORPTION OF P-ENRICHED SOILS IN NEW YORK FOR ENVIRONMENTAL APPLICATIONS

Wei Zhang, Joshua W. Faulkner, Shree K. Giri, Larry D. Geohring, Tammo S. Steenhuis

Abstract

The phosphorus (P) sorption isotherm experiment is a widely used tool in environmental applications for assessing soil's vulnerability to P loss to runoff or drainage. The sorbed legacy P (S_0) (i.e. the P retained in soils from previous P applications) participates in sorption processes, but cannot readily be determined in a sorption experiment. Thus, it is important to accurately estimate S_0 for P-enriched soils (e.g. the soils that heavily receive fertilizer, manure, farm wastewater, or sewage sludge). Two curve-fitting procedures (i.e. one-step method and two-step method) with Langmuir models have been used to estimate S_0 and other sorption parameters, including the P sorption maxima (S_{max}), the bonding energy constant (k), and the zero-sorption equilibrium concentration (EPC_0). This study evaluated these two methods on sixteen samples of Langford, Volusia, and Mardin channery silt loam soils at surface (0-8 cm) and subsurface (61-91 cm) in New York. The results indicate that the two methods agreed well in estimating S_{max}, and the estimates of k were close. The S_0 estimates by the two methods had a good agreement for surface soils, but a poor agreement for subsurface soils, which may be of little concern because of small S_0 of subsurface soils. Although the one-step method yielded greater EPC_0 estimates, the EPC_0 estimates by the two methods had an excellent linear correlation for P-enriched surface soils, suggesting that both methods could work equally if only the

relative magnitudes of EPC_0 among soils are needed. Overall, both methods are acceptable to fit the Langmuir isotherms.

Keywords: phosphorus, sorption isotherm, Langmuir model

Introduction

Phosphorus (P), although an essential element for all life forms, is considered in many cases a limiting mineral nutrient for freshwater lakes, reservoirs, streams, and headwaters of estuarine systems (Correll, 1998). Over-enrichment of P in these waters usually leads to eutrophication, resulting in algal or cyanobacterial blooms, anoxia, and fish kills. Phosphorus export from agricultural production sources contributes significantly to the P accumulation in surface waters (Carpenter et al., 1998). After field applications of chemical P fertilizer, manure, farm wastewaters, or sewage sludge, the P transport through landscape is largely dependent on soil's P sorption properties. Soils accumulate P when receiving P in excess of vegetation removal (Kao and Blanchar, 1973; Sui and Thompson, 2000; Siddique and Robinson, 2003). One portion of the accumulated P from previous P applications readily takes part in P sorption processes between soil and solution (Zhou et al., 2005), thus is prone to the loss to runoff or drainage. This labile pool of the soil P is termed as the sorbed legacy P (S_0) here. Its magnitude is often significant in P-enriched soils, which is of little concern in agronomic applications, but is far more important in environmental applications regarding soil P loss.

Phosphorus sorption properties of soils are mainly studied by sorption isotherm experiments, which were historically initiated in agronomy for evaluating the P availability for crop uptake (Olsen and Watanabe, 1957; Holford, 1979), but have become popular for assessing the soil P mobility in environmental applications (Gale et al., 1994; Vadas and Sims, 1999; Sui and Thompson, 2000; Siddique and Robinson, 2003). Phosphorus sorption isotherms have been quantitatively described by the

Langmuir, Freundlich, and Tempkin models (Graetz and Nair, 2000; Villapando and Graetz, 2001; Barrow, 2008). The Langmuir model has the advantage over the Freundlich and Tempkin models in environmental applications because the soil's maximum capacity to sorb P (i.e. the P sorption maxima, S_{max}) and the P bonding energy constant (k) can be determined (Graetz and Nair, 2000; Villapando and Graetz, 2001). These two parameters have been used to evaluate the soil P loss potential: the soil P saturation degree (S_0/S_{max}) and the maximum P buffering capacity index ($S_{max}k$) (Holford, 1979; Sharpley, 1995; Sui and Thompson, 2000; Sims et al., 2002; Zhang et al., 2005; Bolster and Hornberger, 2007). In addition, the zero-sorption equilibrium concentration (i.e. the P concentration in soil water that causes neither P sorption nor desorption, EPC_0) has also been employed to assess the soil P loss potential (Vadas and Sims, 1999; Graetz and Nair, 2000; Zhou et al., 2005).

In a P sorption isotherm experiment, the difference of P between the initial sorption solution and the final sorption solution is the amount of P sorbed by soils, referred herein as the apparent soil P sorption (S'). The apparent soil P sorption does not include the sorbed legacy P (S_0). Ignoring S_0 could be problematic in environmental applications that utilize P sorption isotherms for P-enriched soils, as a result of erroneous estimates of sorption parameters and consequent misevaluation of the soil P loss potential. Thus, many researchers have put considerable effort in estimating S_0.

In the past, two types of methods have been used to estimate the sorbed legacy P (S_0), namely, the extraction methods and the curve-fitting methods. In the extraction methods, S_0 was estimated using experimental measurements from an extraction method, including the Olsen-extractable P (Siddique and Robinson, 2003), the Mehlich-1 or Mehlich-3 extractable P (Sallade and Sims, 1997; Brock et al., 2007), the Morgan-extractable P (Brock et al., 2007), the isotopically exchangeable P (Olsen and

Watanabe, 1957), and the anion-exchange resin-impregnated membrane extractable P (Villapando and Graetz, 2001). In the curve-fitting methods, S_0 was estimated by two curve-fitting procedures associated with the Langmuir isotherm equation (Gale et al., 1994; Reddy et al., 1998; Graetz and Nair, 2000; Pant and Reddy, 2001; Zhou et al., 2005), referred here as the two-step method and the one-step method, as explained in detail in the following model section. The curve-fitting methods have advantages over the extraction methods, because the extraction methods usually use an extractant with different chemistry from that of sorption solutions, thus the tested soil P does not necessarily agree with S_0. Villapando and Graetz (2001) had to use a correction factor to compensate this discrepancy. The curve-fitting methods avoid this problem since S_0 is estimated from the sorption isotherms. Currently, it is not known how well these two curve-fitting methods agree with each other in estimating S_0 and other sorption parameters, including S_{max}, k, and EPC_0.

Therefore, the objective of this study was to evaluate the two Langmuir curve-fitting methods, the two-step method and the one-step method, in estimating P sorption parameters (i.e. S_0, S_{max}, k, and EPC_0) of three soil series in New York. In addition, we applied the one-step and two-step methods to the Freundlich model and examined the model's suitability for P-enriched soils. The results of this study will help researchers better utilize the P sorption model in P sorption studies.

P Sorption Models

The Langmuir model is extensively used in the contemporary environment-related P sorption study. The model is somewhat theoretically based and allows one to estimate the P sorption maxima (Olsen and Watanabe, 1957; Villapando and Graetz, 2001; Essington, 2004; Bolster and Hornberger, 2007; Bolster, 2008), although the use of the model was challenged for heterogeneous surface of soils (Sparks, 2003). Pant and Reddy (2001) argued that every P compound in soils is independently equilibrated

with P in solution, and the heterogeneous soil systems behave as a mixture of homogeneous surfaces.

The total amount of P sorbed in soils per unit soil mass, S (mg kg^{-1}), and the equilibrium P concentration, C (mg L^{-1}), in solution follow the Langmuir model as:

$$S = \frac{S_{max} kC}{1 + kC} \qquad (1)$$

where S_{max} (mg kg^{-1}) is the maximum of P that can be sorbed on unit soil mass, and k (L mg^{-1}) is the bonding energy constant.

Isotherms are usually determined with batch experiments in which flasks are shaken for a predetermined time period (typically 24 hours). In these flasks, M (g) of dry soil and V (mL) of aqueous solution with P concentration of C_i (mg L^{-1}) are added. At the end of experiments, the aqueous P concentration is C. The amount of P removed from solution (i.e. adsorbed to the soil particles) per unit soil mass, S' (mg kg^{-1}), can be expressed as:

$$S' = \frac{(C_i - C)V}{M} \qquad (2)$$

The total amount of P sorbed in the soil (S) is defined as the sum of the sorbed legacy P, S_0 (mg kg^{-1}), before the solution is added and the new amount that is sorbed from solution (S'):

$$S = S' + S_0 \qquad (3)$$

Generally the value of S_0 is unknown and needs to be determined. It can be neglected if it is small (Olsen and Watanabe, 1957). In cases where S_0 is significant (e.g. P-enriched soils), two-curve fitting methods, the two-step method and the one-step method, have been developed to determine S_0.

The two-step method proposed by Gale et al. (1994) has been popular due to its simplicity (Reddy et al., 1998; Graetz and Nair, 2000; Pant and Reddy, 2001). It assumes a linear sorption isotherm at low concentrations as:

$$S' = KC - S_0 \qquad (4)$$

where K (L kg^{-1}) is the partition coefficient.

In the two-step method, the apparent isotherm (S' versus C) at low concentrations is first fitted with eq. 4 to obtain S_0. Adding S_0 to S' (eq. 3) yields the total sorbed P (S) in soils. The entire isotherm (S versus C) is then fitted with the Langmuir model (eq. 1) to estimate S_{max} and k.

The one-step method developed by Zhou et al. (2005) assumes that the Langmuir model is also valid for low concentrations. Combining eqs. 1, 2, and 3 produces:

$$\frac{(C_i - C)V}{M} = \frac{S_{max} kC}{1 + kC} - S_0 \qquad (5)$$

For soils in P-free initial solutions (C_i=0), the equilibrium P concentration (C) in solution is C_0 (mg L^{-1}). From eq. 5, S_0 can be expressed as:

$$S_0 = \frac{S_{max} kC_0}{1 + kC_0} + \frac{C_0 V}{M} \qquad (6)$$

Combining eqs. 1, 3 and 6, S' can be found as a function of C:

$$S' = \frac{S_{max} kC}{1 + kC} - \left(\frac{S_{max} kC_0}{1 + kC_0} + \frac{C_0 V}{M}\right) \qquad (7)$$

In the one-step method, the apparent isotherm (S' versus C) is directly fitted with eq. 7 using a nonlinear least square fitting algorithm to estimate S_{max} and k, while C_0 is experimentally measured (Zhou et al., 2005). Then, S_0 is calculated from eq. 6.

The zero-sorption equilibrium concentration (EPC_0), an indicator of the potential of P loss to runoff or drainage, is defined as the aqueous P concentration that does not cause either P sorption or desorption (Graetz and Nair, 2000; Vadas and Sims, 1999; Zhou et al., 2005). Hence, S' is zero. For the two-step method, EPC_0 can be determined as:

$$EPC_0 = S_0 / K \qquad (8)$$

For the one-step method, EPC_0 can be determined as:

$$EPC_0 = \frac{S_{max} kC_0 /(1+kC_0) + C_0 V / M}{S_{max} k /(1+kC_0) - kC_0 V / M} \qquad (9)$$

Knowing sorption parameters of S_{max} and k, the maximum buffering capacity (*MBC*) of soils, the index of soils' resistance to the change of P concentration in soil solution with adding or removing P (Holford, 1979; Sui and Thompson, 2000), is derived as:

$$MBC = \left(\frac{dS'}{dC}\right)_{C\to 0} = \left[\frac{S_{max} k}{(1+kC)^2}\right]_{C\to 0} = S_{max} k \qquad (10)$$

The values of *MBC*, also being the slope of isotherms at $C \to 0$, dictate the steepness of isotherms at low concentrations. In the case that S_{max} does not differ as much as k does among soils, the bonding energy constant (k) determines the shape of isotherms. The soils' *MBC* values are also environmentally relevant since soils with larger *MBC* would in principle have a greater tendency to maintain their original aqueous P concentration in the event of the inflow of higher P concentrations.

To examine the suitability of the Freundlich model for use on P-enriched soils, we present this application as well. The traditional Freundlich model is (Barrow, 2008):

$$S = K_f C^n \qquad (11)$$

where K_f (mg^{1-n} kg^{-1} L^n) is the Freundlich sorption energy constant, and n is a dimensionless correction factor. Similar to the Langmuir models, in the Freundlich two-step method S_0 is estimated by fitting the apparent isotherm (S' versus C) at the low concentrations to eq. 4 and S is calculated by eq. 3. The entire isotherm (S versus C) is then fitted with eq. 11 to obtain K_f and n. The EPC_0 estimate is determined by eq. 8. In the Freundlich one-step method, the model equations are (see Appendix for detailed derivation):

$$S_0 = K_f C_0^n + \frac{C_0 V}{M} \qquad (12)$$

$$S' = K_f C^n - \left(K_f C_0^n + \frac{C_0 V}{M}\right) \qquad (13)$$

$$EPC_0 = \left(C_0^n + \frac{C_0 V}{M K_f} \right)^{1/n} \qquad (14)$$

The apparent isotherm (S' versus C) is fitted to eq. 13 to estimate K_f and n. Then, S_0 and EPC_0 are calculated from eq. 12 and 14.

Materials and Methods

Site Description

The soils in this study were collected from three vegetative treatment areas (VTAs) located at Tompkins County, Wyoming County and Delaware County in New York. The soil was classified as a Langford channery silt loam (fine-loamy, mixed, active, mesic Typic Fragiudepts) at the Tompkins County site, a Volusia channery silt loam (fine-loamy, mixed, active, mesic Aeric Fragiaquepts) at the Wyoming County site, and a Mardin channery silt loam (coarse-loamy, mixed, active, mesic Typic Fragiudepts) at the Delaware County site (NRCS, 2008). The three soil series are typical glaciated soils in the northeastern U.S., and have extensive distributions in New York and northern Pennsylvania.

The Tompkins County and Wyoming County VTAs were planted in a mixture of reed canarygrass (*Phalaris arundinacea*), redtop (*Agrostis alba*), and tall fescue (*Festuca elatior*), and have received the farm silage bunker runoff by gravity flow since the spring of 2005 and the summer of 2006, respectively. The Delaware County VTA is located in a pasture primarily used for hay production and receives the intermittent dosing of farm barnyard runoff collected in a storage tank since the summer of 2005. These nutrient-laden wastewaters contained 300 - 2000 mg L^{-1} dissolved organic carbon (DOC), 18 - 170 mg L^{-1} ammonium-nitrogen, 13 - 55 mg L^{-1} soluble reactive P (SRP), and 80 - 350 mg L^{-1} dissolved Ca. The annual P application rate at the Tompkins County site was estimated to be 126 kg P ha^{-1}, which is much

greater than the P removal rate of 28 kg P ha^{-1} by grass vegetation (Czymmek and Ketterings, 2007).

Soil Sampling and Analyses

Several sets of surface (0-8 cm) and subsurface (61-91 cm) soil pair located down-slope of wastewater surface distribution points were collected at the Tompkins County site, Wyoming County site, and Delaware County site on October 19, 2006, October 10, 2006, and October 18, 2007, respectively. Soil samples from the Tompkins County site were denoted as T1S, T1D, T2S, T2D, T4S, and T4D, the ones from the Wyoming County site as W1S, W1D, W2S, W2D, W4S, and W4D, and the ones from the Delaware county site as D1S, D1D, D3S, and D3D (refer to Table 2.1 for the labeling convention). The soil samples were air-dried, ground, and passed through a 2 mm-sieve. The soil analysis was conducted for air-dried soil samples by the Cornell Nutrient Analysis Laboratory (CNAL), Cornell University, Ithaca, NY. Soil pH was measured in water at 1:1 soil:water ratio. The soil organic matter (OM) was determined by loss on ignition. Soil samples were extracted with sodium acetate solution (0.72 *N* NaOAc+0.52 *N* CH_3COOH), known as the Morgan extraction. The extractants were analyzed for P using the ascorbic acid method with a flow analyzer (ALPKEM RFA/2, OI Analytical, College Station, TX) and for cations including Ca, Fe, and Al by inductively coupled plasma atomic emission spectroscopy (ICP-AES) (JY70 TYPEII, Jobin Yvon, Edison, NJ). The above soil analyses followed the methods of NRCS (2004) and Sims and Wolf (1995). The nitric acid-digestion elements, including P, Ca, Fe, and Al, were determined by ICP-AES (SPECTRO-CIROS^{CCD}, SPECTRO Analytical Instruments Inc., Mahwah, NJ) after the microwave-assisted digestion with HNO_3 (USEPA, 2007).

Selected chemical properties of soils are summarized in Table 2.1. The soil tests demonstrate a variety of soil chemical properties. The soils had OM ranging from

0.6% to 8.1% and various degree of P-enrichment with the Morgan extractable P ranging from 0.7 to 262 mg kg^{-1}. The higher Morgan extractable P of the surface soils in the Wyoming County site may partially be a result of silage and manure stockpiling on the ground, prior to the VTA construction. The Morgan extractable cations also covered a wide range, with Ca ranging from 347 to 4067 mg kg^{-1}, Fe from 1.5 to 48.5 mg kg^{-1}, and Al from 7.9 to 44.2 mg kg^{-1}. The nitric acid-digestion elements showed the similar variability. The soil pH was between 6.2 and 8.1. While the soil series are listed as acidic in the soil survey (NRCS, 2008), liming and the application of dairy manure and dairy farm wastewater could have increased the soil pH, similar to that reported by Barkle et al. (2000) and Cabrera et al. (2009).

Table 2.1. Selected chemical properties of soils from three vegetative treatment areas sites at Tompkins County (T), Wyoming County (W), and Delaware County (D) in New York.

Soils[†]	pH	OM[‡] (%)	Morgan extractable elements (mg kg^{-1})				Nitric acid-digestion elements (mg kg^{-1})			
			P	Ca	Fe	Al	P	Ca	Fe	Al
T1S	7.5	5.6	40.1	3143	13.1	19.3	1738	4968	26617	37500
T1D	7.6	1.3	2.0	1284	10.0	35.2	494	1741	28406	19626
T2S	7.7	5.4	92.2	3079	5.7	12.8	1783	4524	24048	22361
T2D	7.8	1.1	1.5	1411	4.0	18.3	609	2338	27267	21950
T4S	6.7	5.2	60.1	2274	3.3	9.8	1648	3743	26994	21826
T4D	7.8	0.8	0.7	1312	3.9	26.8	466	2059	29760	18403
W1S	7.4	6.4	259	3619	3.6	8.8	2233	7696	20399	19318
W1D	7.7	2.5	25.2	2127	33.5	21.6	825	4875	21162	15525
W2S	7.4	7.7	262	3526	4.7	8.7	2175	6504	18158	14793
W2D	8.1	1.4	7.9	1412	48.5	22.6	577	2835	26532	20135
W4S	7.1	8.1	236	4067	4.3	7.9	3030	6522	17560	18233
W4D	7.6	1.0	10.5	1167	1.5	15.7	603	2236	23171	18039
D1S	7.2	7.4	79.8	2190	3.4	12.4	611	913	26150	16673
D1D	6.7	0.6	11.1	423	13.0	44.2	376	478	29993	15198
D3S	6.2	5.8	12.8	1422	5.5	40.2	363	1014	27404	13886
D3D	6.6	1.1	4.4	347	16.7	73.2	297	464	27086	13228

[†] Soil samples were labeled as: site = Tompkins County site (T), Wyoming County site (W), and Delaware County site (D); location = a higher number indicates a greater distance down-slope of wastewater surface distribution points; depth = surface (S) and subsurface (D).
[‡] OM = organic matter.

Sorption Isotherms

One gram of air-dried soils was placed in the series of 50 mL polypropylene centrifuge tubes and mixed with 20 mL 0.01 M potassium chloride (KCl) solutions spiked with 0, 1, 5, 10, 50, 100, and 200 mg/L P as KH_2PO_4. Duplicate tests were carried out for each soil sample. The centrifuge tubes were shaken on a reciprocal shaker at a speed of 180 cycle/min for 24 hours at 25 ± 3 ºC. The supernatants were filtered through a 0.45 μm mixed cellulose ester membrane (Pall Life Sciences, Ann Arbor, MI). The filtrates were acidified with concentrated hydrochloric acid and stored in the refrigerator at 4 ºC before analysis. Filtrate was analyzed for soluble reactive P (SRP) by a flow-injection P analyzer (Flowsystem-3000, OI Analytical, College Station, TX) using the ascorbic colorimetric method (USEPA, 1983). The initial P concentrations were also measured. The difference between the initial concentration and the final concentration was calculated as the apparent sorbed P (S') by eq. 2.

Following the procedures in the model section, the averaged isotherms were fitted using both the one-step and two-step methods by the unweighted trust-region nonlinear least square regression algorithm in Matlab (The MathWorks, Inc., Natick, MA). The estimates of S_{max}, k, S_0, and EPC_0 from both methods in the Langmuir models were plotted in 1:1 scatter plots and linear regressions through the origin were performed to examine the agreement between estimates. The Freundlich models were also examined on their goodness-of-fit and the agreement of parameter estimates by the one-step and two-step methods.

Results and Discussion

As mentioned previously, the isotherms were fitted to the Langmuir models by the one-step method and the two-step method to estimate S_{max}, k, S_0, EPC_0, and MBC, which are shown in Table 2.2 together with the adjusted R^2, root mean square error

(RMSE), and the parameter 95% confidence intervals. The measured and fitted Langmuir isotherms of T2S and T2D are shown in Figure 2.1 as examples. The apparent isotherms (S' versus C) in Figure 2.1 were fitted by the one-step method. The linear fitting of the apparent isotherm at low concentrations (eq. 4) in the two-step method is shown in the inset of Figure 2.1. Both the Langmuir one-step and two-step methods fitted the sorption data satisfactorily. The adjusted R^2 values ranged from 0.90 to 0.99 for both the Langmuir one-step and two-step methods, suggesting a good model fit. The RMSE values were from 15 to 78 mg kg^{-1} (Table 2.2), which were in the same range with the RMSE values (7 to 90 mg kg^{-1}) calculated from the SSE (i.e. sum of squared error) values reported by Bolster and Hornberger (2007) and Bolster (2008). The 95% confidence interval widths in the Langmuir one-step method were 0.4 ± 0.2 times of the S_{max} estimates and 2.3 ± 0.7 times of the k estimates, and the similar parameter uncertainties were observed for the Langmuir two-step method. These parameter uncertainties agreed with the reported ones (see Fig. 5 in Bolster and Hornberger, 2007). Thus, our Langmuir models offered the satisfactory goodness of fit, at least equivalent to the results of other studies.

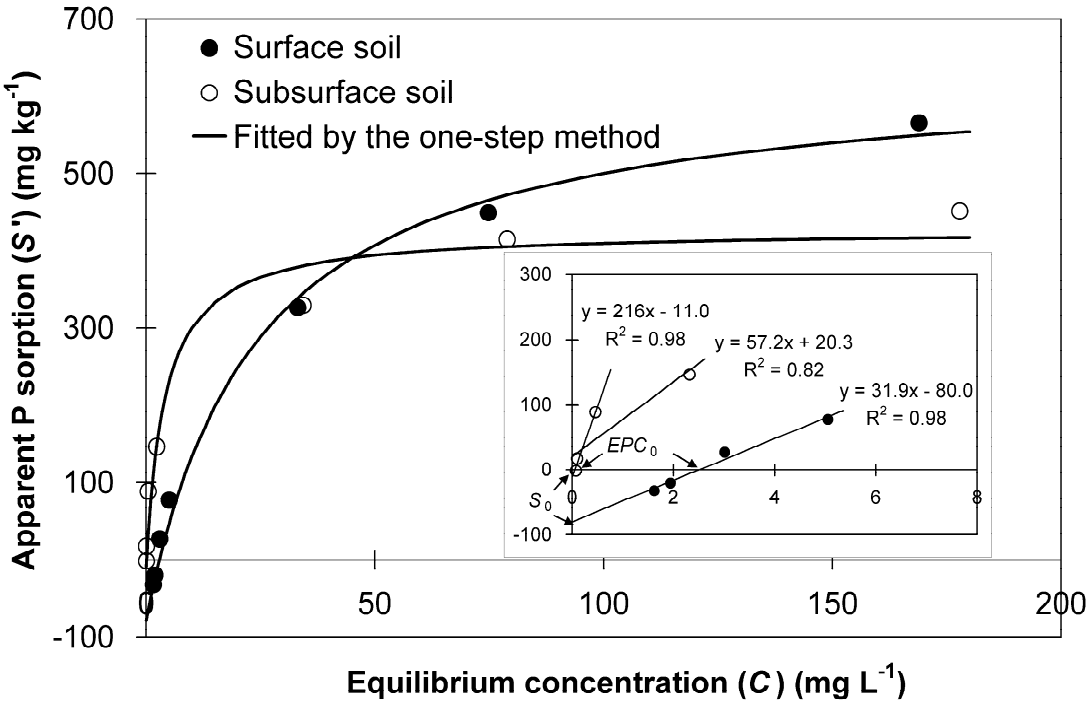

Figure 2.1. Typical observed and fitted Langmuir sorption isotherms of surface and subsurface soils (T2S and T2D). The inset showed the estimation of the sorbed legacy P (S_0) and the zero-sorption equilibrium concentration (EPC_0) by fitting linear isotherms at low concentrations.

Table 2.2. Estimated sorption parameters by the one-step method and the two-step method in the Langmuir models.

	Soils	S_{max} † (mg kg^{-1})	k† (L mg^{-1})	Adjusted R^2	RMSE † (mg kg^{-1})	S_0† (mg kg^{-1})	EPC_0† (mg L^{-1})	MBC† (L kg^{-1})
One-step method	T1S	872 (116)‡	0.075 (0.058)‡	0.98	40	50‡	0.80‡	65‡
	T1D	450 (95)	0.225 (0.324)	0.93	52	9	0.09	101
	T2S	716 (73)	0.042 (0.021)	0.99	21	78	2.91	30
	T2D	437 (66)	0.243 (0.251)	0.96	37	9	0.09	106
	T4S	405 (71)	0.057 (0.069)	0.96	29	80	4.34	23
	T4D	329 (76)	0.403 (0.631)	0.90	47	6	0.05	133
	W1S	613 (128)	0.031 (0.032)	0.97	34	129	8.61	19
	W1D	643 (155)	0.053 (0.061)	0.96	48	26	0.80	34
	W2S	605 (176)	0.023 (0.026)	0.96	37	127	11.7	14
	W2D	562 (122)	0.138 (0.205)	0.94	57	13	0.17	78
	W4S	705 (62)	0.026 (0.012)	0.99	15	187	14.1	18
	W4D	388 (80)	0.241 (0.328)	0.93	46	10	0.23	93
	D1S	1147 (345)	0.012 (0.009)	0.98	35	92	7.00	14
	D1D	314 (86)	0.120 (0.185)	0.90	41	6	0.15	38
	D3S	1197 (445)	0.024 (0.027)	0.96	75	16	0.54	29
	D3D	416 (109)	0.164 (0.274)	0.90	56	7	0.14	68
Two-step method	T1S	851 (112)	0.094 (0.059)	0.98	41	57 (72)‡	0.63‡	80
	T1D	448 (96)	0.243 (0.322)	0.93	52	9 (134)	0.04	109
	T2S	704 (70)	0.046 (0.017)	0.99	21	80 (45)	2.51	32
	T2D	436 (68)	0.264 (0.250)	0.96	38	11 (114)	0.05	115
	T4S	398 (82)	0.052 (0.039)	0.96	28	69 (29)	3.90	21
	T4D	327 (77)	0.427 (0.632)	0.90	46	6 (107)	0.02	140
	W1S	602 (125)	0.033 (0.021)	0.97	33	127 (31)	7.26	20
	W1D	614 (133)	0.089 (0.093)	0.95	53	46 (61)	0.58	55
	W2S	580 (148)	0.029 (0.022)	0.96	37	136 (37)	8.68	17
	W2D	556 (115)	0.199 (0.249)	0.94	60	24 (64)	0.13	111
	W4S	694 (61)	0.029 (0.007)	0.99	16	194 (19)	11.3	20
	W4D	385 (82)	0.246 (0.308)	0.93	46	8 (108)	0.05	95
	D1S	1061 (300)	0.016 (0.011)	0.98	42	109 (61)	4.70	17
	D1D	312 (89)	0.108 (0.161)	0.91	40	0 (0)	0.00	34
	D3S	1175 (435)	0.027 (0.029)	0.96	78	22 (65)	0.25	32
	D3D	412 (112)	0.157 (0.250)	0.91	55	2 (133)	0.02	65

† S_{max} = the P sorption maxima; k = the bonding energy constant; RMSE = root mean squared error; S_0 = the sorbed legacy P; EPC_0 = the zero-sorption equilibrium concentration; MBC = the maximum buffering capacity.

‡ Adding and subtracting the values in the parenthesis on parameter estimates generates the 95% confidence intervals. For S_{max} and k, those values were directly obtained from the Langmuir model fitting using the one-step and two-step methods. For S_0 in the two-step method, the 95% confidence intervals were from the linear isotherm fitting. The S_0 values in the one-step method, the EPC_0 values, and the MBC values were calculated from the fitted parameters, thus no 95% confidence intervals could be provided.

The Freundlich one-step method produced unrealistically large K_f and S_0 (for brevity, detailed data not shown), while considerable parameters uncertainty were observed for K_f and n (i.e., the 95% confidence interval widths were 2.5 ± 2.2 times of the K_f estimates and 1.9 ± 1.9 times of the n estimates). The Freundlich two-step method had similar goodness of fit, compared to that of the Langmuir models, with the adjusted R^2 values ranging from 0.94 to 0.99 and the RMSE values from 19 to 70 mg kg^{-1}. The 95% confidence interval widths were 0.9 ± 0.2 times of the K_f estimates and 0.5 ± 0.1 times of the n estimates. While the EPC_0 estimates by the two Freundlich methods were close, the estimates of K_f, n, and S_0 differed drastically by over 89%. In addition, the Freundlich sorption parameters are less meaningful in evaluating the soil P loss potential, compared to the Langmuir sorption parameters, because the Langmuir sorption parameters can be used to determine the soil P saturation degree (S_0/S_{max}) and the maximum P buffering capacity index ($S_{max}k$) (Sharpley, 1995; Graetz and Nair, 2000; Villapando and Graetz, 2001; Zhang et al., 2005; Bolster and Hornberger, 2007). Therefore, in the following sections, we focused on the results of the Langmuir models and the Freundlich models were not further considered.

Surface and subsurface soils generally showed distinct sorption behavior in that the isotherms of subsurface soils appeared steeper than that of surface soils at low concentrations (e.g. observing the difference between T2S and T2D in Figure 2.1). This is supported by the fact that the *MBC* values of subsurface soils are greater than that of surface soils by a factor of 1.4 to 6.9 (Table 2.2), and the isotherm steepness monotonically increases with increasing *MBC* at low concentrations. The steeper isotherms of subsurface soils had a narrow range of isotherm linearity at very low concentrations, which demands additional considerations for the two-step method. Taking T2S and T2D as examples, the concentration range of isotherm linearity (R^2 = 0.98) was 1.62 - 5.06 mg L^{-1} for T2S (the inset of Figure 2.1), which corresponded to

the four lowest concentration points with the initial concentration from 0 to 10 mg L^{-1}. For T2D, the concentration range of isotherm linearity ($R^2 = 0.98$) was 0.08 - 0.43 mg L^{-1} (the inset of Figure 2.1), which corresponded to the three lowest concentration points with the initial concentration from 0 to 5 mg L^{-1}. Graetz and Nair (2000) recommended that the linear isotherm at low concentrations shall have a R^2 value greater than 0.95. This criterion was met for the lowest four concentration points of surface soil isotherms, but only for the lowest three concentration points of subsurface soil isotherms, as shown in the inset of Figure 2.1. The isotherms of other soils showed similar trends (data not shown).

The 1:1 scatter plots of S_{max}, k, S_0, and EPC_0 estimated from the Langmuir one-step and two-step methods for surface and subsurface soils are presented in Figure 2.2 and Figure 2.3, respectively. The estimates of S_{max} by both methods agreed very well, with a regression slope of 0.97 for surface soil and 0.98 for subsurface soil, and an R^2 of 0.99 for both soil depths (Figure 2.2A and Figure 2.3A). This good agreement is a result of the dependency of S_{max} on P sorption at high equilibrium concentrations (Essington, 2004). Thus, the assumption of isotherm linearity at low concentrations in the two-step method should not significantly affect S_{max} estimates. The estimates of k from both methods were fairly close, with the estimates by the two-step method being 13% and 7% higher on average for surface and subsurface soils, respectively (Figure 2.2B and Figure 2.3B). Eliminating a high value in Figure 2.2B resulted in a slope of 1.04 with a 95% confidence interval of (0.91, 1.15), indicating no significant difference from 1, similar to Figure 2.3B. Thus, the k values estimated by both methods were indeed not significantly different. For the sorbed legacy P (S_0), the results were similar for surface soils (Figure 2.2C). However, the estimates of S_0 differed by 48% for subsurface soils with the R^2 value of the regression line being 0.80 and the slope being significant different with 1 (Figure 2.3C), implying a poor

agreement. Fortunately, the estimation of S_0 for subsurface soils may be less important, considering the small S_0 and Morgan extractable P of subsurface soils (Table 2.1 and 2.2). The EPC_0 estimates from both methods correlate with each other well for surface soils ($R^2 = 0.99$, Figure 2.2D), but exhibit a slightly poorer correlation for subsurface soils ($R^2 = 0.89$, Figure 2.3D). Even so, the one-step method overestimated EPC_0 over 22% (Figure 2.2D and Figure 2.3D). The EPC_0 estimates from the one-step method are determined from the Langmuir isotherm fitting, which is more dependent on P sorption at high concentrations as mentioned before. This dependency in the one-step method causes lower estimated sorption than the observed values at low concentrations, thus a shift of EPC_0 to greater values when the isotherm crosses the zero sorption line (i.e., $S'=0$). The two-step method estimates EPC_0 by fitting a linear isotherm at low concentrations as shown in the inset of Figure 2.1, which can be considered a more accurate procedure. If only the relative magnitude of EPC_0 among soils is needed for comparison purpose, both methods could work equally for surface soils since their estimates of EPC_0 are linearly correlated (Figure 2.2D). For subsurface soils, the EPC_0 values ranging from 0.05 to 0.80 mg L^{-1} are relatively small and not as much concern as that of surface soils (0.54 to 14.1 mg L^{-1}) when considering the P loss (Table 2.2). Since the EPC_0 value is interpreted as the potential of soil P loss to runoff or drainage (Vadas and Sims, 1999), the greater estimates of EPC_0 from the one-step method could lead to more environmentally conservative management practices.

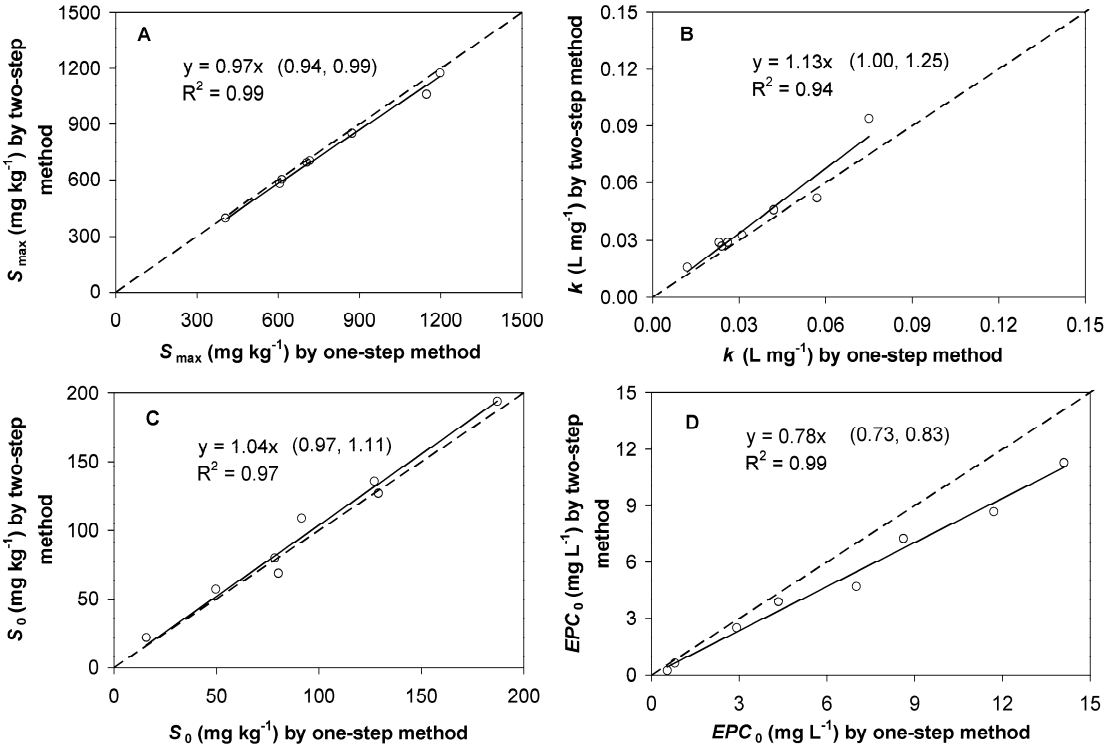

Figure 2.2. Comparison between sorption parameters estimated by the one-step method and the two-step method for surface soils: A. the P sorption maxima (S_{max}); B. the bonding energy constant (k); C. the sorbed legacy P (S_0); and D. the zero-sorption equilibrium concentration (EPC_0). The 95% confidence intervals of the slopes are shown in the parenthesis.

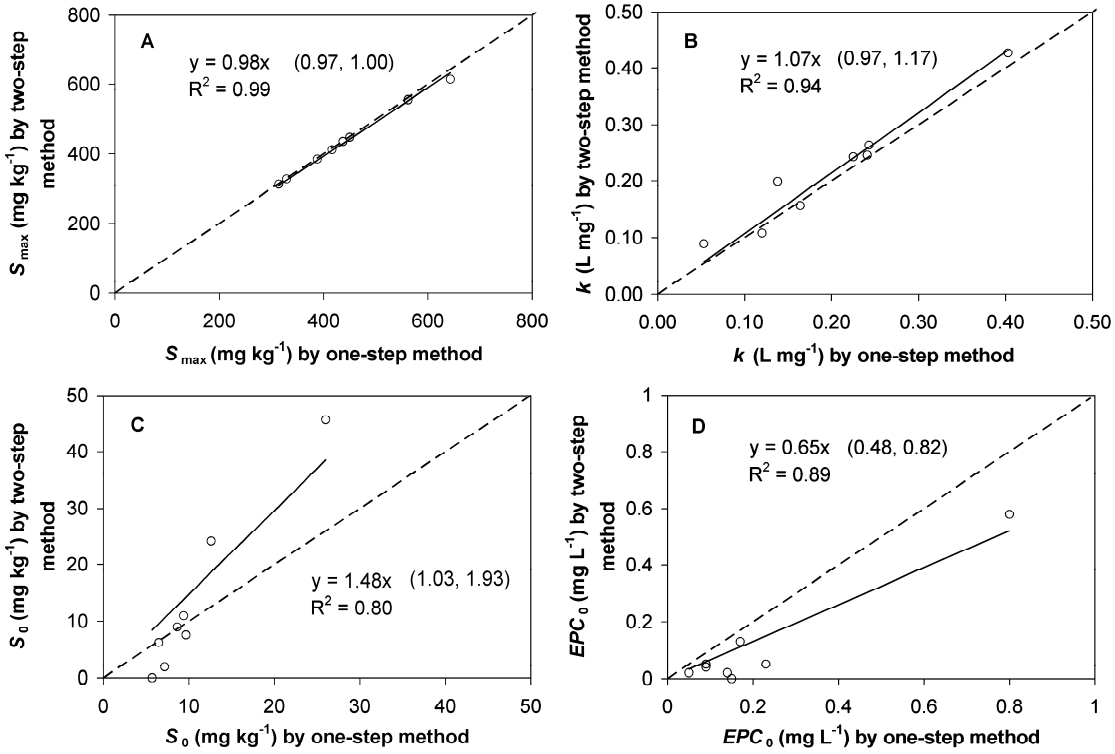

Figure 2.3. Comparison between sorption parameters estimated by the one-step method and the two-step method for subsurface soils: A. the P sorption maxima (S_{max}); B. the bonding energy constant (k); C. the sorbed legacy P (S_0); and D. the zero-sorption equilibrium concentration (EPC_0). The 95% confidence intervals of the slopes are shown in the parenthesis.

Overall, both the one-step method and the two-step method are acceptable to fit the Langmuir isotherms for P-enriched soils. The two methods work equally well for estimating the P sorption maxima (S_{max}) and the bonding energy constant (k). Although there was a large difference in the sorbed legacy (S_0) estimates for subsurface soils, it may be neglected considering the small magnitude of S_0 of the subsurface soils. Since the one-step method overestimated EPC_0, the two-step method could thus be a preferred method if the accurate estimation of EPC_0 is needed.

Conclusions

The accurate estimation of the sorbed legacy P (S_0) is important in a sorption study on P-enriched soils that heavily receive fertilizer, manure, farm wastewater, and sewage sludge. Ignoring S_0 may result in erroneous estimates of Langmuir sorption parameters, including the P sorption maxima (S_{max}), the bonding energy (k), and the zero-sorption equilibrium concentration (EPC_0), and consequent misevaluation of the potential of soil P loss to runoff or drainage. The two curve-fitting methods in the Langmuir models (i.e., the one-step method and the two-step method) have been used to estimate S_0. The one-step method differs with the two-step method in that it assumes the Langmuir isotherm at low concentrations, while the latter assumes a linear isotherm. These two methods were compared for their estimates of S_{max}, k, S_0, and EPC_0 on three soil series in New York. The S_{max} estimates by the two methods agreed well, and the results of k were close. The estimates of S_0 by the two methods had a good agreement for surface soils, but a poor agreement for subsurface soils, which may be neglected because of the small magnitude of S_0 of the subsurface soils. Although the one-step method yielded greater EPC_0 estimates, the EPC_0 estimates by the two methods had an excellent linear correlation for P-enriched soils. In conclusion, both methods are considered acceptable to fit the Langmuir isotherms for P-enriched soils.

Acknowledgement

This work was supported primarily by Conservation Innovation Grant (CIG) 48866/A001 from the US Department of Agriculture (USDA), Natural Resources Conservation Service (NRCS) and partly by a Mini-Grant from USDA-funded Agricultural Ecosystems Program (AEP) at Cornell University.

This is a non-final version of an article published in final form in Soil Sci. 174(10): 523–530. The published version can be accessed through the Soil Science's website at:

http://journals.lww.com/soilsci/Abstract/2009/10000/Evaluation_of_Two_Langmuir_Models_for_Phosphorus.1.aspx

APPENDIX

Here we present the derivation of the equations for the Freundlich one-step method. The traditional Freundlich model is shown in eq. 11. The apparent sorbed P (S') and the total sorbed P (S) are defined in eqs. 2 and 3. Combining eqs. 11, 2, and 3, we find the equation given by Barrow (2008) for P-enriched soils:

$$S' = \frac{(C_i - C)V}{M} = K_f C^n - S_0 \qquad \text{(A1)}$$

For soils in P-free initial solutions ($C_i = 0$), the aqueous equilibrium P concentration (C) is C_0. From eq. A1, we derive eq. 12:

$$S_0 = K_f C_0^n + \frac{C_0 V}{M} \qquad \text{(A2)}$$

Further, we substitute eq. A2 (or eq. 12) into eq. A1 and derive eq. 13:

$$S' = K_f C^n - (K_f C_0^n + \frac{C_0 V}{M}) \qquad \text{(A3)}$$

We then set $S' = 0$ (i.e., the P sorption and desorption are equal). From eq. A3 (or eq. 13), we find the zero-sorption equilibrium concentration (EPC_0) (i.e., eq. 14):

$$EPC_0 = \left(C_0^n + \frac{C_0 V}{M K_f} \right)^{1/n} \qquad \text{(A4)}$$

REFERENCES

Barkle, G.F., R. Stenger, P.L. Singleton, and D.J. Painter. 2000. Effect of regular irrigation with dairy farm effluent on soil organic matter and soil microbial biomass. *Aust. J. Soil Res.* 38(6): 1087–1097.

Barrow, N.J. 2008. The description of sorption curves. *Eur. J. Soil Sci.* 59: 900–910.

Bolster, C.H., and G.M. Hornberger. 2007. On the use of linearized Langmuir equations. *Soil Sci. Soc. Am. J.* 71(6): 1796–1806.

Bolster, C.H. 2008. Revisiting a statistical shortcoming when fitting the Langmuir model to sorption data. *J. Environ. Qual.* 37(5): 1986–1992.

Brock, E.H., Q.M. Ketterings, and P.J.A. Kleinman. 2007. Measuring and predicting the phosphorus sorption capacity of manure-amended soils. *Soil Sci.* 172(4): 266–278.

Cabrera, V.E., L.J. Stavast, T.T. Baker, M.K. Wood, D.S. Cram, R.P. Flynn, and A.L. Ulery. 2009. Soil and runoff response to dairy manure application on New Mexico rangeland. *Agric. Ecosyst. & Environ.* 131: 255–262.

Carpenter, S.R., N.F. Caraco, D.L. Correll, R.W. Howarth, A.N. Sharpley, and V.H. Smith. 1998. Nonpoint pollution of surface waters with phosphorus and nitrogen. *Ecol. Appl.* 8:559–568.

Czymmek, K.J., and Q.M. Ketterings. 2007. Removal of phosphorus by field crops. Agronomy Fact Sheet Series No. 28, Department of Crop and Soil Sciences, Cornell University, Ithaca, NY.

Correll, D.L. 1998. The role of phosphorus in the eutrophication of receiving waters: A review. *J. Environ. Qual.* 27: 261–266.

Essington, M.E. 2004. Soil and water chemistry: An integrative approach. CRC Press. Boca Raton, FL.

Gale, P.M., K.R. Reddy, and D.A. Graetz. 1994. Phosphorus retention by wetland soils used for treated wastewater disposal. *J. Environ. Qual.* 23: 370–377.

Graetz, D.A., and V.D. Nair. 2000. Phosphorus sorption isotherm determination. In Methods of phosphorus analysis for soils, sediments, residuals, and waters. G.M. Pierzynski (ed). Southern Cooperative Series Bulletin No. 396. Manhattan, KS.

Holford, I.C.R. 1979. Evaluation of soil phosphate buffering indices. *Aust. J. Soil Res.* 17: 495–504.

Kao, C.W., and R.W. Blanchar. 1973. Distribution and chemistry of phosphorus in an Albaqualf soil after 82 years of phosphate fertilization. *J. Environ. Qual.* 2(2): 237–240.

NRCS. 2004. Soil survey laboratory methods manual. Soil survey investigations report No. 42. Burt, R. (Ed). National Resources Conservation Service. Washington, DC.

NRCS. 2008. National cooperative soil survey: web soil survey 2.0. Natural Resources Conservation Service. Washington, DC. http://websoilsurvey.nrcs.usda.gov/ accessed on 2/18/2008.

Olsen, S.R., and F.S. Watanabe. 1957. A method to determine a phosphorus adsorption maximum of soils as measured by the Langmuir isotherm. *Soil Sci. Soc. Am. J.* 21: 144–149.

Pant, H.K. and K.R. Reddy. 2001. Phosphorus sorption characteristics of estuarine sediments under different redox conditions. *J. Environ. Qual.* 30: 1474–1480.

Reddy, K.R., G.A.O. Conner, and P.M. Gale. 1998. Phosphorus sorption capacities of wetland soils and stream sediments impacted by dairy effluent. *J. Environ. Qual.* 27: 438–447.

Sallade, Y.E., and J.T. Sims. 1997. Phosphorus transformations in the sediments of Delaware's agricultural drainageways: I. Phosphorus forms and sorption. *J. Environ. Qual.* 26: 1571–1579.

Sharpley A.N. 1995. Dependence of runoff phosphorus on extractable soil phosphorus. *J. Environ. Qual.* 24: 920–926.

Siddique, M.T. and J.S. Robinson. 2003. Phosphorus sorption and availability in soils amended with animal manures and sewage sludge. *J. Environ. Qual.* 32: 1114–1121.

Sims, J.T. and A. Wolf. 1995. Recommended Soil Testing Procedures for the Northeastern United States. Northeast Regional Bull. #493. Agricultural Experiment Station, University of Delaware, Newark, DE.

Sims, J.T., R.O. Maguire, A.B. Leytem, K.L. Gartley, and M.C. Pautler. 2002. Evaluation of Mehlich 3 as an Agri-environmental soil phosphorus test for the Mid-Atlantic United States of America. *Soil Sci. Soc. Am. J.* 66: 2016–2032.

Sparks, D.L. 2003. Environmental soil chemistry. Academic Press. San Diego, CA.

Sui, Y. and M.L. Thompson. 2000. Phosphorus sorption, desorption, and buffering capacity in a biosolids-amended mollisol. *Soil Sci. Soc. Am. J.* 64: 164–169.

USEPA. 1983. Phosphorus, all forms. Method 365.1 (Colorimetric, Automated, Ascorbic Acid). pp.365-1.1-365-1.7. In Methods for Chemical Analysis of Water and Wastes, EPA-600/ 4-79-020. US Environmental Protection Agency. Cincinnati, OH.

USEPA. 2007. Method 3051A: Microwave assisted acid digestion of sediments, sludges, soils, and oils. U.S. Environmental Protection Agency. Washington, DC.

Vadas, P.A. and J.T. Sims. 1999. Phosphorus sorption in manured Atlantic coastal plain soils under flooded and drained conditions. *J. Environ. Qual.* 28: 1870–1877.

Villapando, R.R. and D.A. Graetz. 2001. Phosphorus sorption and desorption properties of the spodic horizon from selected Florida spodosols. *Soil Sci. Soc. Am. J.* 65: 331–339.

Zhang, H., J.L. Schroder, J.K. Fuhrman, N.T. Basta, D.E. Storm, and M.E. Payton. 2005. Path and multiple regression analysis of phosphorus sorption capacity. *Soil Sci. Soc. Am. J.* 69: 96–106.

Zhou, A., H. Tang, and D. Wang. 2005. Phosphorus adsorption on natural sediments: Modeling and effects of pH and sediment composition. *Water Res.* 39:1245–1254.

CHAPTER 3

EFFECT OF SOIL REDUCTION ON PHOSPHORUS SORPTION OF AN ORGANIC-RICH SILT LOAM

Wei Zhang, Joshua W. Faulkner, Shree K. Giri, Larry D. Geohring,

Tammo S. Steenhuis

Abstract

Phosphorus (P) flux from agricultural landscapes to surface waters may cause eutrophication. In the northeastern U.S., P transport largely depends on P sorption of soils in variable source areas (VSAs) or in land treatment systems. Soil redox fluctuation commonly occurs in these areas. Nevertheless, the effect of soil redox on P sorption has been variable in the literature. This study investigated P sorption of an organic-rich northeastern glaciated silt loam (Langford) under air-dried, field-wet, and reduced conditions using batch P sorption experiments. Additionally, the influence of farm wastewater on soil P sorption was studied. Major results indicated that soil reduction increased the maximum amount of P that can be sorbed (S_{max}) and decreased the aqueous P concentration at which P sorption and desorption are equal (EPC_0), both determined from a modified Langmuir isotherm model. The slightly reduced field-wet soils had no significant difference for S_{max}, due to limited soil reduction. Using the diluted wastewater as the sorption solution matrices instead of 0.01 M KCl solution, the soils generally exhibited greater S_{max} and lower EPC_0 except for EPC_0 of reduced soil S2, implying more complex P sorption in the field. Identified P sorption mechanisms include phosphate precipitation, ligand exchange with organic matter, and adsorption onto Fe hydroxides. Transformation of Fe compounds during soil reduction is primarily responsible for the changes of soil P sorption.

Keywords: phosphorus, sorption, redox, vegetative treatment areas

Introduction

Agriculture in the United Sates significantly contributes to the phosphorus (P) loading of surface waters, and the P enrichment in recipient waters may cause eutrophication (Carpenter et al., 1998). Phosphorus transport in the agricultural landscapes of the northeastern U.S. largely depends on P sorption of soils in some areas that are periodically saturated during the year. A few areas are of particular interest, including variable source areas (VSAs) and land treatment systems (Gburek et al., 2002; Kim et al., 2006; Walter et al., 2000). While in most agricultural soils the moisture content is usually at field capacity or less, saturated conditions often occur in undulating landscapes containing glaciated soils with relatively permeable shallow top soil underlain by a dense slowly permeable fragipan (e.g. the northeastern U.S.). The areas that are prone to saturation are known as VSAs, since the extent of saturation varies with rainfall and other factors. Walter et al. (2000) estimated that VSAs could be 10% of total watershed area and generate 20% of total annual runoff in the New York City watershed. When these areas are located in agricultural fields, they often receive P input through manure spreading. Land treatment systems, including vegetative treatment areas (VTAs), also experience alternating wetting and drying cycles due to wastewater loading combined with direct rainfall. The VTAs are widely used to treat dairy farm wastewaters (i.e., milkhouse wastewater, barnyard runoff, and silage bunker runoff), which typically contain high P concentrations, with soluble reactive phosphorus (SRP) ranging from 16 to 55 mg L^{-1} (Kim et al., 2003, 2006; Schellinger and Clausen, 1992; Schwer and Clausen, 1989; Yang et al., 1980). When these areas are close to and hydrologically linked with field ditches or natural waterways, their P export becomes important.

Soil saturation fluctuation (i.e., water table changes) usually controls the changes of soil redox in the northeastern U.S. and elsewhere (Callebaut et al., 1982; Cogger et

al., 1992; Eshel and Banin, 2002; Pickering and Veneman, 1984). In the wetting period, soil saturation results in oxygen depletion and concurrent soil reduction mediated by microbial activity (Gotoh and Patrick, 1974; Hutchison and Hesterberg, 2004). In the drying period, the water table is lowered and the soils are re-oxidized. The changing soil redox corresponds with changes in soil mineralogy and chemistry, which in turn affects soil P retention (Sims and Pierzynski, 2005). Thus, the typical laboratory P sorption experiments carried out under aerobic conditions are not likely representative of environmental applications in VSAs and VTAs, where the alternating soil reduction and re-oxidation processes occur frequently. Obviously, the fate and transport of P in VSAs and VTAs demand further study on the P retention of soils under varying redox conditions. Such information pertaining to the northeastern soils is sparse.

A number of studies investigated P sorption of various soils under reduced conditions due to agronomic and environmental interests (Gale et al, 1994; Holford and Patrick, 1981; Khalid et al., 1977; Pant et al., 2002; Pant and Reddy, 2001; Patrick et al., 1973; Patrick and Khalid, 1974; Sah and Mikkelsen, 1986; Willett and Higgins, 1978; Vadas and Sims, 1998, 1999). Despite much research effort, varying results have been observed regarding the soil P sorption changes under reduced conditions compared to aerobic conditions. Some researchers reported that reduced soils released more soluble P (Ann et al., 2000; Khalid et al., 1977; Pant and Reddy, 2001; Patrick et al., 1973; Patrick and Khalid, 1974; Young and Ross, 2001). In contrast, Holford and Patrick (1981) observed lower P concentrations in the soil solution of a reduced rice soil; Vadas and Sims (1998, 1999) noticed that reduced poultry litter-amended soils released less soluble P. Elevated P release under reduced conditions is attributed mainly to: reductive dissolution of Fe phosphate (Patrick et al., 1973) or ferric hydroxide (Gotoh and Patrick, 1974; Holford and Patrick, 1981); competitive

adsorption by dissolved organic matter (DOM) (Bhatti et al., 1998; Guppy et al., 2005); and formation of aqueous ternary DOM-Fe-PO_4 or DOM-Al-PO_4 complexs (Hutchison and Hesterberg, 2004). While increased P sorption is due to the transformation of crystalline ferric hydroxide to amorphous ferrous or ferric hydroxide, resulting in more reactive surface sites (Holford and Patrick, 1981; Khalid et al., 1977; Patrick and Khalid, 1974; Vadas and Sims, 1999), lowered P sorption may result from the reductive dissolution of Fe compounds under conditions unsuitable for the re-precipitation of Fe hydroxides (e.g. low pH) (Vadas and Sims, 1999).

Given the importance of soil redox on soil P sorption, the frequent redox transition in VSAs and VTAs, the variable results in the past, and the sparse information on the northeastern soils, the objectives of this study were to investigate the effect of soil reduction on P sorption of a northeastern glaciated silt loam and further identify the plausible P sorption mechanisms. We selected an organic-rich silt loam located in a VTA for this study, and P sorption on air-dried, field-wet, and reduced soils (i.e., representing varying redox conditions or soil moisture regime) were compared to elucidate the effect of soil redox. The influence of farm wastewater on P sorption was also examined to provide more insight on P sorption in the field.

Materials and Methods

Soil Sampling and Analyses

Soil samples were collected from a VTA in Tompkins County, New York, in October, 2006. The VTA is a designated grass area and has been receiving farm silage bunker runoff by gravity flow since the spring of 2005. Field study indicated that the water table fluctuated and frequently reached the soil surface (Faulkner et al., 2010), while the soil water redox measured at the approximate 61 cm depth ranged from 40 to 420 mV during the year. The wastewater discharged to the VTA contained 300-2000

mg L^{-1} dissolved organic carbon (DOC), 18-115 mg L^{-1} ammonium-nitrogen, and 13-55 mg L^{-1} soluble reactive P (SRP). The annual P application rate was estimated to be 126 kg P ha^{-1}, much greater than the expected P removal rate of 28 kg P ha^{-1} by the grass vegetation (Czymmek and Ketterings, 2007). Thus, soil P sorption is an important process to retain P.

The soil is a Langford channery silt loam (fine-loamy, mixed, active, mesic Typic Fragiudepts) and has an extensive distribution in the glaciated Appalachian Plateau of central and southern New York and north-west Pennsylvania (NRCS, 2008). The Langford soil consists of a 55 cm-deep moderately well drained silt loam underlain by a slowly permeable silt loam restrictive layer (i.e., fragipan). Three surface soils (0-8 cm) and one subsurface soil (61-91 cm) in the VTA wastewater flow path were used in this study. The subsurface soil was located in the fragipan. The surface soils were denoted as S1, S2, and S4 and the subsurface soil as D2. The labeling convention refers to depth (S = surface and D = subsurface) and location (a greater number indicating a greater distance from wastewater source). The soil samples were air-dried, ground, and passed through a 2 mm sieve before use. Field-wet soil samples were also collected at location 2 and in a cornfield (abbreviated as C) adjacent to the VTA in November, 2007. The soils were labeled as S2N, D2N, SC, and DC. The field-wet soils were sealed in Ziploc® bags and stored in a refrigerator at 4 ºC after collection and used within 24 hours. Subsamples of the field-wet soils were also air-dried. Soil analyses were conducted on the air-dried soil samples by the Cornell Nutrient Analysis Laboratory, Cornell University, Ithaca, NY. Soil pH was measured in water using a 1:1 soil:water ratio (w/v). The soil organic matter (OM) was determined by loss on ignition. Total soil carbon (TC) and nitrogen (TN) were determined by a CN analyzer (NC 2100, CE Instruments, Hindley Green, Wigan, UK). Soil samples were extracted with sodium acetate solution (0.72 *N* NaOAc+0.52 *N*

CH_3COOH, Morgan extraction) and analyzed for P using the ascorbic acid method with a flow analyzer (ALPKEM RFA/2, OI Analytical, College Station, TX) and for cations (i.e., Ca, Fe, Al, and Mn) by inductively coupled plasma-atomic emission spectrometry (ICP-AES) (JY70 TYPEII, Jobin Yvon, Edison, NJ). The above soil analyses followed recommended procedures of NRCS (2004) and Sims and Wolf (1995). The nitric acid-digestion elements, including P, Ca, Fe, Al, and Mn, were determined by ICP-AES (SPECTRO-CIROS^{CCD}, SPECTRO Analytical Instruments Inc., Mahwah, NJ) after a microwave-assisted digestion with HNO_3 (USEPA, 2007). Particle size analysis was conducted on separate soil samples collected at the same locations in July, 2007, following the standard methods (NRCS, 2004). Selected physicochemical properties of the soils are shown in Table 3.1.

Table 3.1. Physicochemical properties of soils.

Soils		S1	S2	S4	D2	S2N	D2N	SC	DC
pH		7.47	7.65	6.69	7.75	7.10	7.60	7.30	6.80
OM (%) †		5.60	5.41	5.21	1.13	5.40	4.10	1.40	0.70
TN (%) †		0.35	0.36	0.33	0.09	0.41	0.09	0.24	0.05
TC (%) †		3.49	3.46	3.19	0.59	3.74	0.66	2.72	0.36
Morgan extractable elements (mg kg^{-1})	P	40.1	92.2	60.1	1.5	112	5.5	20.5	3.0
	Ca	3143	3079	2274	1411	2565	1320	2050	415
	Fe	13.1	5.7	3.3	4.0	8.5	14.0	2.0	5.5
	Al	19.3	12.8	9.8	18.3	10.0	17.0	17.5	38.5
	Mn	40.9	24.2	9.0	6.20	47.5	108	8.5	4.5
Nitric acid-digestion elements (mg kg^{-1})	P	1738	1783	1648	609	1306	393	719	256
	Ca	4968	4524	3743	2,338	3756	2403	2845	1708
	Fe	26617	24048	26994	27,267	13786	22637	15592	16020
	Al	37500	22361	21826	21950	12994	14248	12700	9696
	Mn	565	573	741	539	363	438	445	269
Particle size (% by weight) ‡	Sand	28.4	25.9	23.4	25.4	–	–	–	–
	Silt	53.7	57.7	55.8	54.7	–	–	–	–
	Clay	17.9	16.4	20.8	19.9	–	–	–	–
USDA Class.		silt loam	silt loam	silt loam	Silt loam	–	--	--	--

† OM = soil organic matter; TN = soil total nitrogen; TC = soil total carbon.
‡Analyses were conducted on separate soil samples collected at the same locations and depths in the summer of 2007.

Table 3.2. Batch P sorption isotherm experiments on soil samples conducted in duplicate.

Experiment	Objectives	Soil	Redox condition	Sorption solution matrices	Soil/water ratio (g/mL)
Set I	effect of soil reduction on P sorption	S1	air-dried	0.01 M KCl	1:20
			Reduced		
		S2	air-dried		
			Reduced		
		S4	air-dried		
			Reduced		
		D2	air-dried		
			Reduced		
		S2N	air-dried		1.4:20
			field-wet		
		D2N	air-dried		2.5:20
			field-wet		
		SC	air-dried		1.5:20
			field-wet		
		DC	air-dried		1.7:20
			field-wet		
Set II	effect of farm wastewater matrices on P sorption[†]	S2	air-dried	1/2 wastewater	1:20
			Reduced		
		D2	air-dried		
			Reduced		

[†] comparison was made with the experiments using 0.01 M KCl for the same soils.

Sorption Isotherm Experiments

Batch P sorption isotherm experiments were conducted in duplicate for soil samples under air-dried, field-wet, and reduced conditions, using either 0.01 M potassium chloride (KCl) solution (0.01 M KCl) or farm wastewater diluted to half in deionized water (1/2 wastewater) as sorption solution matrices. In a 24-hour P sorption experiment, the microbial P immobilization is likely to be minimal for air-dried and field-wet soils (Giesler et al., 2005). We conducted paired sorption experiments with and without biocide (0.02% sodium azide) in duplicate for soil S1 under air-dried conditions, and soil S1 and S2 under reduced conditions (i.e., the biocide was added after soils were reduced by anaerobic incubation as discussed later).

No significant difference in P sorption parameters existed between the two treatments (i.e., with or without biocide) for both air-dried and reduced soils as suggested by Student's t-tests (data not shown). Therefore, we did not inhibit microbial activity in further sorption experiments. Experiments are summarized in Table 3.2 and explained below in detail.

Experiment Set I: Effect of Soil Reduction

Experiment I-A: Air-dried Soils

One gram of an air-dried soil sample was placed in a series of 50 mL polypropylene centrifuge tubes and mixed with 20 mL 0.01 M KCl solution containing 0, 1, 5, 10, 50, 100, and 200 mg L^{-1} P as KH_2PO_4. The centrifuge tubes were shaken on a reciprocal shaker at a speed of 180 cycle min^{-1} for 24 hours at 25±3 ºC. Preliminary tests indicated that the 24-hour period was adequate to capture the major P sorption. The suspension was centrifuged. The pH and redox potential (Eh) were measured with a pH/mV/Ion meter (Accumet® AP61, Fisher Scientific). The Eh measurements were corrected using the standard hydrogen electrode as a reference by adding 200 mV. The supernatants were filtered through a 0.45 μm mixed cellulose ester membrane (Pall Life Sciences, Ann Arbor, MI). One drop of concentrated hydrochloric acid was added to the filtrates to preserve the samples, which were stored in the refrigerator at 4 ºC before analysis. The soluble reactive P (SRP) concentrations of the initial sorption solution and the supernatants of the sorption experiments were measured by a flow analyzer (Flowsystem-3000, OI Analytical, College Station, TX) using the ascorbic colorimetric method (USEPA, 1983). The difference between the initial SRP concentration and the supernatant SRP concentration is the P sorbed by soils.

Table 3.3. Chemical conditions of sorption experiments using 0.01 M KCl solution. *n* is the number of tests, the value in the parenthesis is one standard deviation, and the value in the bracket is the redox potential or pe+pH at the end of anaerobic incubation.

Soils		Eh[§] (mV)	pH	pe+pH[§]	Final equilibrium constituents of P-free initial solutions (mg L^{-1})			
					Ca	Fe	Mn	SRP[¶]
S1	air-dried (n = 4)[†]	372 (0)	7.06 (0.01)	13.3	44.4 (0.8)	0.29 (0.00)	0.01 (0.00)	0.88 (0.04)
	reduced (n = 4)	[60 (16)] 236 (34)	7.20 (0.12)	[8.21] 11.2	52.3 (4.2)	0.69 (0.12)	1.72 (0.04)	0.40 (0.11)
S2	air-dried (n = 2)	372 (0)	7.03 (0.01)	13.3	49.4 (1.3)	0.36 (0.01)	0.09 (0.04)	1.62 (0.08)
	reduced (n = 4)	[81 (21)] 180 (43)	7.23 (0.05)[†]	[8.59] 10.3	53.8 (5.7)	1.39 (1.07)	1.76 (0.39)	1.06 (0.37)[‡]
S4	air-dried (n = 2)	389 (6)	6.46 (0.02)	13.9	43.9 (4.9)	0.48 (0.16)	0.07 (0.00)	1.97 (0.02)
	reduced (n = 2)	[61 (0)] 260 (15)	7.04 (0.02)	[8.07] 11.4	43.0 (0.4)	0.54 (0.05)	3.52 (0.02)	0.24 (0.02)
D2	air-dried (n = 2)	443 (3)	6.84 (0.25)	13.3	39.6 (0.7)	0.14 (0.02)	0.20 (0.01)	0.08 (0.01)
	reduced (n = 2)	[108 (18)] 246 (8)	7.15 (0.02)	[8.96] 11.3	39.5 (0.7)	0.00 (0.00)	1.19 (1.68)	0.08 (0.00)
S2N	air-dried (n = 2)	382 (4)	6.70 (0.01)	13.1	47.7 (0.7)	0.08 (0.01)	0.03 (0.00)	1.55 (0.05)
	field-wet (n = 2)	323 (6)	7.05 (0.02)	12.5	32.9 (1.3)	0.18 (0.03)	0.03 (0.00)	0.62 (0.07)
D2N	air-dried (n = 2)	379 (0)	6.64 (0.00)	13.0	71.7 (3.2)	0.06 (0.01)	0.02 (0.00)	0.10 (0.01)
	field-wet (n = 2)	346 (8)	6.95 (0.01)	12.8	70.0 (8.4)	0.04 (0.02)	0.03 (0.01)	0.03 (0.00)
SC	air-dried (n = 2)	369 (1)	6.65 (0.04)	12.9	47.8 (1.4)	0.05 (0.03)	0.00 (0.00)	0.20 (0.02)
	field-wet (n = 2)	352 (4)	6.99 (0.06)	12.9	40.3 (5.1)	0.37 (0.45)	0.00 (0.00)	0.19 (0.01)
DC	air-dried (n = 2)	377 (1)	6.58 (0.05)	12.9	20.8 (0.0)	0.36 (0.21)	0.00 (0.00)	0.05 (0.01)
	field-wet (n = 2)	360 (4)	6.75 (0.03)	12.8	18.6 (1)	0.01 (0.01)	0.00 (0.00)	0.02 (0.01)

[†] the measurements were conducted for 2 tests.
[‡] the results with the elimination of one outlier.
[§] Eh = redox potential, and pe = Eh/59.2.
[¶] SRP = soluble reactive P.

Experiment I-B: Field-wet Soils

The sorption experiments for field-wet soils followed the same procedures as that of the air-dried soils previously described, except a different soil:water ratio was used. Based on recorded wet soil mass, the amount of dry soil mass used in the experiments and the soil:water ratios were calculated after the measurement of soil moisture content by the gravimetrical method. Soil moisture content by weight was measured in triplicates and was 0.52 for S2N, 0.22 for D2N, 0.36 for SC, and 0.17 for DC. The soil:water ratio was then calculated to be 1.4:20 for S2N, 2.5:20 for D2N, 1.5:20 for SC, and 1.7:20 for DC. To compare the P sorption between the field-wet soils and the air-dried soils, the sorption isotherm experiments were also conducted for the air-dried subsamples of S2N, D2N, SC, and DC using the soil:water ratio calculated above. The Eh measurement indicated that the field-wet soils appeared to be only slightly reduced relative to the air-dried soils (Table 3.3).

Experiment I-C: Reduced Soils

The sorption isotherm experiments for reduced soils generally followed the same procedures of shaking, separation, and analyses as the previously described experiments, but differed in the method of P addition to the soil suspensions. The P was added after the soils reached reduced conditions. One gram of each air-dried soil was mixed with 20, 19.98, 19.9, 19.8, 19, 18, and 16 mL 0.01 M KCl solution in 40 mL borosilicate glass vials, sealed by polypropylene caps with a PTFE resin/silicone septa, and purged with high-purity nitrogen gas (99.999%) at 20 kPa for 2 minutes. The pressure was selected to produce adequate agitation in the soil suspension without over-pressurizing the vials. Preliminary soil incubation experiments suggested that if placed in the ambient environment, the soils could not be reduced to a greater degree, probably due to oxygen diffusion into the incubation vials. Thus, the incubation vials were kept in an anaerobic chamber (COY Laboratory Products INC, Grass Lake,

Michigan) for 21 days at room temperature. At the end of incubation, 0, 0.02, 0.1, 0.2, 1, 2, and 4 mL of 1000 mg L^{-1} P in 0.01 M KCl solution were added into the respective vials to produce the same P concentration series as described before. Next, the vials were moved out of the chamber and subjected to the sorption procedures. The redox potential (Eh) measurements confirmed that the soils were reduced after the incubation (Table 3.3, Essington, 2004). The Eh increased at the end of sorption experiments probably due to oxygen diffusion into the vials during the shaking, but was still much lower compared to the Eh of the air-dried and field-wet soils.

Experiment Set II: Effect of Farm Wastewater

Soil S2 and D2 were also tested using diluted farm wastewater. Dairy farm wastewater (silage bunker runoff) was collected during a rainfall event in November, 2007. The wastewater was filtered through Whatman #1 filter paper and kept in the refrigerator at 4 ºC for later use. The procedures of sorption experiments for the air-dried and reduced soils were the same as previously described except the sorption solution matrices were different. Instead of using 0.01 M KCl solution, 10 mL actual wastewater was mixed with deionized water (1/2 wastewater) and used for soil reduction incubation of S2 and D2. The redox potential of soil solutions was 47 ± 42 mV for soil S2 and 17 ± 10 mV for soil D2 at the end of anaerobic incubation. At the end of sorption experiments, the redox potential increased to 151 ± 9 mV for soil S2 and 166 ± 1 mV for soil D2, while the pH was 7.18 ± 0.04 for soil S2 and 7.14 ± 0.06 for soil D2. Additionally, 10 mL aged wastewater was mixed with deionized water and used for air-dried S2 and D2. Before being used in the air-dried soil experiments, the wastewater was kept in the refrigerator at 4 ºC for 27 days, a period similar to the anaerobic incubation duration, to allow for the wastewater aging. The increased turbidity and decreased organic carbon content in the aged wastewater suggested the

likelihood of microbial organic decomposition. The chemical composition of newly collected wastewater and aged wastewater is shown in Table 3.4.

Table 3.4. Selected chemical composition of farm wastewater.

	Dissolved chemical constituents (mg L^{-1})				
	SRP†	Ca	Fe	Mn	DOC†
Newly collected wastewater	7.70	486	0.51	0.81	580
Aged wastewater	0.21	485	0.48	0.78	215

† SRP = soluble reactive P and DOC = dissolved organic carbon.

Post-sorption Examination

The final sorption solutions with zero initial P concentration in the sorption experiments using 0.01 M KCl were analyzed for soluble Ca, Fe, and Mn with the ICP-AES. For some selected experiments, additional analyses were conducted for the entire series of the final solutions to determine soluble Ca, Fe, Mn, and dissolved organic carbon (DOC). DOC was determined by a TOC analyzer (Model 1010, OI Analytical, College Station, TX).

Fitting of Sorption Data

A modified Langmuir model was used to characterize the P sorption of the VTA soils (Zhou et al., 2005; Zhang et al., 2008). The model equations are listed below; the derivations of the equations are given by Zhou et al. (2005).

$$S' = \frac{(C_i - C)V}{M} \qquad (1)$$

$$S' = \frac{S_{\max} kC}{1 + kC} - \left(\frac{S_{\max} kC_0}{1 + kC_0} + \frac{C_0 V}{M}\right) \qquad (2)$$

$$S_0 = \frac{S_{\max} kC_0}{1 + kC_0} + \frac{C_0 V}{M} \qquad (3)$$

$$EPC_0 = \frac{S_0}{k(S_{\max} - S_0)} = \frac{S_{\max} kC_0 / (1 + kC_0) + C_0 V / M}{S_{\max} k / (1 + kC_0) - kC_0 V / M} \qquad (4)$$

where S' (mg kg^{-1}) = the amount of P sorbed by the soil from the solution (i.e., apparent P sorption); C_i (mg L^{-1}) = the initial P concentration in the solution; C (mg L^{-1}) = the final equilibrium concentration in the solution; V (mL) = the volume of

solution; M (g) = the mass of soil sample; S_{max} (mg kg^{-1}) = the P sorption maxima; k (L mg^{-1}) = the bonding energy constant; C_0 (mg L^{-1}) = the final equilibrium concentration for the P-free initial solution (i.e., $C_i = 0$); S_0 (mg kg^{-1}) = the labile pool of soil P from the historical P applications that readily participate the P exchange between the solid and liquid phases (i.e., the sorbed legacy P); EPC_0 (mg L^{-1}) = the zero-sorption equilibrium concentration at which the amount of P sorbed and desorbed are equal (i.e., $S' = 0$).

Sorption isotherms (S' vs C) were fitted to the modified Langmuir model (Eq. 2) by the trust-region nonlinear least square regression algorithm in the Matlab (The MathWorks, Inc., Natick, MA) to estimate S_{max} and k. The C_0 was either measured for the experiments in 0.01 M KCl (Experiment Set I) or fitted as a variable for the experiments in 1/2 wastewater (Experiment Set II). After S_{max} and k were estimated, S_0 and EPC_0 were determined from Eq. 3 and 4, respectively.

Statistical Analyses

Statistical comparisons of treatments were conducted for estimated sorption parameters, including S_{max}, k, EPC_0, and S_0 for air-dried, field-wet, and reduced soils, and the effect of the wastewater on P sorption. Comparisons were performed using Student's t-test for two samples, assuming unequal variance, in Excel 2003 (Microsoft, Redmond, WA).

Results and Discussion

All sorption data fitted the modified Langmuir model well with a coefficient of determination (r^2) greater than 0.91 (data not shown). First, estimated sorption parameters are compared for the effect of soil reduction (Experiment Set I) and farm wastewater matrices (Experiment Set II) on soil P sorption. Then, the sorption mechanisms are discussed in detail by examining the sorption solution chemistry.

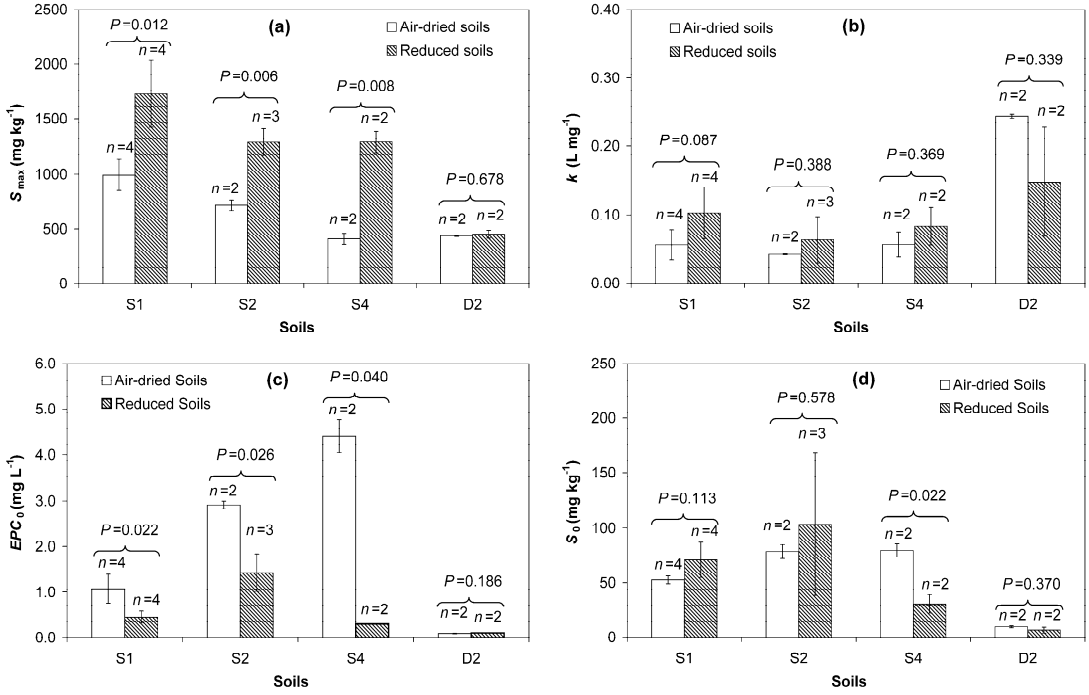

Figure 3.1. Comparison of estimated sorption parameters between the air-dried and reduced soils: (a) the P sorption maxima (S_{max}) comparison; (b) the bonding energy constant (k) comparison; (c) the zero-sorption equilibrium concentration (EPC_0) comparison; (d) the sorbed legacy P (S_0) comparison. Error bars represent standard deviations. Sample size (n) and P-value (two-tail) are listed above the columns.

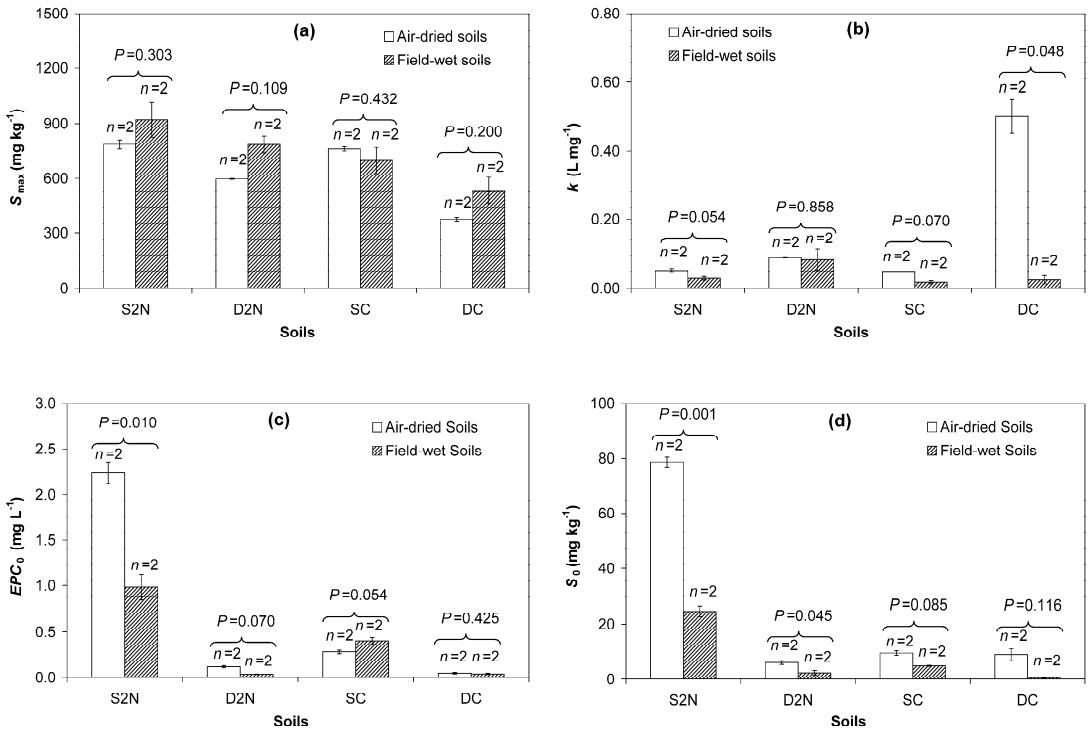

Figure 3.2. Comparison of estimated sorption parameters between the air-dried and field-wet soils: (a) the P sorption maxima (S_{max}) comparison; (b) the bonding energy constant (k) comparison; (c) the zero-sorption equilibrium concentration (EPC_0) comparison; (d) the sorbed legacy P (S_0) comparison. Error bars represent standard deviation. Sample size (n) and P-value (two-tail) are listed above the columns.

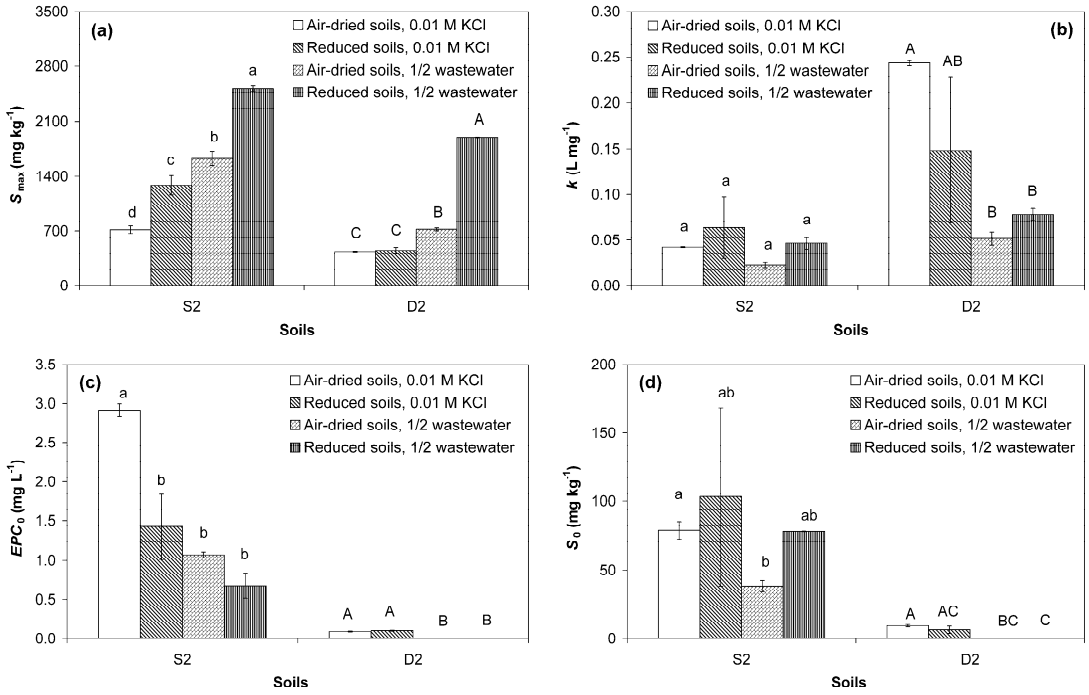

Figure 3.3. Effect of wastewater sorption matrices on P sorption of the air-dried and reduced soils (S2 and D2): (a) the P sorption maxima (S_{max}) comparison; (b) the bonding energy constant (k) comparison; (c) the zero-sorption equilibrium concentration (EPC_0) comparison; (d) the sorbed legacy P (S_0) comparison. Error bars represent standard deviations. Difference in means at the 0.05 significance level (two-tail) is indicated by different lowercase letters for S2 and uppercase letters for D2 (No cross-comparison between S2 and D2).

Experiment Set I: Effect of Soil Reduction

The estimated sorption parameters for air-dried and reduced soils are compared in Figure 3.1 (Experiment Set I-A and C). Compared to the air-dried condition, the surface soil S1, S2, and S4 exhibited significantly greater sorption maxima (S_{max}) and lower zero-sorption equilibrium concentrations (EPC_0) under reduced conditions at the 0.05 significance level, while the subsurface soil D2 did not show any significant difference for both S_{max} and EPC_0 (Figure 3.1a and c). The lack of significant change in the P sorption of the soil D2 upon soil reduction may be because the soil had less nutrients for microbial consumption during soil incubation, which resulted in smaller changes in soil chemistry mediated by microbial activity. Compared to the surface soils (S1, S2, and S4), the subsurface soil D2 had lower content of organic matter (OM) by a factor of 5, total nitrogen (TN) by a factor of 3, and total carbon (TC) by a factor of 6 (Table 3.1). In addition, there were no consistently significant differences in the bonding energy constants (k) and the sorbed legacy P (S_0) between these two treatments (Figure 3.1b and d). One may find it surprising that EPC_0 decreased for soil S1 and S2 under reduced conditions, while S_0 did not show a similar trend. Possible explanations are that either the large variation of S_0 for reduced soil S1 and S2 may unfortunately exclude any discernable trend, or from Eq. 4, EPC_0 is inversely proportional to S_{max} and k so that the change of S_{max} and k may be adequate to lower EPC_0.

The estimated sorption parameters for field-wet and air-dried soils are shown in Figure 3.2 (Experiment Set I-B). The S_{max} was not significantly different for these two treatments ($P > 0.109$, Figure 3.2a). Similar to the previous comparison, the surface soil S2N had a significantly lower EPC_0 under field-wet conditions ($P = 0.010$, Figure 3.2c), while the subsurface soil D2N did not. The bonding energy constants (k) were not significantly different between the air-dried and field-wet soil S2N, D2N, and SC

at the 0.05 significance level except for the soil DC (Figure 3.2b). For the sorbed legacy P (S_0), the air-dried soil S2N and D2N showed greater values ($P < 0.045$, Figure 3.2d). The insignificant difference for the cornfield surface soil (SC) in EPC_0 and S_0 may be because of its lower OM, Morgan extractable P, Fe, and Mn. The lack of significant differences in S_{max} may be because the field-wet soils were only slightly reduced (Table 3.3).

The above results indicate that soil reduction altered the soil P sorption more consistently by increasing S_{max} and decreasing EPC_0, compared to the changes of k and S_0. Previous studies have already shown the effect of soil reduction on P sorption is variable, likely stemming from varied soil properties and experimental conditions (Ann et al., 2000; Holford and Patrick, 1981, Khalid et al., 1977; Pant and Reddy, 2001; Patrick et al., 1973; Patrick and Khalid, 1974; Vadas and Sims, 1998, 1999; Young and Ross, 2001). This study further demonstrated that the effect is highly site-specific.

Experiment Set II: Effect of Farm Wastewater

While the study using 0.01 M KCl sorption solution provides some insight on the effect of soil reduction (or soil saturation) on P sorption, the field runoff or farm wastewater has a far more complex chemical composition than the electrolyte solution. The effect of the organic-rich wastewater on P sorption of air-dried and reduced soils was examined and results are displayed in Figure 3.3.

Using 1/2 wastewater generally resulted in greater S_{max} and lower EPC_0 than using 0.01 M KCl (Figure 3.3a and c), except for EPC_0 of reduced soil S2 ($P = 0.066$). No consistent effect was observed for k and S_0 (Figure 3.3b and d), although the usage of diluted wastewater appeared to have a greater effect on air-dried soils. For instance, the air-dried D2 had lower k and S_0, and the air-dried S2 had lower S_0 in 1/2 wastewater, while the reduced soils did not show any significant difference. In

addition, when using 1/2 wastewater, a significant difference was noted for S_{max} between air-dried conditions and reduced conditions, but not for k, EPC_0, and S_0 (Figure 3.3).

Sorption Mechanisms

Ligand Exchange of Phosphate with Organic Matter

The DOC concentrations in the final solutions of the sorption experiments using 0.01 M KCl increased with increasing apparent P sorption (S') calculated from Eq. 1 (Figure 3.4a, open symbols). Good linear trends were obtained for the air-dried soils with r^2 values greater than 0.92 (Figure 3.4a). The linearity of ascending trends for the reduced soils was weaker, and there were greater variations in the DOC concentrations (Figure 3.4a, trends with filled diamond and triangle). Similar ascending trends were observed by Giesler et al. (2005) and attributed to the competition of phosphate with soil OM occupying the sorption sites. Other studies have also shown that phosphate can displace soil OM (Beck et al., 1999; Bhatti et al., 1998; Kaiser and Zech, 1997). Thus, ligand exchange of phosphate with soil OM may play a role on soil P sorption in 0.01 M KCl solutions. However, for the sorption experiments using 1/2 wastewater, there were not similar increasing linear trends. Rather, the DOC concentrations remained relatively constant with increasing S' (Figure 3.4b). We believe that in the wastewater matrices the ligand exchange process was suppressed because OM is more prone to partition onto soil surface due to a DOC concentration gradient.

Phosphate Precipitation

The relevant cations (Ca, Fe, and Mn) concentrations in the final sorption solutions for selected experiments reveal other plausible sorption mechanisms. The Ca concentrations generally dropped with increasing S' for both air-dried and reduced soils (Figure 3.5). The same pattern was also observed for the experiments using other

soils (S2N, and D2N, data not shown). Since most soils have a cation exchange preference of K^+ over Ca^{2+} (Sparks, 2003), including a Loring silt loam (Oxyaquic Fragiudalf) (Essington, 2004), it is plausible that the Ca concentration decreases were a result of Ca phosphate precipitation, but not the cation exchange. This hypothesis is supported by other studies (Lindsay, 1979; Sims and Pierzynski, 2005; Ugurlu and Salman, 1998). Following the procedure of Lindsay (1979), the solubility diagram for Ca phosphates, variscite ($AlPO_4 \cdot 2H_2O$), and strengite ($FePO_4 \cdot 2H_2O$) is shown in Figure 3.6. For the P concentrations (1-200 mg L^{-1} or Log P = -2.2~4.2) and a typical pH range of 6 to 7.5 (rectangular shaded area in Figure 3.6), P is mainly supersaturated with Ca phosphates. When pH is lower than 6.7, P may also be supersaturated with variscite and strengite. This mineral equilibrium calculation provides further evidence of Ca phosphate precipitation in these experiments. Thus, the Ca phosphate precipitation could explain the increased soil P sorption when using 1/2 wastewater (Figure 3.3), since the Ca concentration decrease was much greater in 1/2 wastewater than in 0.01 M KCl due to the high Ca concentrations of diluted wastewater (Table 3.4 and Figure 3.5). Assuming a 1:1 Ca:P molar ratio in Ca phosphate formations, an approximate calculation based on the decreased Ca concentration and the apparent P sorption (S') at the highest initial concentration (200 mg L^{-1} P) indicated that Ca phosphate precipitation contributed 19 ± 3% of the P sorption when using 0.01 M KCl and 68 ± 19% of it when using 1/2 wastewater. The greater contribution of Ca phosphate precipitation in the experiments of 1/2 wastewater was also indicated by the greater regression slopes in Figure 3.5b.

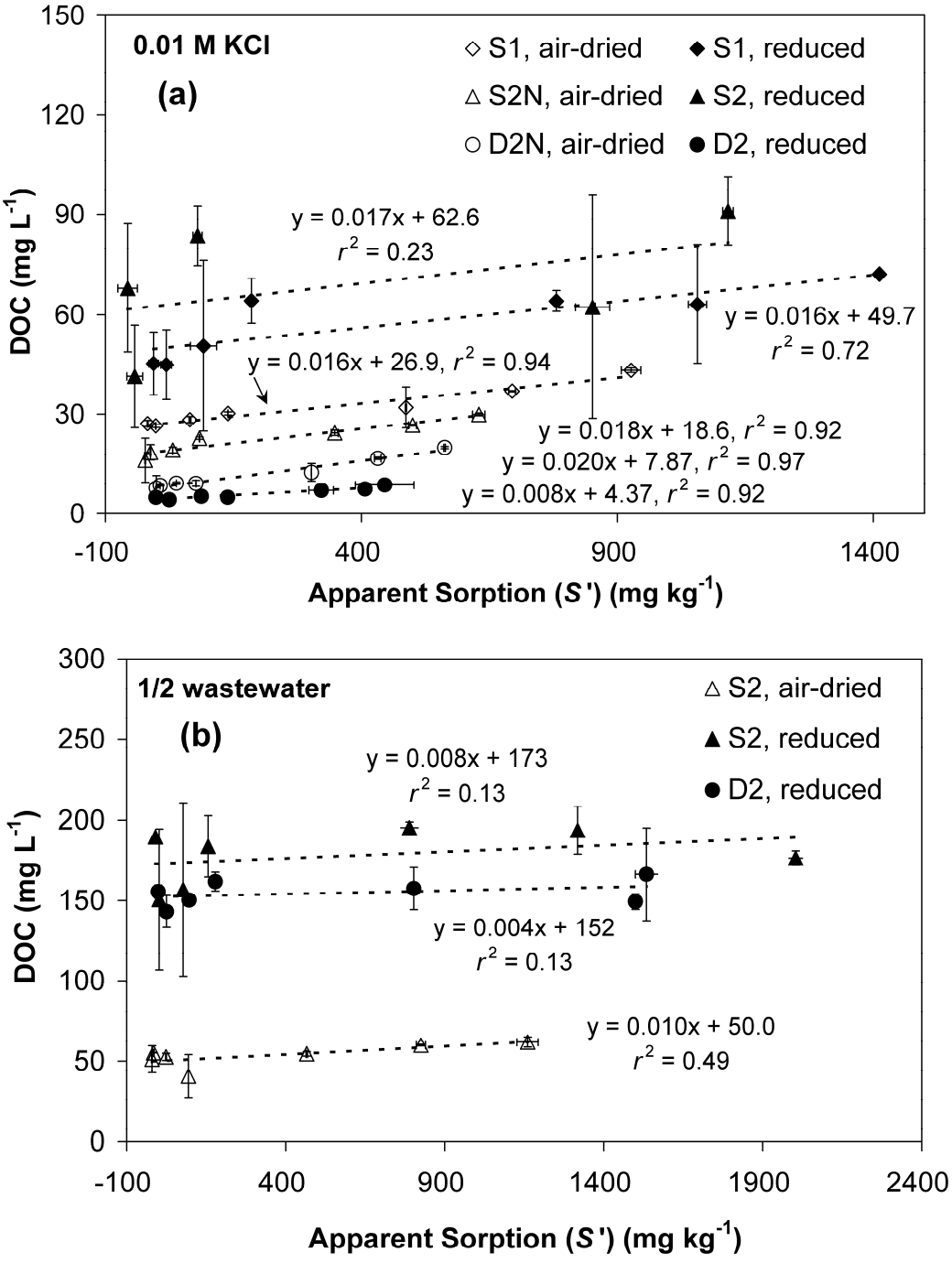

Figure 3.4. Dissolved organic carbon (DOC) concentrations in the final sorption solutions for air-dried or reduced soils in (a) 0.01 M KCl and (b) 1/2 wastewater. Error bars represent standard deviations of two tests.

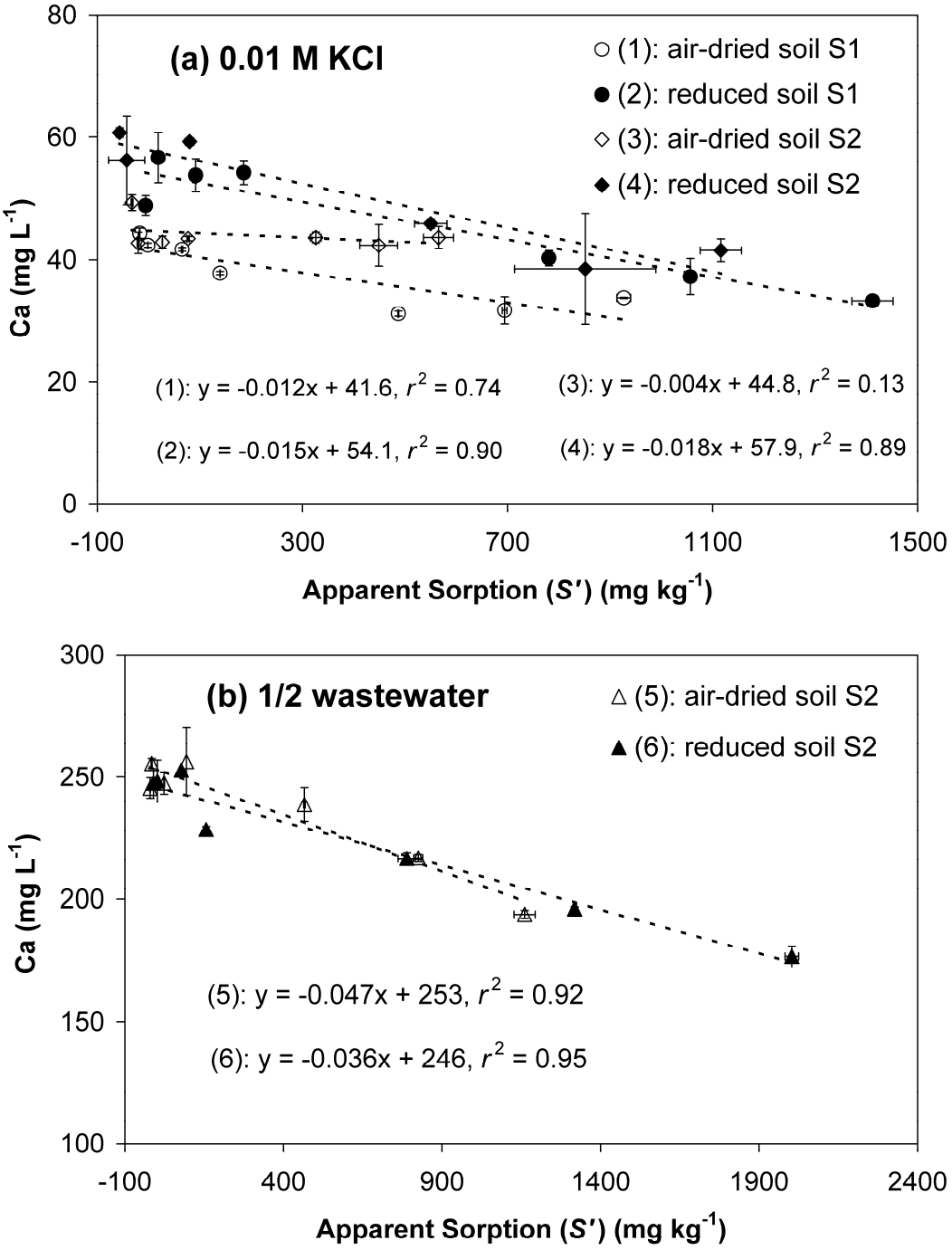

Figure 3.5. Dissolved Ca concentrations in the final sorption solutions for air-dried or reduced soils in (a) 0.01 M KCl and (b) 1/2 wastewater. Error bars represent standard deviations of two tests.

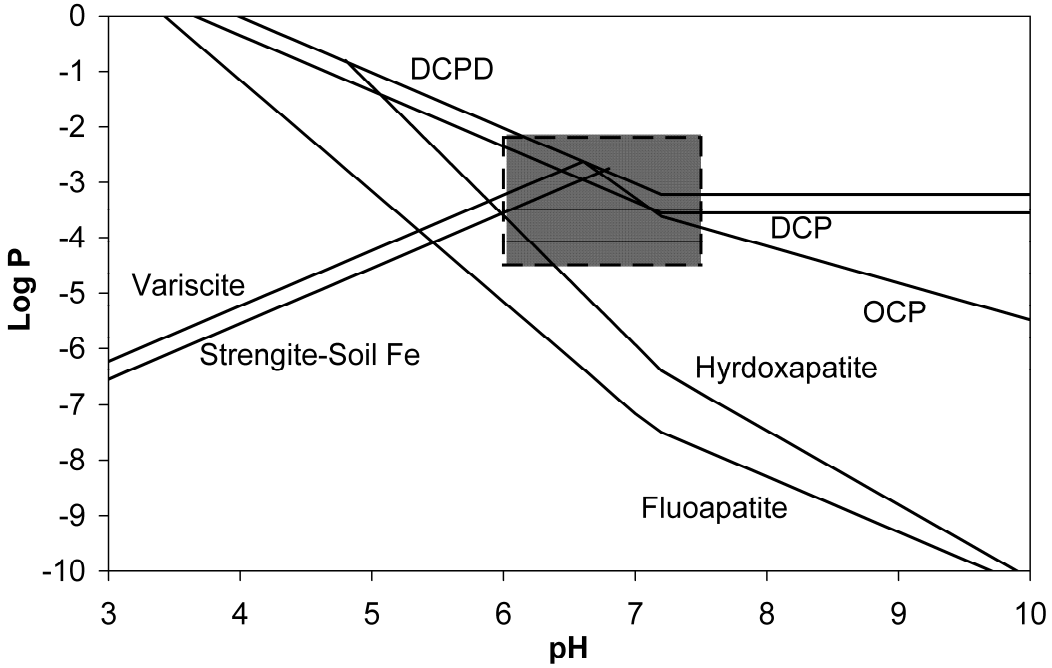

Figure 3.6. Solubility diagram of Ca phosphates compared to strengite and variscite (Ca^{2+} = 0.00045 M for pH < 8.35 and its activity is controlled by calcite for pH ≥ 8.35). The shadow area indicates the range of sorption solutions studied (pH = 6-7.5 and SRP = 1-200 mg L^{-1}). DCPD = brushite, dicalcium phosphate dihydrate, $CaHPO_4 \cdot 2H_2O$; DCP = monetite, dicalcium phosphate, $CaHPO_4$; OCP = octacalcium phosphate, $Ca_4H(PO_4)_3 \cdot 2.5H_2O$.

The Fe and Mn solution concentrations were generally greater for reduced soils than air-dried soils (Table 3.3), due to reductive dissolution of Fe and Mn minerals. While Fe and Mn phosphate precipitations could have occurred, their contribution to P sorption was minimal (less than 2%) due to their low solution concentrations in this study (data not shown). Particularly, vivianite ($Fe_3(PO_4)_2 \cdot 8H_2O$) formation may not be important herein, because vivianite forms below the pe+pH value of 8.34 (Lindsay, 1979) and the pe+pH values at the end of P sorption experiments were from 10.3 to 11.4.

Phosphate Adsorption into Fe Hydroxides

Ferric or ferrous hydroxides are highly relevant to soil P sorption (Lijklema, 1980; Patrick and Khalid, 1974). Analysis of X-ray diffraction data indeed indicated that Fe hydroxides ($Fe(OH)_2$ or $Fe(OH)_3$) was one of major mineral phases in these soils (data not shown). In this study, the pe+pH values of the reduced soils at the end of anaerobic incubation were from 8.07 to 8.96 (Table 3.3), well below 11.5, the value at which structured soil $Fe(OH)_3$ (soil-Fe) is reductively dissolved (Lindsay, 1979). Our preliminary soil reduction incubation experiments also showed that dissolved ferrous Fe was the major species of total soluble Fe in the solutions of the surface soil S1 (86 ± 1%). At the end of the sorption experiments, the pe+pH values were elevated to approximately 11 (Table 3.3). During this re-oxidation process, an amorphous mixture of hydrated ferric or ferrous hydroxide hydroxides would likely be freshly precipitated (Holford and Patrick, 1981; Khalid et al., 1977; Lindsay, 1979; Patrick and Khalid, 1974). The newly formed amorphous ferrous or ferric hydroxides have much greater reactive surface areas than the crystalline Fe oxides or hydroxides, and would result in a greater P sorption (Khalid et al., 1977; Holford and Patrick, 1981; Patrick and Khalid, 1974; Vadas and Sims, 1999; Young and Ross, 2001). Thus, the increased P sorption for reduced soils was mainly caused by the Fe transformation,

while increased DOC and Ca concentrations under reduced conditions may not be the major causes indicated by the negligible difference of regression slopes between air-dried and reduced soils in Figure 3.4 and 3.5. Indeed, Ca phosphate precipitation contributed approximately 23 ± 6% of increased P sorption under reduced conditions. Contribution from ligand exchange of soil OM and phosphate cannot be evaluated due to unknown molecular structure of soil OM. Nonetheless, the more important role of soil OM during its anaerobic decomposition may be related to enhanced soil reduction and amorphous soil Fe formations (Sah and Mikkelsen, 1986).

Additionally, it is unclear if the increased P sorption capacity of reduced soils is solely related to the combination of soil reduction and subsequent re-oxidation. In any case, soil reduction indeed invokes the mechanisms that increase the P sorption of the organic-rich silt loam used in this study. In fact, the re-oxidation following soil reduction is highly relevant to field phenomena, particularly in VTAs and VSAs, where soil saturation commonly reaches the soil surface. The reduced soils in the shallow soil depth may be re-oxidized through air re-entry when soil moisture decreases. Thus, the soil P sorption sites could be increased through this mechanism, which agrees with the concept of soil P sorption site regeneration previously suggested in the literature (Hill and Sawhney, 1981; Sawhney and Hill, 1975). In a rainfall event that generates surface and subsurface runoff in VSAs and VTAs, inevitable P flush out of soils will occur when these areas are nearby streams or field ditches. Thus, improved knowledge of the above mechanism is particularly important to managing agricultural land for treating farm wastes in terms of slowing the soil P saturation or decreasing the available P to the event-flush. Nevertheless, caution is needed when relating this mechanism to the land applications of farm wastes. We believe that this mechanism can only provide temporary P retention, as any retention mechanism may do. Continuously loading soils with manure and farm wastewaters increases the labile

pool of the soil P (i.e., the sorbed legacy P), and rapid P release will occur if a threshold of the ratio of the labile P to the P sorption maxima is exceeded (Maguire and Sims, 2002; Sharpley, 1995; Sims et al., 2002).

Conclusions

Soils in variable source areas (VSAs) and land treatment systems (e.g. vegetative treatment areas (VTAs)) in the northeastern U.S. generally experience an alternating saturated and unsaturated moisture regime (or redox conditions). The redox change invoked by the fluctuating soil moisture likely affects the soil P sorption under these conditions. This study compared the P sorption of an organic-rich northeastern glaciated silt loam under air-dried, field-wet, and reduced conditions. The results indicated that reduced conditions changed the soil P sorption significantly by increasing P sorption maxima (S_{max}) and decreasing zero-sorption equilibrium concentration (EPC_0), relative to the air-dried soils, implying an elevated P sorption capacity. The slightly reduced field-wet soils had no significant difference for S_{max}, because of limited soil reduction. Compared to using an electrolyte solution (0.01 M KCl), using diluted wastewater as the sorption solutions significantly increased S_{max} and decreased EPC_0 (except for EPC_0 of reduced S2), as a result of high Ca concentrations in the wastewater. The P sorption mechanisms are identified as phosphate precipitation, ligand exchange with organic matter, and adsorption onto Fe hydroxides. The transformation of Fe compounds and the associated changes in P sorption onto Fe hydroxides were identified as performing a pivotal role in the effect of soil reduction on P sorption. Therefore, to better understand P transport through the landscapes, more attention should be paid to local hydrology and the effect of soil moisture change (i.e., redox fluctuation) on soil P retention, which may depend on the soil type, the degree of soil reduction, and the property of the land-applied farm wastes.

Acknowledgements

This work was supported primarily by Conservation Innovation Grants (CIG) 48866/A001 from the US Department of Agriculture (USDA), Natural Resources Conservation Service (NRCS) and partly by a Mini-Grant from USDA-funded Agricultural Ecosystems Program (AEP) at Cornell University and other NRCS-USDA grants.

This is a non-final version of an article published in final form in Soil Sci. Soc. Am. J. 74(1): 240–249. The published version can be accessed through the internet at: http://soil.scijournals.org/cgi/content/abstract/74/1/240.

REFERENCES

Ann, Y., K.R. Reddy, and J.J. Delfino. 2000. Influence of redox potential on phosphorus solubility in chemically amended wetland organic soils. *Ecol. Eng.* 14: 169–180.

Beck, M.A., W.P. Robarge, and S.W. Buol. 1999. Phosphorus retention and release of anions and organic C by two Andisols. *Eur. J. Soil Sci.* 50: 157–164.

Bhatti, J.S., N.B. Comerford, and C.T. Johnston. 1998. Influence of oxalate and soil organic matter on sorption and desorption of phosphate onto a spodic horizon. *Soil Sci. Soc. Am. J.* 62: 1089–1095.

Callebaut, F., D. Gabriels, W. Minjauw, and M. de Boodt. 1982. Redox potential, oxygen diffusion rate, and soil gas composition in relation to water table level in two soils. *Soil Sci.* 134(3): 149–156.

Carpenter, S.R., N.F. Caraco, D.L. Correll, R.W. Howarth, A.N. Sharpley, and V.H. Smith. 1998. Nonpoint pollution of surface waters with phosphorus and nitrogen. *Ecol. Appl.* 8: 559–568.

Cogger, C.G., and P.E. Kennedy. 1992. Seasonally saturated soils in the Puget Lowland I. Saturation, reduction, and color patterns. *Soil Sci.* 153(6): 421–433.

Czymmek, K.J., and Q.M. Ketterings. 2007. Removal of phosphorus by field crops. Agronomy Fact Sheet Series No. 28, Department of Crop and Soil Sciences, Cornell University, Ithaca, NY.

Essington, M.E. 2004. Soil and water chemistry: An integrative approach. CRC Press. Boca Raton, Florida.

Eshel, G., and A. Banin. 2002. Feasibility study of long-term continuous field measurement of soil redox potential. Commun. *Soil Sci. Plant Anal.* 33(5&6): 695–709.

Faulkner, J.W., Z.M. Easton, W. Zhang, L.D. Geohring, T.S. Steenhuis. 2010. Design and risk assessment tool for vegetative treatment areas receiving agricultural wastewater: Preliminary results. *J. Environ. Manage.* (accepted).

Gale, P.M., K.R. Reddy, and D.A. Graetz. 1994. Phosphorus retention by wetland soils used for treated wastewater disposal. *J. Environ. Qual.* 23: 370–377.

Gburek, W.J., C.C. Drungil, M.S. Srivivasan, B.A. Needelman, and D.E. Woodward. 2002. Variable-source-area controls on phosphorus transport: Bridging the gap between research and design. *J. Soil Water and Conserv.* 57(6): 534–543.

Giesler, R., T. Andersson, L. Lovgren, and P. Persson. 2005. Phosphate sorption in aluminum- and iron-rich humus soils. *Soil Sci. Soc. Am. J.* 69: 77–86.

Gotoh, S., and W.H. Patrick, Jr. 1974. Transformation of iron in a waterlogged soil as influenced by redox potential and pH. *Soil Sci. Soc. Am. Proc.* 38: 66–71.

Guppy, C.N., N.W. Menzies, P.W. Moody, and F.P.C. Blamey. 2005. Competitive sorption reactions between phosphorus and organic matter in soil: A review. *Aust. J. Soil Res.* 43: 189–202.

Hill, D.E., and B.L. Sawhney. 1981. Removal of phosphorus from waste water by soil under aerobic and anaerobic conditions. *J. Environ. Qual.* 10(3): 401–405.

Holford, I.C.R., and W.H. Patrick, Jr. 1981. Effects of duration of anaerobiosis and reoxidation on phosphate sorption characteristics of an acid soil. *Aust. J. Soil Res.* 19:69–78.

Hutchison, K.J., and D. Hesterberg. 2004. Dissolution of phosphate in a phosphorous-enriched Ultisol as affected by microbial reduction. *J. Environ. Qual.* 33: 1793–1802.

Kaiser, K., and W. Zech. 1997. Competitive sorption of dissolved organic matter fractions to soils and related mineral phases. *Soil Sci. Soc. Am. J.* 61: 64–69.

Khalid, R.A., W.H. Patrick, Jr., and R.D. Delaune. 1977. Phosphorus sorption characteristics of flooded soils. *Soil Sci. Soc. Am. J.* 41: 305–310.

Kim, Y., L.D. Geohring, and T.S. Steenhuis. 2003. Phosphorus removal in vegetative filter strips receiving milkhouse wastewater and barnyard runoff. ASAE Annual International Meeting. Las Vegas, Nevada. 27-30 July 2003. Paper Number: 032075. American Society of Agricultural and Biological Engineering, St. Joseph, MI.

Kim, Y., L.D. Geohring, J.H. Jeon, A.S. Collick, S.K. Giri, and T. S. Steenhuis. 2006. Evaluation of the effectiveness of vegetative filter strips for phosphorus removal with the use of a tracer. *J. Soil and Water Conserv.* 61(5): 293–302.

Lijklema, L. 1980. Interaction of orthophosphate with iron(III) and aluminum hydroxides. *Environ. Sci. Technol.* 14(5): 537–541.

Lindsay, W.L. 1979. Chemical equilibria in soils. John Wiley & Sons, Inc. New York.

Maguire, R.O., and J.T. Sims 2002. Measuring agronomic and environmental soil phosphorus saturation and predicting phosphorus leaching with Mehlich 3. *Soil Sci. Soc. Am. J.* 66: 2033–2039.

NRCS. 2004. Soil survey laboratory methods manual. Soil survey investigations report No. 42. Burt, R. (Ed). National Resources Conservation Service. Washington, DC.

NRCS. 2008. National cooperative soil survey: web soil survey 2.0. Natural Resources Conservation Service. Washington, DC. http://websoilsurvey.nrcs.usda.gov/ accessed on 2/18/2008.

Pant, H.K., V.D. Nair, K.R. Reddy, D.A. Graetz and R.R. Villapando. 2002. Influence of flooding on phosphorus mobility in manure-impacted soil. *J. Environ. Qual.* 31: 1399–1405.

Pant, H.K., and K.R. Reddy. 2001. Phosphorus sorption characteristics of estuarine sediments under different redox conditions. *J. Environ. Qual.* 30: 1474–1480.

Patrick, W.H., Jr., S. Gotoh, and B.G. Williams. 1973. Strengite dissolution in flooded soils and sediments. *Science* 179: 564–565.

Patrick, W.H., Jr., and R.A. Khalid. 1974. Phosphate release and sorption by soils and sediments: effect of aerobic and anaerobic conditions. *Science* 186(4158): 53–55.

Pickering, E.W., and P.L.M. Veneman. 1984. Moisture regimes and morphological characteristics in a hydrosequence in central Massachusetts. *Soil Sci. Soc. Am. J.* 48: 113–118.

Sah, R.N., and D.S. Mikkelsen. 1986. Effects of anaerobic decomposition of organic matter on sorption and transformations of phosphate in drained soils: 1. Effects on phosphate sorption. *Soil Sci.* 142(5): 267–274.

Sawhney, B.L., and D.E. Hill. 1975. Phosphate sorption characteristics of soils treated with domestic waste water. *J. Environ. Qual.* 4(3): 342–346.

Schellinger, G.R., and J.C. Clausen. 1992. Vegetative filter treatment of dairy barnyard runoff in cold regions. *J. Environ. Qual.* 21: 40–45.

Schwer, C.B., and J.C. Clausen. 1989. Vegetative filter treatment of dairy milkhouse wastewater. *J. Environ. Qual.* 18: 446–451.

Sharpley, A.N. 1995. Dependence of runoff phosphorus on extractable soil phosphorus. *J. Environ. Qual.* 24: 920–926.

Sims, J.T., and A. Wolf. 1995. Recommended soil testing procedures for the Northeastern United States. Northeast Regional Bull. #493. Agricultural Experiment Station, University of Delaware, Newark, DE.

Sims, J.T., R.O. Maguire, A.B. Leytem, K.L. Gartley, and M.C. Pautler. 2002. Evaluation of Mehlich 3 as an Agri-environmental soil phosphorus test for the Mid-Atlantic United States of America. *Soil Sci. Soc. Am. J.* 66: 2016–2032.

Sims, J.T., and G.M. Pierzynski. 2005. Chemistry of phosphorus in soils. In *Chemical processes in soils*. Tabatabai, M.A., and D.L. Sparks (Eds.). Soil Science Society of America. Madison, Wisconsin.

Sparks, D.L. 2003. Environmental soil chemistry. Academic Press. San Diego, CA.

Ugurlu, A., and B. Salman. 1998. Phosphorus removal by fly ash. *Environ. Int.* 24(8): 911–918.

USEPA. 1983. Phosphorus, all forms. Method 365.1 (Colorimetric, Automated, Ascorbic Acid). pp.365-1.1-365-1.7. In Methods for Chemical Analysis of Water and Wastes, EPA-600/ 4-79-020. US Environmental Protection Agency. Cincinnati, Ohio.

USEPA. 2007. Method 3051A: Microwave assisted acid digestion of sediments, sludges, soils, and oils. U.S. Environmental Protection Agency. Washington, DC.

Vadas, P.A., and J.T. Sims. 1998. Redox status, poultry litter, and phosphorus solubility in Atlantic Coastal Plain soils. *Soil Sci. Soc. Am. J.* 62: 1025–1034.

Vadas, P.A., and J.T. Sims. 1999. Phosphorus sorption in manured Atlantic coastal plain soils under flooded and drained conditions. *J. Environ. Qual.* 28:1870–1877.

Walter, M.T., M.F. Walter, E.S. Brooks, T.S. Steenhuis, J. Boll, and K.R. Weiler. 2000. Hydrologically sensitive areas: variable source area hydrology implications for water quality risk assessment. *J. Soil and Water Conserv.* 3: 277–284.

Willett, I.R., and M.L. Higgins. 1978. Phosphate sorption by reduced and reoxidized rice soils. *Aust. J. Soil Res.* 16: 319–326.

Yang, S., J.H. Jones, F.J. Olsen, and J.J. Paterson. 1980. Soil as a medium for dairy liquid waste disposal. *J. Environ. Qual.* 9(3): 370–372.

Young, E.O., and D.S. Ross. 2001. Phosphate release from seasonally flooded soils: A laboratory microcosm study. *J. Environ. Qual.* 30: 91–101.

Zhang, W., J.W. Faulkner, L.D. Geohring, and T.S. Steenhuis. 2008. Evaluation of two Langmuir models for phosphorus sorption on various soils under varied conditions. ASABE Annual International Meeting, Providence, Rhode Island, June 29-July 2, 2008. Paper number: 084181.

Zhou, A., H. Tang, and D. Wang. 2005. Phosphorus adsorption on natural sediments: Modeling and effects of pH and sediment composition. *Water Res.* 39: 1245–1254.

CHAPTER 4

COLLOID TRANSPORT AND RETENTION IN UNSATURATED POROUS MEDIA: EFFECT OF COLLOID INPUT CONCENTRATION

Wei Zhang, Verónica L. Morales, M. Ekrem Cakmak, Anthony E. Salvucci, Larry D. Geohring, Anthony G. Hay, Jean-Yves Parlange, Tammo S. Steenhuis

Abstract

Colloids play an important role in facilitating transport of adsorbed contaminants in soils. Recent studies showed that under saturated conditions colloid retention was a function of its concentration. It is unknown if this is the case under unsaturated conditions. In this study, the effect of colloid concentration on colloid retention was investigated in unsaturated columns by increasing concentrations of colloid influents with varying ionic strength. Colloid retention was observed in-situ by bright field microscopy and quantified by measuring colloid breakthrough curves. In our unsaturated experiments, greater input concentrations resulted in increased colloid retention at ionic strength above 0.1 mM, but not at an ionic strength of 0 mM. Bright field microscope images showed that colloid retention mainly occurred at the solid-water interface and wedge-shaped air-water-solid interfaces, whereas the retention at the grain-grain contacts was minor. Some colloids at the air-water-solid interfaces were rotating and oscillating and thus trapped. Computational hydrodynamic simulation confirmed that the wedge-shaped air-water-solid interface could form a "hydrodynamic trap" by retaining colloids in its low velocity vortices. Direct visualization also revealed that colloids once retained acted as new retention sites for other suspended colloids at ionic strength greater than 0.1 mM and thereby could explain the greater retention with increased input concentrations. Derjaguin-Landau-Verwey-Overbeek (DLVO) energy calculations support this concept. Finally, the

results of unsaturated experiments were in agreement with limited saturated experiments under otherwise the same conditions.

Keywords: colloid, transport, retention, unsaturated porous media, concentration dependence, ionic strength, visualization, bright field microscopy, hydrodynamics

Introduction

Understanding colloid transport in unsaturated soils is important because the vadose zone is critical for protecting groundwater (de Jonge et al., 2004; DeNovio et al., 2004; McCarthy and McKay et al., 2004). To date, the majority of studies have focused on colloid transport in groundwater. Under saturated conditions, colloids are retained at the solid-water interface (SWI) and the wedge-shaped grain-grain contacts (Bradford and Torkzaban, 2008). Recent studies using microscopy in unsaturated media have shown that in addition to the retention sites in saturated soils colloids are retained at the air-water interface (AWI) (Wan and Wilson, 1994a,b) and the air-water-solid (AWS) interfaces (Crist et al., 2004, 2005; Zevi et al., 2005). Analysis of breakthrough curves (BTCs) from unsaturated columns found that colloid retention depends on properties of porous media and colloids (Zhuang et al., 2005; Gargiulo et al., 2007; Morales et al., 2009), flow regime (Saiers and Lenhart, 2003a; Gao and Saiers, 2006), solution chemistry including pH, ionic strength, and organic matter (Franchi and O'Melia, 2003; Saiers and Lenhart, 2003b; Torkzaban et al., 2008a), and moisture content (Powelson et al., 2001; Gao and Saiers, 2006; Torkzaban et al., 2008a).

Nonetheless, predicting colloid transport in the vadose zone still remains a challenge (Flury and Qiu, 2008). Studies under saturated conditions have shown that increasing input concentrations may either increase or decrease the percentage of retained colloid (Gannon et al., 1991; Tan et al., 1994; Camesano and Logan, 1998; Bradford and Bettahar, 2006; Bradford et al., 2009a; Haznedaroglu et al., 2009). The

decrease in colloid retention is attributed to the occupation of retention sites by colloids, and subsequent "blocking" of additional attachment by electrostatic repulsion of like-charged particles (Song and Elimelech, 1993; Camesano and Logan, 1998; Ko and Elimelech, 2000). The enhancement in retention is ascribed to "ripening" when interparticle interactions are attractive and the attached colloids become new retention sites for other suspended colloids (Darby and Lawler, 1990; Song and Elimelech, 1993; Liu et al., 1995; Camesano and Logan, 1998). This concentration effect in saturated media is also related to solution ionic strength (Gannon et al., 1991; Tan et al., 1994; Bradford et al., 2009a). Although colloid concentrations in the vadose zone vary at least by four orders of magnitude (DeNovio et al., 2004; Bradford and Torkzaban, 2008), the role of colloid input concentration in unsaturated soils has yet to be explored. This gap of knowledge presents a challenge to the prediction of colloid transport in the vadose zone.

To fill the knowledge gap, our objective was to investigate colloid input concentration effect on colloid transport in unsaturated porous media under varying ionic strengths. Additional experiments in saturated media were conducted to confirm the concentration effect observed in unsaturated media. We mainly focused on the experimental and mechanistic aspects of the concentration effect.

Materials and Methods

Sand and Colloid

Red hydrophilic carboxylated polystyrene microspheres with a diameter of 2.6 μm (Magsphere, Inc., Pasdena, CA) were used as model colloids. The colloids supplied in a 10% (w/v) solution (1×10^5 mg L^{-1} or 1×10^{10} colloids mL^{-1}) were washed with deionized (DI) water, and then subsequently diluted to colloid suspensions of 10, 100, and 1000 mg L^{-1} in 0, 0.1, 0.5, and 1.0 mM NaCl solutions. These colloid suspensions were used as influents in the following column experiments. The NaCl solutions free

of colloids were used as background influents. Colloid concentration was measured by a spectrophotometer at wavelength of 550 nm (SPECTRONIC 501, Milton Roy, Ivyland, PA) and the calibration curves had a linearity range of 0 to 500 mg L^{-1} (r^2 = 0.999).

Angular translucent sand with d_{10} = 0.27 mm, d_{50} = 0.40 mm, d_{90} = 0.53 mm was used (Size 2, AGSCO Corporation, Hasbrouck Heights, NJ), consisting of 99.5% silicon oxide (S_iO_2) and trace amount of aluminum oxide, iron oxide, etc. (Table 4.S1 in Appendix S1). The sand was washed with DI water to remove dust, dried, and stored in a closed container. Quartz fragments were liberated from the DI washed sand by sonication in DI water for 30 min, as per Saiers and Lenhart (2003b). The quartz suspension was then diluted into the NaCl solutions matching the ionic strength of column influents. By dynamic light scattering, the quartz fragments were sized to be 197 nm in diameter (Zetasizer Nano-ZS, Malvern Instruments Ltd., Malvern, Worcestershire, United Kingdom). Electrophoretic mobility (EM) of the colloids and quartz fragments was measured by the zetasizer. The ζ-potential was calculated from the EM values using the tables provided by Ottewill and Shaw (1972) and is shown in Table 4.1.

Table 4.1. Properties of background influents and electrophoretic mobility (EM) and ζ-potential of the quartz sand and carboxylated polystyrene colloids.

IS (mM)	pH	Colloids (2.6 μm)		Quartz Sand	
		EM (μm cm s^{-1} V^{-1})	ζ (mV)	EM (μm cm s^{-1} V^{-1})	ζ (mV)
0	5.9 ± 0.2	-2.86 ± 0.15	-57.2 ± 4.3	-2.42 ± 0.07	-47.5 ± 1.4
0.1	5.9 ± 0.1	-2.54 ± 0.29	-35.4 ± 4.2	-2.69 ± 0.13	-52.8 ± 3.5
0.5	5.9 ± 0.1	-2.24 ± 0.11	-29.7 ± 1.5	-2.79 ± 0.33	-50.3 ± 7.4
1.0	5.8 ± 0.1	-2.11 ± 0.14	-27.9 ± 1.8	-3.01 ± 0.18	-51.7 ± 3.9

Column Experiments

A transparent, acrylic rectangular column of 10-cm-long and 2×2-cm-wide was wet-packed with the sand to a porosity of 0.40 cm^3 cm^{-3}. Breakthrough experiments of colloid input pulse were conducted under a steady state flow rate (q) of 0.3 mL min^{-1}

(i.e., Darcy velocity U = 0.075 cm min^{-1}) and average volumetric moisture content (θ_w) of 0.22 ± 0.03 for unsaturated conditions or 0.40 ± 0.00 for saturated conditions. Fifteen experimental sets were carried out with two to five replications (Table 4.2). Experimental sets 1–12 were conducted under unsaturated conditions and consisted of three colloid input concentrations (C_0 = 10, 100, 1000 mg L^{-1}) and four ionic strengths (IS = 0, 0.1, 0.5, 1.0 mM). In unsaturated experimental set 13, a pulse of bromide solution (101 mg L^{-1}) was applied instead of the colloids to define the characteristics of water flow in the columns. Experimental sets 14 and 15 were conducted under saturated conditions at C_0 = 10 and 1000 mg L^{-1} and IS = 1.0 mM. Experimental sets were replicated until a definite trend was established. Because colloid retention was more variable at lower C_0 and ionic strength, more replicates were conducted for those experimental sets. Column experiment parameters, including C_0, IS, θ_w, and average pore water velocity ($v = U/\theta_w$), are listed in Table 4.2.

Hydrodynamic properties of unsaturated columns, including dispersion coefficient (D), mobile water content (θ_m), and Peclet number (Pe), were determined by fitting the bromide breakthrough curves (BTCs) with a physical two-region nonequilibrium model implemented in CXTFIT 2.0 (Appendix S2). Colloid transport through porous media at a steady state can be described by a dispersion-convection equation including a term for first-order colloid deposition (Kretzschmar and Sticher, 1997; Kretzschamar et al., 1997; Akbour et al., 2002).

$$\frac{\partial C}{\partial t} = D\frac{\partial^2 C}{\partial z^2} - v\frac{\partial C}{\partial z} - k_d C \qquad (1)$$

where C (mg L^{-1}) is the colloid concentration in solution, t (min) is the time, z (cm) is the travel distance, and k_d (min^{-1}) is the colloid deposition rate coefficient. Here D is obtained from the bromide tests, and v is equal to the average pore water velocity. Because the columns had Peclet number (Pe = 70 ± 25, Table 4.S3) greater than 50, the dispersion term in Eq. 1 is ignored and the colloid deposition rate coefficient (k_d)

(min^{-1}) can thus be determined as (Kretzschmar and Sticher, 1997; Kretzschamar et al., 1997; Akbour et al., 2002):

$$k_d = -\frac{v}{L}\ln(M_{ER}) \qquad (2)$$

where L (cm) is the column length, and M_{ER} is the colloid effluent mass recovery. Here M_{ER} was calculated by numerically integrating the area under the BTCs and then dividing the recovered mass by the input mass.

$$M_{ER} = \frac{\sum_{i=1}\left[q(t_i - t_{i-1})(C_i + C_{i-1})\right]}{2t_c q C_0} \qquad (3)$$

where t_i is the time lapsed at the ith effluent sample, C_i is the colloid concentration of the ith effluent sample, and t_c is the colloid pulse duration.

Comparisons of k_d and M_{ER} were conducted using the least significant difference (LSD) method in SPSS 17.0 (SPSS Inc., Chicago, IL).

In-situ Visualization of Colloid Transport

Similarly to Morales et al. (2009), colloid transport was visualized in-situ by digital bright field microscopy (BFM) (KH-7700, Hirox-USA, River Edge, NJ). The BFM lens was mounted horizontally to visualize the pore-scale processes from a lateral view of the columns. Images and videos were periodically taken at pores located 2 to 3 cm from the column top.

Table 4.2. Column experiment properties, effluent mass recoveries, and colloid deposition rate coefficients in unsaturated and saturated media.

	IS (mM)	Bromide	Colloid Input Concentrations (C_0) (mg L^{-1})		
			10	100	1000
Experimental Sets	0	Expt. 13 (3) [a]	Expt. 1 (4)	Expt. 2 (3)	Expt. 3 (3)
	0.1		Expt. 4 (5)	Expt. 5 (3)	Expt. 6 (3)
	0.5		Expt. 7 (4)	Expt. 8 (2)	Expt. 9 (2)
	1.0		Expt. 10 (3)	Expt. 11 (2)	Expt. 12 (2)
	1.0		Expt. 14 (3)	--	Expt. 15 (2)
Moisture Content (θ_w)(v/v)	0	0.22 ± 0.04 [b]	0.23 ± 0.01	0.22 ± 0.03	0.24 ± 0.04
	0.1	--	0.21 ± 0.04	0.22 ± 0.03	0.23 ± 0.01
	0.5	--	0.21 ± 0.02	0.22 ± 0.02	0.25 ± 0.04
	1.0	--	0.22 ± 0.02	0.24 ± 0.01	0.22 ± 0.03
	1.0	--	0.40 ± 0.00	--	0.40 ± 0.01
Pore Water Velocity (v) (cm min^{-1})	0	0.36 ± 0.07	0.33 ± 0.02	0.34 ± 0.04	0.31 ± 0.05
	0.1	--	0.37 ± 0.08	0.34 ± 0.05	0.32 ± 0.01
	0.5	--	0.36 ± 0.03	0.35 ± 0.04	0.31 ± 0.05
	1.0	--	0.35 ± 0.04	0.31 ± 0.02	0.35 ± 0.05
	1.0	--	0.19 ± 0.00	--	0.19 ± 0.00
Effluent Recovery (M_{ER})	0	0.95 ± 0.02	0.65 ± 0.09 aA [c]	0.64 ± 0.03 aA	0.68 ± 0.02 aA
	0.1	--	0.41 ± 0.10 aB	0.32 ± 0.04 abB	0.20 ± 0.10 bB
	0.5	--	0.12 ± 0.05 aC	0.07 ± 0.00 abC	0.02 ± 0.01 bC
	1.0	--	0.16 ± 0.02 aC	0.01 ± 0.01 bC	0.00 ± 0.00 bC
	1.0	--	0.14 ± 0.03 aC [d]	--	0.03 ± 0.00 bD [d]
Deposition Rate Coefficient (k_d) (min^{-1})	0	--	0.015 ± 0.005 aA [c]	0.015 ± 0.001 aA	0.012 ± 0.002 aA
	0.1	--	0.036 ± 0.016 aB	0.040 ± 0.010 aB	0.055 ± 0.016 aA
	0.5	--	0.078 ± 0.020 aC	0.093 ± 0.009 abC	0.117 ± 0.013 bB
	1.0	--	0.065 ± 0.006 aC	0.131 ± 0.002 abD	0.204 ± 0.055 bC
	1.0 [d]	--	0.038 ± 0.005 aD [d]	--	0.067 ± 0.000 bD [d]

[a] The value in the parentheses is the number of replicates for each experiment set; Expt. 1–13 were conducted in unsaturated media, and Expt. 14–15 were in saturated media; [b] The values are presented as means with one standard deviation; [c] Means of effluent recovery and deposition rate coefficient within a row with different lower case letters are significantly different ($P < 0.05$) under identical IS, and means within a column with different upper case letters are significantly different ($P < 0.05$) under identical C_0; [d] Comparison only made with unsaturated experiments at 1.0 mM (one-tail t-test).

DLVO Interaction Energy Calculations and Hydrodynamic Simulation

Colloid retention greatly depends on total Derjaguin-Landau-Verwey-Overbeek (DLVO) interaction energy of colloid interacting with other colloids or the interfaces (e.g., SWI or AWS interfaces) in soil pores (Bradford and Torkzaban, 2008). In the DLVO energy profile, the negative interaction energy at primary energy minimum or secondary energy minimum indicates an attractive force that may result in colloid aggregation or attachment, while the positive energy means a repulsive force that

promotes the colloid stability or mobility. Thus, total DLVO interaction energies were calculated as the sum of Lifshitz-van der Waals, electric double layer, and Born repulsion interactions for Colloid–SWI, Colloid–Colloid, and Colloid–AWI interactions. Born repulsion was included to account for the interaction energy resulting from the overlap of the electron clouds of atoms, similar to the approach of Hahn et al. (Hahn et al., 2004). Attachment efficiency (α) determining whether particle collision with the interfaces results in attachment was estimated from DLVO energies using a Maxwell model (Appendix S3).

Colloid retention is also highly dependent on pore-scale hydrodynamics (Johnson et al., 2007; Bradford et al., 2009b; Torkzaban et al, 2008b). To explain the observed colloid retention at the AWS interfaces, two-dimensional flow field in the wedge-shaped AWS interface formed by a sand grain and a meniscus was simulated by numerically solving the Stokes and continuity equations using COMSOL Multiphysics v3.5a software package (COMSOL, Inc., Burlington, MA). A non-slip boundary (i.e., zero velocity) was set at the sand surface, whereas a slip boundary (i.e., the normal component of velocity is zero and the tangential component of total stress is zero) was defined at the meniscus. More detailed information about the experimental, the DLVO calculations, and the hydrodynamic simulation are provided in the Appendix.

Results

Column Breakthrough Experiment

The bromide BTCs in unsaturated columns were best fitted with a physical two-region nonequilibrium model ($R^2 > 0.992$). The results showed that 63 ± 9% of water in the unsaturated columns were mobile and 37 ± 9% of water located in small pores or wedges were immobile or stagnant (Table 4.S3 in Appendix), which agrees with the value in the literature (Gao and Saiers, 2006). The conservative bromide was eluted almost completely with an effluent mass recovery of 95 ± 2% (Table 4.2).

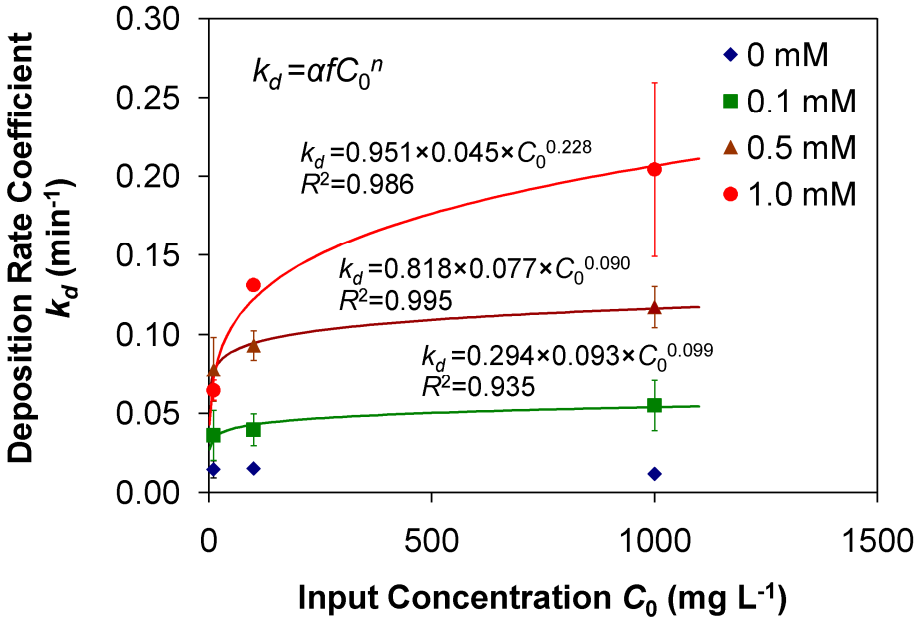

Figure 4.1. Colloid deposition rate coefficients as a function of colloid input concentration and ionic strength in unsaturated media. In the equation, α is attachment efficiency, and f and n are fitting parameters (Appendix S3).

Colloid mass recoveries in effluent (M_{ER}) and deposition rate coefficients (k_d) for the unsaturated and saturated columns based on the BTCs (detailed in Figure 4.S1) are presented in Table 4.2 and Figure 4.1. As expected (Liu et al., 1995; Saiers and Lenhart, 2003; de Jonge et al., 2004; McCarthy and McKay, 2004; Bradford and Torkzaban, 2008), these results confirmed that increasing ionic strength significantly enhanced colloid retention (Table 4.2, Figure 4.1). Additionally, when input concentrations increased, the effluent mass recovery decreased and colloid retention increased at ionic strength of 0.1 mM or greater. At any non-zero ionic strength k_d is a power function of input concentrations (Figure 4.1). The greater the influent ionic strength, the stronger effect the concentration had on colloid retention, judging from the greatest exponent of the regression at 1 mM ionic strength. In saturated experiments, the colloid retention was less than that of unsaturated experiments

(Powelson and Mills, 2001; Torkzaban et al., 2008a), and similarly increased with input concentrations (Table 4.2).

DLVO Interaction Energy Profiles

A negative primary or secondary energy minimum in the DLVO energy profiles is required for colloids to be attracted to the grain surfaces or other colloids. The DLVO energy profiles in Figure 4.2 for Colloid-SWI and Colloid-Colloid interactions indicate that a negative primary energy minimum does not exist. Secondary energy minima exist for ionic strength of 0.1 mM or greater, but not for the 0 mM solutions. Because the depth of the secondary minimum increases with ionic strength (Figure 4.2), colloids become more attracted to other colloids or grains as ionic strength increases. The attachment efficiency (α) for Colloid-SWI interactions increased from 0 at 0 mM to 0.294 at 0.1 mM, 0.818 at 0.5 mM, and 0.951 at 1 mM. The similar trend was observed for Colloid-Colloid interactions (Table 4.S4). Colloids are not attracted to the AWI at any ionic strength (Figure 4.S3), resulting in zero attachment efficiency.

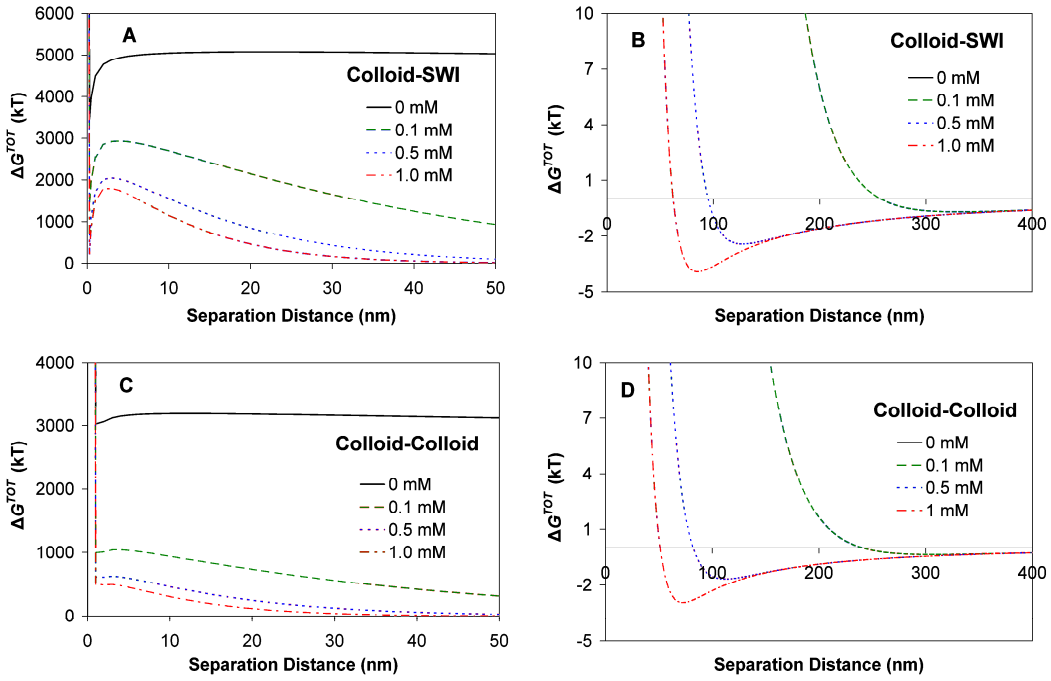

Figure 4.2. Total DLVO interaction energy (ΔG^{TOT}) for a colloid interacting with the solid-water interface (SWI) and another colloid at ionic strength of 0, 0.1, 0.5, and 1.0 mM: (A) Primary energy barrier for Colloid-SWI interaction; (B) Second energy minimum for Colloid-SWI interaction; (C) Primary energy barrier for Colloid-Colloid interaction; (D) Secondary energy minimum for Colloid-Colloid interaction.

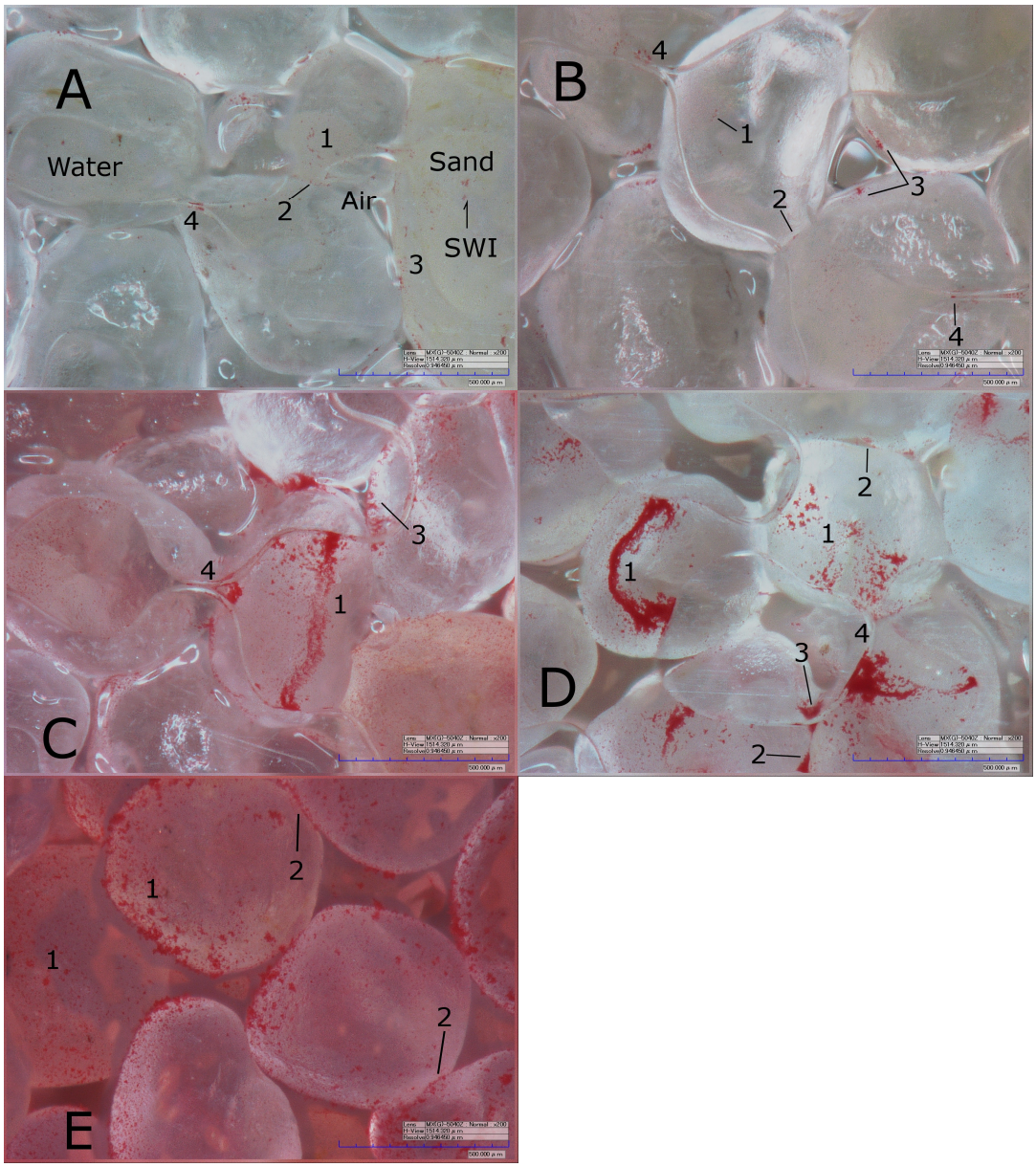

Figure 4.3. Observed retention sites of colloids in unsaturated (A, B, C, D) and saturated (E) experiments with C_0 = 1000 mg L^{-1} under four ionic strengths (IS): (A) IS = 0 mM; (B) IS = 0.1 mM; (C) IS = 0.5 mM; (D) IS = 1.0 mM; (E) IS = 1.0 mM. Retention site 1 = the SWI, 2 = the grain-grain contacts, 3 = the AWS interface, 4 = the AWS pore space formed by the adjacent menisci and the SWI. Microscopic view is rotated 90° counterclockwise due to horizontal mounting of the microscope lens. The flow direction was from left and right, representing the downward flow in the column experiments. Scale bar = 500 µm.

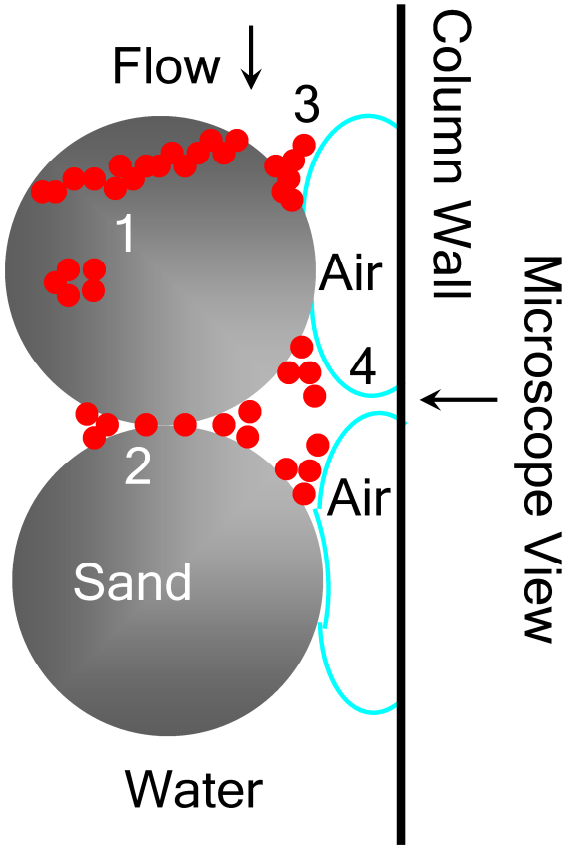

Figure 4.4. Schematic of colloid retention sites in unsaturated media: (1) the solid-water interface (SWI); (2) the grain-grain contacts; (3) the air-water-solid (AWS) interface; (4) the AWS pore space formed by the adjacent menisci and the SWI.

Colloid Retention: Visualization

Images of colloid retained in unsaturated columns after the colloid pulse passed confirmed that more colloids can be retained at greater ionic strength (Figure 4.3). Although the retention at the grain-grain contacts existed, it appeared minor compared with the retention at the SWI and AWS interfaces (Figure 4.3). The retention at the SWI and AWS interface becomes more dominant as the ionic strength increases (Figure 4.3). In saturated condition, colloid retention occurred both at the SWI and the grain-grain contacts with the SWI being the dominant retention site (Figure 4.3E). More visuals are provided in Appendix S5 including 3 video clips (Table 4.S5). To aid in interpretation, Figure 4.4 schematically shows the observed retention sites: (1) the SWI; (2) the wedge-shaped grain-grain contacts; (3) the wedge-shaped AWS interfaces; (4) the AWS pore space formed by the adjacent menisci and the SWI, a particular case of the site 3.

In the wedge-shaped AWS pore space loosely retained colloids were observed to spin or oscillate (*V1.mpg* in Appendix S5). At the SWI colloids were retained in strips or patches, whereas at wedge-shaped grain-grain contacts and AWS interfaces the retained colloids formed aggregates as shown in Figure 4.3, Figure 4.S5A, and *V2.mpg*. In addition, mobile colloids were filtered by amorphous colloid aggregates in the AWS interfaces, and suspended colloids attached to the previously immobilized colloids and formed a thick colloid strip on the SWI as shown in *V2.mpg* and *V3.mpg*.

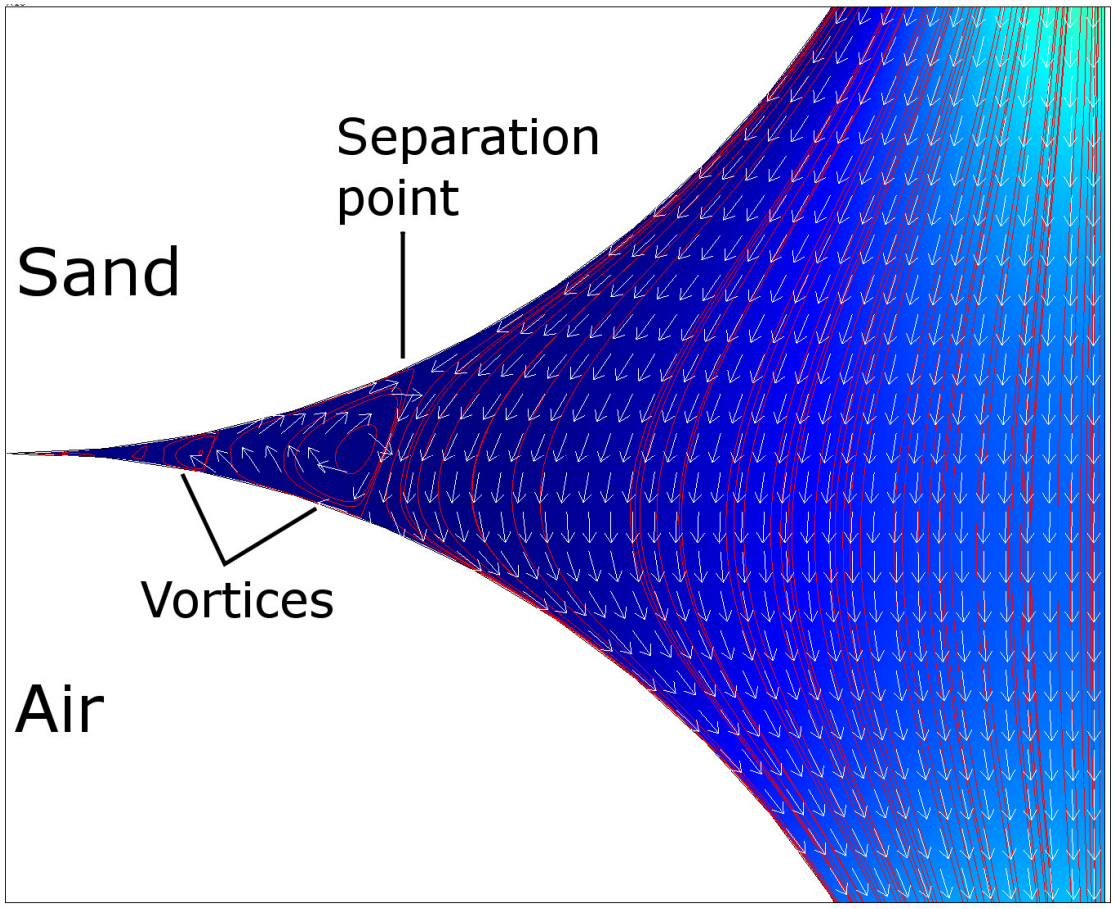

Figure 4.5. Simulated flow velocity field at the wedge-shaped air-water-solid (AWS) interface. Separation of streamlines (red lines) from the sand and meniscus surface creates an immobile region with vortices where water rotates as shown by the normalized water velocity (white arrows).

Discussion

Colloid Retention Sites: Mechanisms

In this section, we will first discuss the retention sites involving only the grain surfaces and water phase, thus common to both saturated and unsaturated media. Then, we will discuss the sites relating to the air phase. Elucidation of these retention mechanisms is advantageous in explaining the observed concentration effect.

Colloid retention at the grain surface (i.e., the SWI) is common in both saturated and unsaturated media. Relatively more colloids are retained at the SWI as ionic strength increases (Figure 4.3), because the interface becomes more attractive to colloids, shown by the increasing depth of secondary energy minimum (Figure 4.2). Colloid retention at the SWI by the attractive secondary energy minimum has been well established (Franchi and O'Melia, 2003; Hahn et al., 2004; Hahn and O'Melia, 2004). Despite having a repulsive Colloid-SWI interaction at IS = 0 mM (no secondary energy minimum in Figure 4.2B), a small amount of colloid were retained (Figure 4.3A). It is known that natural sand surfaces are typically coated with patchy Al or Fe oxides that carry positive charges at neutral pH (Liu et al., 1995; Johnson and Elimelech, 1996; Ryan and Elimelech, 1996) and could act as retention sites for colloids. To test this hypothesis, a subsample of the sand was cleaned by HNO_3 acid wash to remove Al and Fe oxides. The ζ-potential of that sand surface was much more negative than the only water washed sand (Table 4.1 and Table 4.S2 in Appendix S1), implying that Al or Fe oxides indeed provide positive charge sites. At higher ionic strength, the retention by patchy oxides is masked by retention at the secondary energy minimum.

Colloid retention also occurred at the grain-grain contacts in both saturated and unsaturated media (Figure 4.3, and *V2.mpg*). In saturated media, the colloid retention at the wedge-shaped grain-grain contacts under unfavorable attachment conditions

(i.e., in the presence of an energy barrier) has been reported and attributed to straining or wedging (Bradford et al., 2006; Johnson et al., 2007; Bradford and Torkzaban, 2008). The flow funneling and low velocity vortices (i.e., the flow stagnation zone) in the grain-grain contacts facilitate the colloid straining or wedging in this pore space (Johnson et al., 2007; Torkzaban et al., 2008b; Bradford et al., 2009b;). The number of colloids transported to these regions depends on the attraction energy between the grain surface and colloids (e.g., the secondary energy minimum) (Torkzaban et al., 2008b). When colloids become easily attracted to the grain surface, the grain-grain contacts become a less important retention site (Johnson et al., 2007), which agrees with our observation.

Colloid retention in the AWS interfaces occurs uniquely in unsaturated media. The retention at the AWS interfaces in this study cannot be explained by capillary force previously suggested (Steenhuis et al., 2006; Gao et al., 2008; Shang et al., 2009), because the colloids cannot penetrate the air-water interface due to the high DLVO energy barrier for Colloid-AWI interaction (Figure 4.S3) and the stable menisci at the steady state conditions. We observed that some colloids were trapped in the vortices of low velocity in the wedges of the AWS interfaces because loosely retained colloids were spinning or oscillating as shown in *V1.mpg*. In order to explain this observation, we simulated the flow field in this region with a non-slip boundary at the grain surface and a slip boundary at the meniscus using COMSOL. The wedge-shaped pore space caused immobile regions near the gaps between the grain and the meniscus, where water, instead of mixing with the bulk flow, rotates in an infinite set of nested ring vortices of low velocity (Figure 4.5). Also, the flow is funneled into the wedge-shaped pore space clearly shown by the streamline in Figure 4.5. This is similar to the flow pattern in the wedge at the grain-grain contacts in saturated media (Bradford et al., 2009b), validated by the COMSOL simulation with two non-slip

boundaries at the grain surfaces (Torkzaban et al., 2008b). The existence of this flow stagnation zone also resonates with the 37 ± 9% immobile water fraction estimated from the bromide tests (Table 4.S3). Thus, the flow funneling and the vortices of low velocity at the wedge-shaped AWS interfaces were partially responsible to the observed retention. Additionally, the hydrodynamic factors are coupled with the DLVO secondary energy minimum, which together determines the number of colloids transported to and the formation of colloid aggregates at this region (Bradford et al., 2007; Bradford and Torkzaban, 2008; Tong et al., 2008; Torkzaban et al., 2008b; Bradford et al., 2009b).

Input Concentration-dependent of Colloid Retention Induced by Ripening

In addition to the enhanced retention with greater ionic strength, colloid retention increases with input concentrations at non-zero ionic strength (Figure 4.1). This concentration effect has to be related to the SWI and the AWS interfaces because they are the dominant retention sites. As shown in the video suspended colloids are "captured" by already retained colloids at the SWI and AWS interfaces. The DLVO Colloid-Colloid interactions indicate that colloids may attach to each other at the secondary energy minima at non-zero ionic strength (Figure 4.2). The initial colloid retention might be proportional to colloid concentrations in solution, and the consequent capture should become more effective as the retention sites grow (Figure 4.1), resulting in increased overall attachment efficiency (Camesano and Logan, 1998). At greater input concentration the growth of retention sites is faster, thus could partially explain the observed concentration effect. Additionally, colloid aggregation in the bulk solution could be a factor as well. At the zero ionic strength, this ripening-type effect was absent due to the repulsive intraparticle interaction (Figure 4.2).

This coupling of the concentration effect with ionic strength has only been reported in saturated media (Gannon et al., 1991; Tan et al., 1994; Bradford et al.,

2009a). Gannon et al. (1991) and Tan et al. (1994) observed that bacteria (*Pseudomonas sp.* strain KL2) retention decreased as its input concentration increased from 10^8 cells mL^{-1} to 10^9 cell mL^{-1} in 10 mM NaCl solution, but remained unchanged in DI water. It was attributed to the filling of the finite retention sites controlled by ionic strength. Bradford et al. (2009a) reported that the concentration effect of carboxylated polystyrene colloids was absent at both low and high ionic strength (6 and 106 mM), but became evident at the intermediate ionic strength (31 and 56 mM). Here we showed the concentration effect of carboxylated polystyrene colloids at ionic strength of 0.1 mM or greater due to reduced electrostatic repulsion from the relative small ζ-potential (Table 4.1).

In saturated media increasing input concentration was reported to cause lower retention for several bacteria strains and carboxylated polystyrene colloids (Gannon et al., 1991; Tan et al., 1994; Bradford and Bettahar, 2006; Bradford et al., 2009a; Haznedaroglu et al., 2009). The opposite was observed for bacteria *Pseudomonas florescens P17* (Camesano and Logan, 1998), which is in agreement with our results. Since Bradford et al. (2009a) used similar colloids with this study we were able to cross-compare with their results. Compared with this study using angular quartz sand at near-neutral pH of 6 to 7, Bradford et al. (2009a) observed the opposite concentration effect in saturated spheroidal quartz sand at pH of 10. The water saturation degree cannot explain the discrepancy, because our saturated experiments gave the similar results with our unsaturated experiments. Rather the discrepancy stems from the difference in the system pH, surface potential of colloids and sands, and grain shape. The ζ-potential of their colloid and sand were more negative and the Fe and Al oxides were negatively charged at pH of 10, which resulted in greater electrostatic repulsion. The angularity of our sand could also contribute to the greater colloid aggregation and ripening (Tong et al., 2008).

Finally, Tong et al. (2008) conjectured that in saturated media the flow funneled to the grain-grain contacts may induce colloid aggregation (or ripening). Similarly, the funneling flow toward the AWS interfaces shown in Figure 4.5 could play an equal role in unsaturated media. In light of the above discussion, the concentration dependence of colloid retention in unsaturated porous media depends on intricate interplays of solution chemistry (e.g., ionic strength and pH), hydrodynamics, and properties of porous media and colloids (e.g., surface potential and grain shape).

Implications

The findings of this study have interesting implications to the transport of microorganisms, abiotic colloids, and colloid-associated contaminants in the vadose zone. Because more colloids are retained at greater ionic strength, the greatest transport will occur with rainfall that has a lower ionic strength than soil solution. Additionally, the concentration effect, intriguingly, implies that colloids are less well retained in the subsoil where the concentration is lower, because most surface-originated colloids are being retained at the topsoil. This dependence is often not included in models, which may underpredict the risk of groundwater contamination. For a pathogen with a low infectious dose (e.g., Cryptosporidium parvum) improving the prediction of colloid transport is desirable.

Acknowledgement

This research was funded by National Science Foundation (0635954), Binatonal Agricultural Research and Development Fund (IS-3962-07), and U.S. Department of Agriculture.

This is a non-final version of an article published in final form in Environmental Science & Technology. The published version can be accessed through the American Chemical Society's website at: http://pubs.acs.org/doi/suppl/10.1021/es100272f.

APPENDIX

S1. Properties of the Quartz Sand

Typical chemical composition and sieve analysis are shown at Table 4.S1 according to the manufacturer.

Table 4.S1. Typical chemical composition and sieve analysis of the quartz sand.

Composition	Content (% by weight)	Size (mm)	Percent retained (% by weight)
Silicon dioxide	99.5	0.595	0.036
Aluminum oxide	0.02	0.500	0.134
Iron oxide [a]	0.05	0.420	0.258
Sodium oxide	0.05	0.297	0.416
Calcium oxide	0.01	0.250	0.103
Zirconium oxide	0.01	0.210	0.043
Loss on ignition	0.1	0.177	0.01

[a] can include FeO, Fe_2O_3, or metallic iron.

To remove Fe and Al oxides and organics the sand was thoroughly cleaned according to Lenhart and Saiers (2002). Briefly, the DI water washed sand was boiled in 50% concentrated HNO_3 for 2 hours, gently shaken in 0.002 N NaOH for 2 hours on an orbital shaker (Bellco Glass, Inc., Vineland, NJ), and lastly immersed in 0.001 M HNO_3 for 12 to 14 hours. Between each cleaning treatment and after the acid wash, the sand was repeatedly rinsed with DI water until the pH reached the pH of the DI water. The electrophoretic mobility and ζ-potential of the acid-cleaned quartz sand are presented in Table 4.S2. The colloidal quartz particle size was measured to be 235 nm by the dynamic light scattering using the zetasizer, which is very close to the size of the colloidal particle liberated from the DI washed sand (197 nm). Compared to the values of the DI washed sand in Table 4.1, the ζ-potential of the acid-cleaned quartz sand was much lower.

Table 4.S2. Electrophoretic mobility (EM) and ζ-potential of the acid-cleaned quartz sand.

IS (mM)	pH	Acid-Cleaned Quartz Sand	
		EM (μm cm s^{-1} V^{-1})	ζ (mV)
0	5.9 ± 0.2	-2.74 ± 0.05	-55.2 ± 1.2
0.1	5.9 ± 0.1	-3.51 ± 0.16	-77.8 ± 6.5
0.5	5.9 ± 0.1	-3.47 ± 0.24	-65.3 ± 6.7
1.0	5.8 ± 0.1	-3.36 ± 0.19	-57.9 ± 4.3

S2. Column Experiments

A vertical rectangular column (10 height × 2 width × 2 length cm), made of transparent acrylic, was used for breakthrough experiments and to observe internal transport processes with bright field microscopy (BFM). The cover at the top of the column was designed with a gap of approximately 0.5 mm thickness to allow air exchange during imbibition or drainage. The column was initially wet-packed with the sand to a porosity of 0.40 cm^3 cm^{-3}. In unsaturated experiments, the column was allowed to freely drain to field capacity. A dual-channel peristaltic pump (MasterFlex® C/L, Cole-Parmer, Vernon Hills, IL) with a flow rate set at 0.3 mL min^{-1} precisely matched the inflow and outflow rate (q) and ensured steady state conditions. Once the desired water content was reached, the column was conditioned with the colloid-free background influent to ensure that the effluent background absorbance was stabilized. The colloid influent was ultrasonicated for at least 10 min to disperse the colloids. To begin the column experiments, the inflow was switched to the colloid influent. The uninterrupted colloid pulse was injected for 40 min (t_c) to deliver 12 mL of the colloid suspension. As soon as the entire colloid pulse was injected, the inflow was switched back to the colloid-free background influent, while maintaining the same flow rate, until the effluent colloid concentration returned to zero. It took from 1.6 to 2.4 pore volumes to elute unretained colloids from the column. Effluent samples were collected in acrylic cuvettes in 1.5 mL samples to colloid effluent concentrations. The colloid concentration (C) was determined from sample absorbance with the

background effluent value subtracted from each sample. At the end of the experiments, the water mass in the column was also measured and the average volumetric water content (θ_w = 0.22 ± 0.03) was calculated. The pH of the effluent was consistently maintained to be 7.0 ± 0.1 by the sand. Each column experiment was run for three influent colloid concentrations (C_0 = 10, 100, and 1000 mg L^{-1}) and four ionic strengths (IS = 0, 0.1, 0.5, and 1.0 mM), resulting in twelve combinations of concentrations and ionic strength. For each combination, column experiment was replicated from 2 to 5 times. A bromide tracer test (input concentration of 101 mg L^{-1}) was conducted to characterize the water flow inside the columns using the same experimental protocol, but substituting the colloid pulse with bromide. Bromide concentration was analyzed with ion chromatography (Dionex ICS-2000 with Ion Pac® AS18 column, Dionex, Sunnyvale, CA). Additional column experiments were conducted at C_0 = 10 and 1000 mg L^{-1} and IS = 1.0 mM in saturated media (θ_w = 0.40 ± 0.00) to examine whether the effect of colloid input concentration is similar in both saturated and unsaturated media. Breakthrough curves (BTCs) were generated by plotting C/C_0 value against pore volume and are presented in Figure 4.S1 and Figure 4.S2. The experiment runs were labeled by the combination of IS, C_0, and replicate number. The C_0 of 0.001%, 0.01%, and 0.1% is equivalent to 10, 100, 1000 mg L^{-1}.

To determine hydrodynamic properties of the unsaturated columns, the bromide BTCs were fitted with a two-region nonequilibrium transport model implemented in CXTFIT 2.0 (Toride et al., 1995). For a non-reactive solute, the one dimensional convection-dispersion transport equation at the steady state flow rate is:

$$\frac{\theta_m}{\theta_w}\frac{\partial C}{\partial t} = D\frac{\partial^2 C}{\partial z^2} - v\frac{\partial C}{\partial z} - \frac{\alpha}{\theta_w}\left(C - C_{im}\right) \qquad \text{(S2.1)}$$

where C (mg L^{-1}) is the concentration in the mobile phase, C_{im} (mg L^{-1}) is the concentration in the immobile phase, θ_m is the mobile water content, D (cm^2 min^{-1}) is

the hydrodynamic dispersion coefficient, t (min) is the lapsed time, z is the travel distance, α (min^{-1}) is the first-order mass transfer coefficient for the solute exchange rate between the mobile and immobile regions. The bromide BTCs were fitted to the analytical solution of flux-averaged concentration for Eq. S2.1 in reduced form with a pulse-input boundary condition. The BTCs fitted with the model very well (Figure 4.S2 and Table 4.S3), whereas the other models failed fitting the BTCs. The fitted results are summarized in Table 4.S3.

Table 4.S3. Modeling results of bromide tracer experiments in unsaturated columns.

	Bromide-1	Bromide-2	Bromide-3	Mean
Average volumetric water content (θ_w)	0.26	0.17	0.21	0.22 (0.04) [a]
Pore water velocity (v) (cm min^{-1})	0.29	0.43	0.35	0.36 (0.07)
Dispersion coefficient (D) (cm^2 min^{-1})	0.028	0.086	0.038	0.051 (0.031)
Mobile water fraction (θ_m/ θ_w)	0.74	0.58	0.72	0.68 (0.09)
Mass transfer coefficient (α) (min^{-1})	2.8×10^{-4}	3.2×10^{-4}	4.8×10^{-4}	$3.6\ (1.1) \times 10^{-4}$
R^2	0.997	0.998	0.992	
Pelect number (Pe)	103	50	93	82 (28)

[a] the value in the parenthesis is one standard deviation.

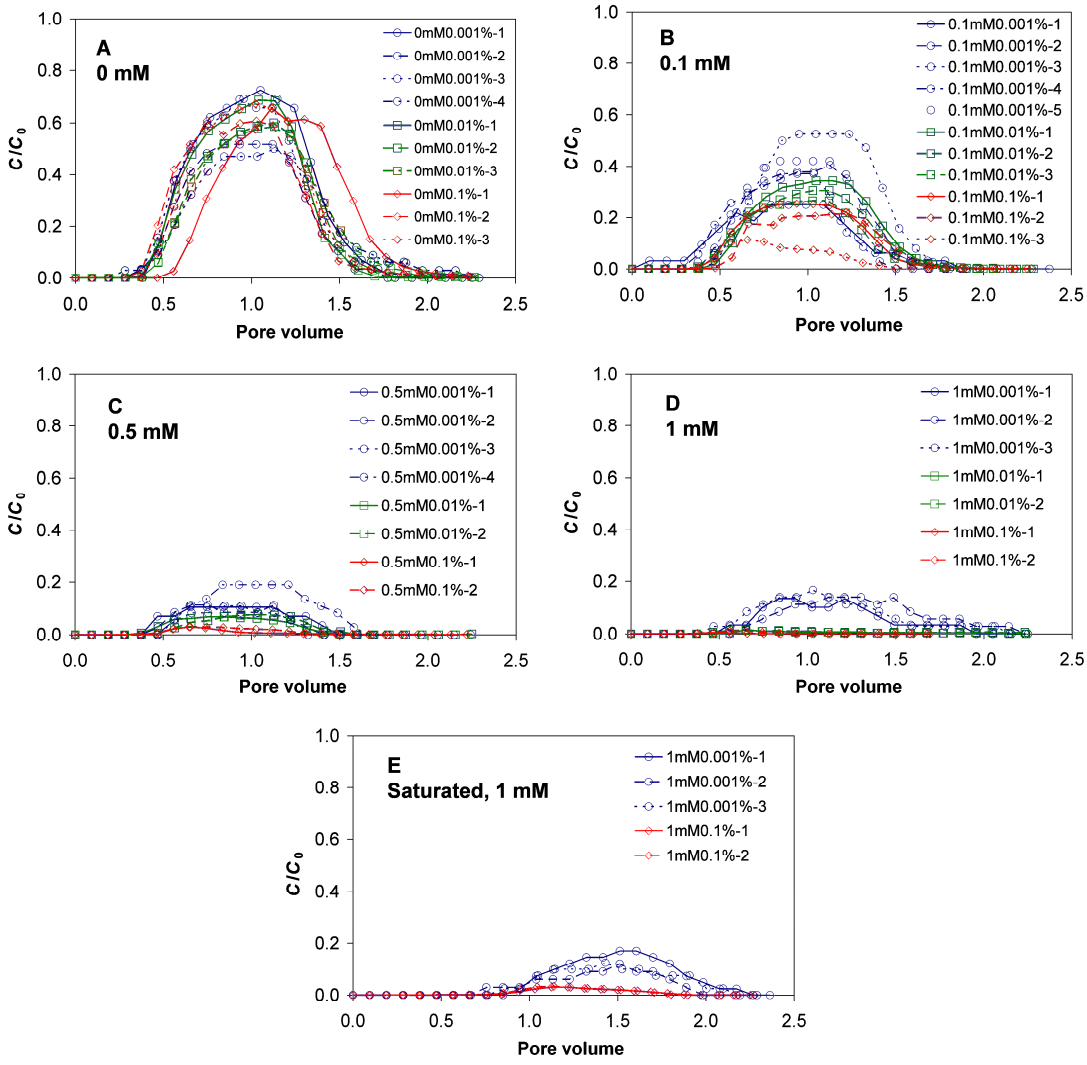

Figure 4.S1. Colloid breakthrough curves for unsaturated and saturated column experiments: (A) Unsaturated, IS = 0 mM; (B) Unsaturated, IS = 0.1 mM; (C) Unsaturated, IS = 0.5 mM; (D) Unsaturated, IS = 1 mM; (E) Saturated, IS = 1 mM.

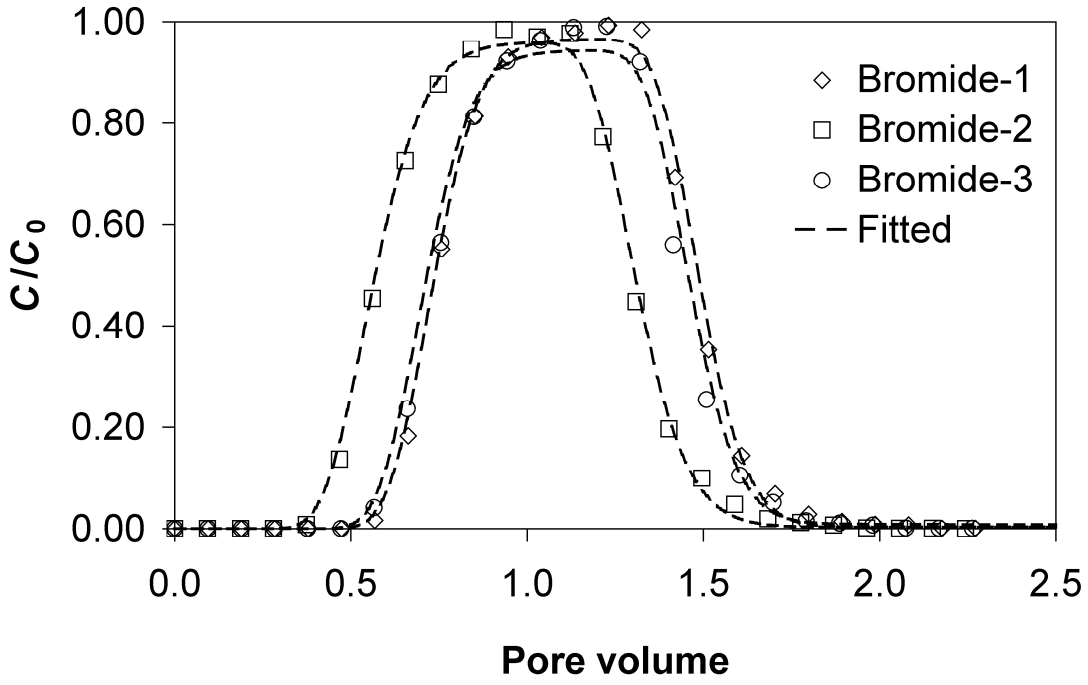

Figure 4.S2. Observed and fitted bromide breakthrough curves in unsaturated experiments.

S3. DLVO Energy Calculations and Deposition Rate Coefficient

The total Derjaguin-Landau-Verwey-Overbeek (DLVO) interaction energy (ΔG^{TOT}), including the Lifshitz-van der Waals (*LW*), electric double layer (*EDL*), and Born repulsion (*BNR*) interactions, is determined with respect to separation distance (x) as:

$$\Delta G^{TOT}(x) = \Delta G^{LW}(x) + \Delta G^{EDL}(x) + \Delta G^{BNR}(x) \quad \text{(S3.1)}$$

The non-retarded Lifshitz-van der Waals interaction energy [$\Delta G^{LW}(x)$] between two spheres in water (i.e., Colloid to Colloid) is evaluated as (Hamaker, 1937):

$$\Delta G^{LW}(x) = -\frac{A}{12}\left\{\frac{y}{r^2+ry+r} + \frac{y}{r^2+ry+r+y} + 2\ln\left(\frac{r^2+ry+r}{r^2+ry+r+y}\right)\right\} \quad \text{(S3.2)}$$

where y = ratio of the radii of two spheres (i.e., equal to 1 for two identical spheres in this study), $r = x/(2a)$ and a is the sphere radius, and A is the Hamaker constant. For

the sphere to plate interactions (i.e., colloids interact with the solid-water interface [SWI] or the air-water interface [AWI]), $\Delta G^{LW}(x)$ is determined by (Norde and Lyklema, 1989):

$$\Delta G^{LW}(x) = -\frac{A}{6}\left\{\frac{2a(x+a)}{x(x+2a)} - \ln\left(\frac{x+2a}{x}\right)\right\} \qquad \text{(S3.3)}$$

On the basis of the Lifshitz theory (Israelachvili, 1992), the Hamaker constant is estimated to be 1.3×10^{-20} J for the colloid-water-colloid interaction, 8.9×10^{-21} J for the colloid-water-sand interaction, and -1.6×10^{-20} J for the colloid-water-air interaction.

Assuming constant surface potentials, the electric double layer interaction energy ($\Delta G^{EDL}(x)$) between a colloid and SWI or AWI can be calculated as (Hogg et al., 1966; Hoek and Agarwal, 2006):

$$\Delta G^{EDL}(x) = \pi\varepsilon\varepsilon_0 a\left\{2\psi_1\psi_2 \ln\left[\frac{1+\exp(-\kappa x)}{1-\exp(-\kappa x)}\right] + (\psi_1^2+\psi_2^2)\ln\left[1-\exp(-2\kappa x)\right]\right\} \qquad \text{(S3.4)}$$

Here ε is the dielectric constant of the medium (i.e., 80.1 for water at 293.15 K), ε_0 is the vacuum permittivity (8.854×10^{-12} C^2 N^{-1} m^{-2}), ψ_1 and ψ_2 are the surface potential of the colloid, and the sand surface or the air-water interface. κ is the reciprocal electric double layer thickness. The electric double layer thickness (i.e., the Debye length [κ^{-1}]) is determined as:

$$\kappa^{-1} = \left(\frac{\varepsilon\varepsilon_0 kT}{2000 N_A I e^2}\right)^{1/2} \qquad \text{(S3.5)}$$

where k is Boltzman constant (1.381×10^{-23} J K^{-1}), T is temperature in Kelvin, N_A is Avogadro constant (6.022×10^{23}), I is ionic strength (mole L^{-1}), and e is the elementary charge (1.602×10^{-19} C). $\Delta G^{EDL}(x)$ between two identical colloids is given by:

$$\Delta G^{EDL}(x) = \pi\varepsilon\varepsilon_0 a\left\{\psi_1^2 \ln\left[\frac{1+\exp(-\kappa x)}{1-\exp(-\kappa x)}\right] + \psi_1^2 \ln\left[1-\exp(-2\kappa x)\right]\right\} \qquad \text{(S3.6)}$$

We used the measured ζ-potential (Table 4.1) in place of the surface potential (van Oss, 1994). The ζ-potential of AWI was estimated to be -65 mV (Graciaa et al., 1995; Schäfer et al., 1998).

The Born repulsion is of short-range and results from the overlap of the electron clouds of atoms. It is often expressed in terms of the empirical Lennard-Jones 6-12 potential. Ruckenstein and Prieve (1976) derived an expression to estimate the Born repulsion between a sphere and a plate.

$$\Delta G^{BNR}(x) = \frac{A\sigma^6}{7560}\left[\frac{8a+x}{(2a+x)^7} + \frac{6a-x}{x^7}\right] \qquad \text{(S3.7)}$$

Here σ is the collision diameter and usually taken as 0.5 nm. For $\Delta G^{BNR}(x)$ between two identical spheres, it is estimated as (Feke et al., 1984):

$$\Delta G^{BNR}(x) = 4A\left(\frac{\sigma}{a}\right)^6 \frac{4!}{10!}\left[\frac{(x/a)^2 - 14x/a + 54}{(x/a-2)^7} + \frac{-2(x/a)^2 + 60}{(x/a)^7} + \frac{(x/a)^2 + 14x/a + 54}{(x/a+2)^7}\right] \text{(S3.8)}$$

We noted that the inclusion of the Born repulsion eliminated the attractive primary minimum for the Colloid-SWI and Colloid-Colloid interactions, but there was an attractive primary minimum associated with the Colloid-AWI interaction due to the negative Hamaker constant.

The total DLVO interaction energies normalized with *kT* are presented in Figure 4.2 and Figure 4.S3. The primary energy barrier heights (ΔG_{pb}) and the secondary energy minimum (SEM) depths ($\Delta G_{2\min}$) of the DLVO energy curves are summarized in Table 4.S4. There was no SEM up to separation distance of 2000 nm for the Colloid-AWI interaction under any condition, and for the Colloid-SWI and Colloid-Colloid interactions at IS = 0 mM. There was SEM for the Colloid-SWI and Colloid-Colloid at IS of 0.1 mM, 0.5 mM, and 1.0 mM.

Attachment efficiency (α) is calculated from a Maxwell model that considers colloid deposition in secondary energy minima (Hahn and O'Melia, 2004; Shen et al., 2007).

$$\alpha = 1 - \int_{\sqrt{\Delta G_{2\min}}}^{\sqrt{\Delta G}} \frac{4}{\pi^{1/2}} E^2 \exp(-E^2) dE \qquad \text{(S3.9)}$$

where E^2 is the kinetic energy of particle normalized by kT, and ΔG is the sum of the primary energy barrier height and the secondary energy minimum depth. The estimated values of α are listed in Table 4.S4.

In colloid filtration theory for saturated porous media, deposition rate coefficient (k_d) can be estimated as (Tufenkji and Elimelech, 2004):

$$k_d = \frac{3}{2} \frac{1-\theta_0}{d_c} v \alpha \eta_0 \qquad \text{(S3.10)}$$

where d_c is the diameter of the collector, and η_0 is the theoretical single-contact efficiency. For unsaturated porous media, colloid filtration theory is not applicable. Nonetheless, assuming α increases with the amount of deposited colloids for the ripening-type effect (Camesano and Logan, 1998), analogous to colloid filtration theory, we have

$$k_d = g(\theta_0, \theta_w, d_c, v, \eta_0) \cdot \alpha R_p S \qquad \text{(S3.11)}$$

where g is a filter parameter that is dependent on filter properties, water content, and hydrodynamics, R_p is a ripening factor, and S is the amount of deposited colloid. It is assumed that the deposited colloid is of the Freundlich-type with colloid input concentration (C_0), i.e., $S = K_f C_0^{\,n}$, where K_f and n are fitting parameters. Then, we derived an empirical equation.

$$k_d = g \alpha R_p K_f C_0^n = \alpha f C_0^n \qquad \text{(S3.12)}$$

Here f is the product of constants g, R_p, and K_f, and n indicates the degree of concentration dependence. We also tested a Langmuir-type deposition, but the Freundlich-type fitted better with our data.

Table 4.S4. DLVO primary energy barrier and second energy minimum (SEM) of colloid interacting with the solid-water interface (SWI), colloids, and the air-water interface (AWI).

IS (mM)	Interactions	Primary Energy Barrier		Second Energy Minimum		Attachment Efficiency (α)
		Height (kT)	Distance (nm)	Depth (kT)	Distance (nm)	
0	Colloid-SWI	5.07×10^3	22	No SEM up to 2000 nm		0
	Colloid-Colloid	3.19×10^3	12	No SEM up to 2000 nm		0
	Colloid-AWI	9.56×10^3	0.3	No SEM up to 2000 nm		0
0.1	Colloid-SWI	2.93×10^3	4	-0.70	330	0.294
	Colloid-Colloid	1.04×10^3	4	-0.36	308	0.132
	Colloid-AWI	4.57×10^3	0.3	No SEM up to 2000 nm		0
0.5	Colloid-SWI	2.05×10^3	3	-2.43	128	0.818
	Colloid-Colloid	6.27×10^2	3	-1.67	112	0.658
	Colloid-AWI	3.47×10^3	0.3	No SEM up to 2000 nm		0
1.0	Colloid-SWI	1.80×10^3	3	-3.93	85	0.951
	Colloid-Colloid	4.95×10^2	3	-2.95	73	0.883
	Colloid-AWI	3.26×10^3	0.3	No SEM up to 2000 nm		0

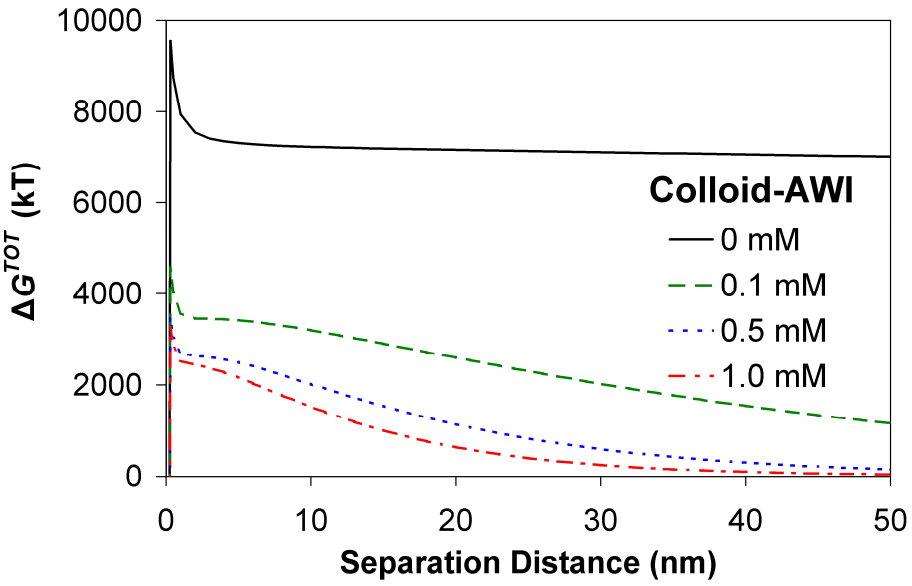

Figure 4.S3. Total DLVO interaction energy (ΔG^{TOT}) for colloid interacting with the air-water interface (AWI) at IS of 0, 0.1, 0.5, and 1.0 mM.

S4. Hydrodynamic Simulation

Two-dimensional flow field in the wedge-shaped AWS interface was simulated by using two spheres in contact model proposed by Torkzaban et al. (2008). Two spheres are a sand grain and an air bubble with diameter of 0.36 mm. The symmetrical boundary on the right side of the domain is located at 20 μm from the spheres. Flow velocity field at steady state, creeping incompressible flow conditions within the pore space was established by numerically solving the Stokes and continuity equations using COMSOL Multiphysics v3.5a software package (COMSOL, Inc., Burlington, MA).

$$\nabla p = \mu \nabla^2 v \qquad \text{(S4.1)}$$

$$\nabla \cdot v = 0 \qquad \text{(S4.2)}$$

where p is the fluid pressure(Pa), μ is the dynamic viscosity of the water (Pa·s), and v is the water velocity (m s^{-1}). Computational mesh was refined to submicron-sized triangular elements, especially at the boundary intersections within the domain in order to avoid any possible artifact. Sand grain surface was set to be no-slip boundary (i.e., velocity = zero), whereas a slip boundary (i.e., the normal component of velocity is zero and the tangential component of the total stress is zero) was defined at the air-water interface (i.e., the meniscus). The right side of the domain was set to be symmetry boundary to account for the effect of neighboring sand grain and air bubbles on fluid flow. Finally, a constant pressure difference between the inlet and outlet boundary was applied in order to achieve the desired pore water velocity of 5×10^{-5} m s^{-1}, which is the approximate average pore water velocity in the column experiments.

S5. In-situ Visualization of Colloid Transport

We summarized the visualization results in this section (Table 4.S5). In the videos (*V1.mpg*, *V2.mpg*, *V3.mpg*) colloids are better observed in the full-screen view (available at http://pubs.acs.org/doi/suppl/10.1021/es100272f). It may be necessary to

download the videos and view them at the full-screen mode. Video *V1.mpg* mainly showed that other than the firmly attached colloids, some colloids retained in the air-water-solid (AWS) interfaces were loosely captured because they were spinning and oscillating in the wedge-shaped AWS pore space formed by the two adjacent menisci and the solid-water interface (SWI). Video *V2.mpg* mainly shows the colloid retention at the grain-grain contacts was minor, compared with the dominant retention at the SWI and the AWS interfaces. In addition, *V2.mpg* also shows that the mobile colloids were filtered by the amorphous colloid aggregates at the AWS interface. Video *V3.mpg* shows that suspended colloids attached to the retained colloids at the SWI and AWS interfaces. In all three videos, major colloids retention at the SWI and AWS interfaces can be easily observed.

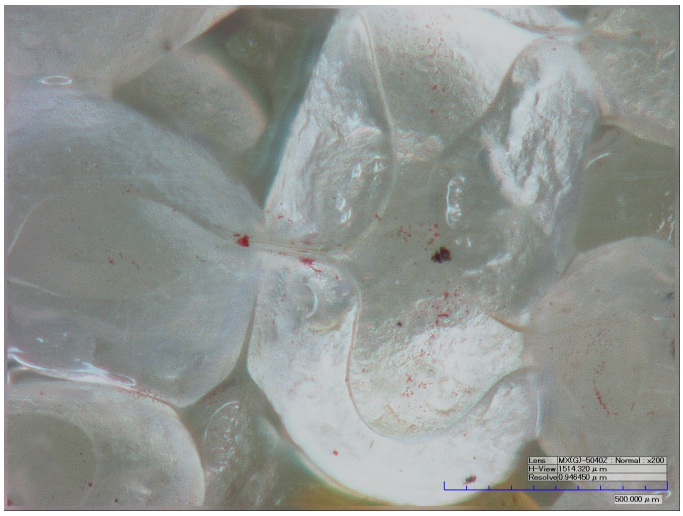

Figure 4.S4. Image taken on the 110th min at the end of experiment with IS = 0.1 mM and C_0 = 0.1% (0.1mM0.1%-3).

Table 4.S5. Summary of videos and images collected in column experiments.

Visuals	Experimental Conditions			Collection Time (min)
	IS (mM)	C_0 (mg L^{-1})	Replicate No.	
V1.mpg				
	0	1000	2	10; 55
	0.1	100	3	38; 54.6
	0.5	1000	2	16
	1.0	100	1	15.4; 22
	1.0	100	2	9.4; 20; 34
V2.mpg				
	0.1	1000	3	4; 6.8; 18.5; 21.1; 35.6; 42
	0.5	100	1	38; 40; 47.4
V3.mpg	1.0	1000	2	3; 4.6; 9; 16; 18.2; 25; 30; 32.6; 41; 47; 71
Figure 3A	0	1000	2	76
Figure 3B	0.1	1000	3	43
Figure 3C	0.5	1000	2	100
Figure 3D	1.0	1000	2	88
Figure 3E	1.0	1000	1	120
Figure S4	0.1	1000	3	110
Figure S5A	0.5	100	1	120
Figure S5B	0.5	1000	2	26
Figure S6	1.0	100	1	120

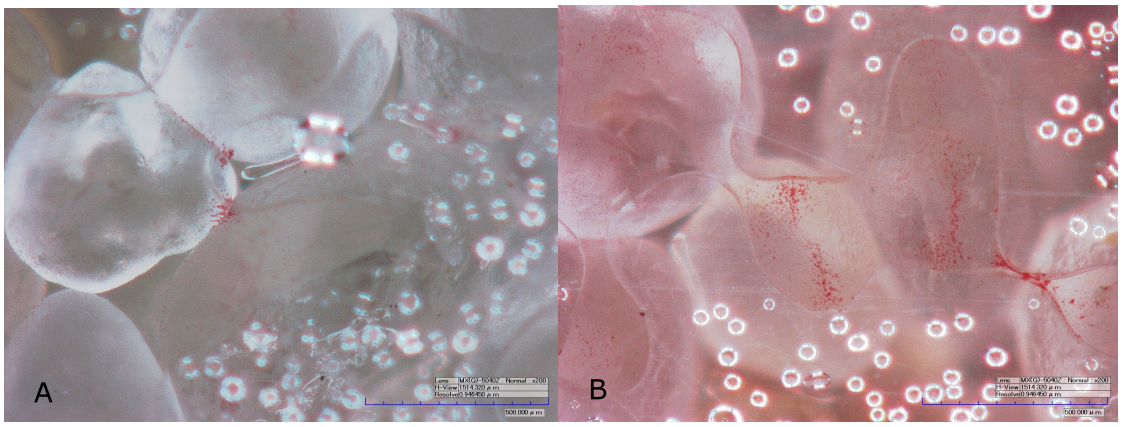

Figure 4.S5. Images collected in the experiments at 0.5 mM ionic strength. (A) C_0 = 0.01% (0.5mM0.01%-1); (B) C_0 = 0.1% (0.5mM0.1%-2).

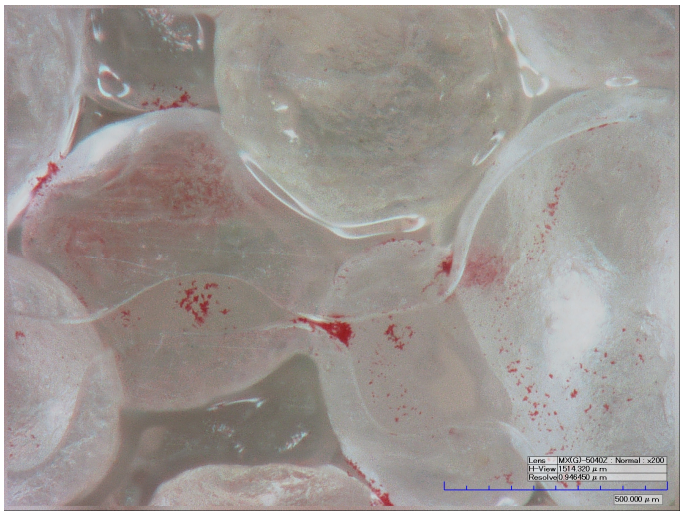

Figure 4.S6. Images recorded at the end of the experiment with IS = 1.0 mM and C_0 = 0.01% (1.0mM0.01%-1).

APPENDIX REFERENCES

Camesano, T.A., and B.E. Logan. 1998. Influence of fluid velocity and cell concentration on the transport of motile and nonmotile bacteria in porous media. *Environ. Sci. Technol.* 32(11): 1699–1708.

Feke, D.L., N.D. Prabhu, Jr.J.A. Mann, and III.J.A. Mann. 1984. A formulation of the short-range repulsion between spherical colloidal particles. *J. Phys. Chem.* 88(23): 5735–5739.

Graciaa, A., G. Morel, P. Saulner, J. Lachaise, and R.S. Schechter. 1995. The ζ-potential of gas bubbles. *J. Colloid and Interface Sci.* 172: 131–136.

Hahn, M.W., and C.R. O'Melia. 2004. Deposition and reentrainment of Brownian particles in porous media under unfavorable chemical conditions: some concepts and applications. *Environ. Sci. Technol.* 38(1): 210–220.

Hamaker, H.C. 1937. The London-van der Waals attraction between spherical particles. *Physica.* 4: 1058–1072.

Hoek, E.M.V., and G.K. Agarwal. 2006. Extended DLVO interactions between spherical particles and rough surfaces. *J. Colloid Interface Sci.* 298: 50–58.

Hogg, R., T.W. Healy, and D.W. Fuerstenau. 1966. Mutual coagulation of colloidal dispersions. *Trans. Faraday Soc.* 62: 1638–1651.

Israelachvili, J.N. 1992. Intermolecular and surface forces. Academic Press: San Diego, CA.

Lenhart, J.J., and J.E. Saiers. 2002. Transport of silica colloids through unsaturated porous media: Experimental results and model comparisons. *Environ. Sci. Technol.* 36(4): 769–777.

Norde, W., and J. Lyklema. 1989. Protein adsorption and bacterial adhesion to solid-surfaces—A colloid-chemical approach. *Colloids Surf.* 38: 1–13.

Ruckenstein, E., and D.C. Prieve. 1976. Adsorption and desoprtion of particles and their chromatographic separation. *AIChE J.* 22(2): 276–283.

Schäfer, A., H. Harms, and A.J.B. Zehnder. 1998. Bacterial accumulation at the air-water interface. *Environ. Sci. Technol.* 32(23): 3704–3712.

Shen, C., B. Li, Y. Huang, and Y. Jin. 2007. Kinetics of coupled primary- and secondary-minimum deposition of colloids under unfavorable chemical conditions. *Environ. Sci. Technol.* 41(20): 6976–6982.

Toride, N., F.J. Leij, and M.T. van Genuchten. 1995. The CXTFIT code for estimating transport parameters from laboratory and fi eld tracer experiments. Research Rep. No. 137; U.S. Salinity Lab., Agriculture Research Service, U.S. Department of Agriculture: Riverside, CA.

Torkzaban, S., S.S. Tazehkand, S.L. Walker, and S.A. Bradford. 2008. Transport and fate of bacteria in porous media: Coupled effects of chemical conditions and pore space geometry. *Water Resour. Res.* 44: W04403, doi:10.1029/2007WR006541.

Tufenkji, N., and M. Elimelech. 2004. Correlation equation for predicting single-collector efficiency in physicochemical filtration in saturated porous media. *Environ. Sci. Technol.* 38(2): 529–536.

van Oss, C.J. 1994. Interfacial forces in aqueous media. Marcel Dekker: New York.

REFERENCES

Akbour, R.A., J. Douch, M. Hamdani, and P. Schmitz. 2002. Transport of kaolinite colloids through quartz sand: Influence of humic acid, Ca^{2+}, and trace metals. *J. Colloid Interface Sci.* 253: 1–8.

Bradford, S.A., and M. Bettahar. 2006. Concentration dependent transport of colloids in saturated porous media. *J. Contam. Hydrol.* 82: 99-117.

Bradford, S.A., J. Šimůnek, M. Bettahar, M.T. van Genuchten, and S.R. Yates. 2006. Significance of straining in colloid deposition: Evidence and implications. *Water Resour. Res.* 42: W12S15, doi:10.1029/2005WR004791.

Bradford, S.A., S. Torkzaban, and S.L. Walker. 2007. Coupling of physical and chemical mechanisms of colloid straining in saturated porous media. *Water Res.* 41: 3012–3024.

Bradford, S.A., and S. Torkzaban. 2008. Colloid transport and retention in unsaturated porous media: A review of interface-, collector-, and pore-scale processes and models. *Vadose Zone J.* 7(2): 667–681.

Bradford, S.A., H.N. Kim, B.Z. Haznedaroglu, S. Torkzaban, and S.L. Walker. 2009a. Coupled factors influencing concentration-dependent colloid transport and retention in saturated porous media. *Environ. Sci. Technol.* 43(18): 6996–7002.

Bradford, S.A., S. Torkzaban, F. Leij, J. Šimůnek, M.T van Genuchten. 2009b. Modeling the coupled effects of pore space geometry and velocity on colloid transport and retention. *Water Resour. Res.* 45: W02414, doi:10.1029/2008WR007096.

Camesano, T.A., and B.E. Logan. 1998. Influence of fluid velocity and cell concentration on the transport of motile and nonmotile bacteria in porous media. *Environ. Sci. Technol.* 32(11): 1699–1708.

Crist, J.T., J.F. McCarthy, Y. Zevi, P. Baveye, J.A. Throop, and T.S. Steenhuis. 2004. Pore-scale visualization of colloid transport and retention in partly saturated porous media. *Vadose Zone J.* 3: 444–450.

Crist, J.T., Y. Zevi, J.F. McCarthy, J.A. Throop, and T.S. Steenhuis. 2005. Transport and retention mechanisms of colloids in partially saturated porous media. *Vadose Zone J.* 4: 184–195.

Darby, J.L., and D.F. Lawler. 1990. Ripening in depth filtration: Effect of particle size on removal and head loss. *Environ. Sci. Technol.* 24(7): 1069–1079.

de Jonge, L.W., C. Kjaergaard, and P. Moldrup. 2004. Colloids and colloid-facilitated transport of contaminants in soils: An introduction. *Vadose Zone J.* 3: 321–325.

DeNovio, N.M., J.E. Saiers, and J.N. Ryan. 2004. Colloid movement in unsaturated porous media: Recent advances and future directions. *Vadose Zone J.* 3: 338–351.

Flury, M., and H. Qiu. 2008. Modeling colloid-facilitated contaminant transport in the vadose zone. *Vadose Zone J.* 7(2): 682–697.

Franchi, A., and C.R. O'Melia. 2003. Effects of natural organic matter and solution chemistry on the deposition and reentrainment of colloids in porous media. *Environ. Sci. Technol.* 37(6): 1122–1129.

Gannon, J., Y. Tan, P. Baveye, and M. Alexander. 1991. Effect of sodium chloride on transport of bacteria in a saturated aquifer material. *Appl. Environ. Microbiol.* 57(9): 2497–2501.

Gao, B., and J.E. Saiers. 2006. Pore-scale mechanisms of colloid deposition and mobilization during steady and transient flow through unsaturated granular media. *Water Resour. Res.* 42: W01410, doi:10.1029/2005WR004233.

Gao, B., T.S. Steenhuis, Y. Zevi, V.L. Morales, J.L. Nieber, B.K. Richards, J.F. McCarthy, and J.-Y. Parlange. 2008. Capillary retention of colloids in unsaturated porous media. *Water Resour. Res.* 44: W04504, doi:10.1029/2006WR005332.

Gargiulo, G., S. Bradford, J. Šimůnek, P. Ustohal, H. Vereecken, and E. Klumpp. 2007. Bacteria transport and deposition under unsaturated conditions: The role of the matrix grain size and the bacteria surface protein. *J. Contam. Hydrol.* 92: 255–273.

Hahn, M.W., and C.R. O'Melia. 2004. Deposition and reentrainment of Brownian particles in porous media under unfavorable chemical conditions: Some concepts and applications. *Environ. Sci. Technol.* 38(1): 210–220.

Hahn, M.W., D. Abadzic, and C.R. O'Melia. 2004. Aquasols: On the role of secondary minima. *Environ. Sci. Technol.* 38(22): 5915–5924.

Haznedaroglu, B.Z., H.N. Kim, S.A. Bradford, and S.L. Walker. 2009. Relative transport behavior of *Escherichia coli* O157:H7 and *Salmonella enterica* Serovar Pullorum in packed bed column systems: Influences of solution chemistry and cell concentration. *Environ. Sci. Technol.* 43(6): 1838–1844.

Johnson, R.R., N. Sun, and M. Elimelech. 1996. Colloid transport in geochemically heterogeneous porous media: Modeling and measurements. *Environ. Sci. Technol.* 30(11): 3284–3293.

Johnson, W.P., M. Tong, and X. Li. 2007. On colloid retention in saturated porous media in the presence of energy barriers: The failure of α, and opportunities to predict η. *Water Resour. Res.* 43: W12S13, doi:10.1029/2006WR005770.

Ko, C.-H., and M. Elimelech. 2000. The "shadow effect" in colloid transport and deposition dynamics in granular porous media: Measurement and mechanisms. *Environ. Sci. Technol.* 34(17): 3681–3689.

Kretzschmar, R., and H. Sticher. 1997. Transport of humic-coated iron oxide colloids in a sandy soil: Influence of Ca^{2+} and trace metals. *Environ. Sci. Technol.* 31(12): 3497–3504.

Kretzschmar, R., K. Barmettler, D. Grolimund, Y.-D. Yan, M. Borkovee, and H. Sticher. 1997. Experimental determination of colloid deposition rates and collision efficiencies in natural porous media. *Water Resour. Res.* 33(5): 1129–1137.

Liu, D., P.R. Johnson, and M. Elimelech. 1995. Colloid deposition dynamics in flow through porous media: Role of electrolyte concentration. *Environ. Sci. Technol.* 29(12): 2963–2973.

McCarthy, J.F., and L.D. McKay. 2004. Colloid transport in the subsurface: Past, present, and future challenges. *Vadose Zone J.* 3: 326–337.

Morales, V.L., B. Gao, and T.S. Steenhuis. 2009. Grain surface-roughness effects on colloid retention in the vadose zone. *Vadose Zone J.* 8(1): 11–20.

Ottewill, R.H., and J.N. Shaw. 1972. Electrophoretic studies on polystyrene latices. *J. Electroanal. Chem. Interfacial Electrochem.* 37: 133–142.

Powelson, D.K., and A.L. Mills. 2001. Transport of *Escherichia coli* in sand columns with constant and changing water contents. *J. Environ. Qual.* 30: 238–245.

Ryan, J.N., and M. Elimelech. 1996. Colloid mobilization and transport in groundwater. *Colloids and Surf., A* 107: 1–56.

Saiers, J.E.; and J.J. Lenhart. 2003a. Colloid mobilization and transport within unsaturated porous media under transient-flow conditions. *Water Resour. Res.* 39(1): 1019, doi:10.1029/2002WR001370.

Saiers, J.E., and J.J. Lenhart. 2003b. Ionic strength effects on colloid transport and interfacial reactions in partially saturated porous media. *Water Resour. Res.* 39(9): 1256, doi:10.1029/2002WR001887.

Shang, J., M. Flury, and Y. Deng. 2009. Force measurements between particles and the air-water interface: Implications for particle mobilization in unsaturated porous media. *Water Resour. Res.* 45: W06420, doi:10.1029/2008WR007384.

Song, L., and M. Elimelech. 1993. Dynamics of colloid deposition in porous media: Modeling the role of retained particles. *Colloid Surf., A* 73: 49–63.

Steenhuis, T.S., A. Dathe, Y. Zevi, et al. 2006. Biocolloid retention in partially saturated soils. *Biologia* 61: S229–S233.

Tan, Y., J.T. Gannon, P. Baveye, and M. Alexander. 1994. Transport of bacteria in an aquifer sand: Experiments and model simulations. *Water Resour. Res.* 30(12): 3243–3252.

Tong, M., H. Ma, and W.P. Johnson. 2008. Funneling of flow into grain-to-grain contacts drives colloid-colloid aggregation in the presence of an energy barrier. *Environ. Sci. Technol.* 42(8): 2826–2832.

Torkzaban, S., S.A. Bradford, M.T. van Genuchten, and S.L. Walker. 2008a. Colloid transport in unsaturated porous media: The role of water content and ionic strength on particle straining. *J. Contam. Hydrol.* 96: 113–127.

Torkzaban, S., S.S. Tazehkand, S.L. Walker, and S.A. Bradford. 2008b. Transport and fate of bacteria in porous media: Coupled effects of chemical conditions and pore space geometry. *Water Resour. Res.* 44: W04403, doi:10.1029/2007WR006541.

Wan, J., and J.L. Wilson. 1994a. Visualization of the role of the gas-water interface on the fate and transport of colloids in porous media. *Water Resour. Res.* 30(1): 11–23.

Wan, J., and J.L. Wilson. 1994b. Colloid transport in unsaturated porous media. *Water Resour. Res.* 30(4): 857–864.

Zevi, Y., A. Dathe, J.F. McCarthy, B.K. Richards, and T.S. Steenhuis. 2005. Distribution of colloid particles onto interfaces in partially saturated sand. *Environ. Sci. Technol.* 39(18): 7055–7064.

Zhuang, J., J. Qi, and Y. Jin. 2005. Retention and transport of amphiphilic colloids under unsaturated flow conditions: Effect of particle size and surface property. *Environ. Sci. Technol.* 39(20): 7853–7859.

CHAPTER 5

TRANSPORT AND RETENTION OF BIOCHAR PARTICLES IN POROUS MEDIA: EFFECT OF PH, IONIC STRENGTH, AND PARTICLE SIZE

Wei Zhang, Jianzhi Niu, Verónica L. Morales, Xincai Chen, Anthony G. Hay, Johannes Lehmann, Tammo S. Steenhuis

Abstract

Biochar land application can potentially be used for carbon sequestration, improving soil quality, and reducing non-point source pollution. Understanding biochar mobility is important because its transport in soil greatly influences its stability and dynamics of soil microbial communities and organic matter. Here, the transport of biochar particles was studied in saturated and unsaturated sand columns by breakthrough experiments under three pH and two ionic strength (IS) levels. Breakthrough curves (BTCs) in saturated experiments were best fitted to a convection-dispersion model with kinetic and equilibrium deposition sites, whereas the BTCs in unsaturated experiments were well fitted with a two-region model that includes particle deposition in the mobile and immobile regions. Biochar retention was enhanced by lowering pH and increasing IS, corroborating the trends of fitted deposition rate coefficients. Under both saturated and unsaturated conditions, effluent mass recoveries decreased respectively by a factor of 6.6 or 15 when pH decreased from 10 to 4 at 10 mM IS, and by a factor of 1.4 or 3.9 when IS increased from 10 mM to 100 mM at pH 7. Biochar retention was greater in unsaturated media, implying that saturated flow elutes more biochar particles. The particles larger than 5.4% of median grain diameter were filtered out of suspension during passage through the media, whereas the retention of smaller particles was clearly dependent on solution chemistry. Similar to other types of colloids, this study highlights the importance of

pH, IS, particle size, and soil water saturation in controlling biochar movement by soil matrix flow.

Keywords: biochar; black carbon; colloid; transport; porous media; carbon sequestration

Introduction

Land application of black carbon produced from low-temperature biomass pyrolysis (i.e., biochar, agrichar, or charcoal) is a promising practice for carbon sequestration, improving soil quality, and reducing agricultural chemical fertilizer use and non-point source pollutions (Marris et al., 2006; Lehmann et al., 2006; Lehmann, 2007a,b; Renner, 2007; Fraiser, 2010). In addition to engineered pyrolysis, black carbon is also formed by forest fire, slash-and-burn agriculture, and incomplete combustion of fossil fuel (Mitra et al., 2002; Czimczik et al., 2005; Rumpel et al., 2006). Hereafter black carbon, biochar, and charcoal are simply refereed as biochar (BC). A preferable approach in the pyrolysis process is to combine production of bioenergy and biochar so that one portion of biomass is converted to bioenergy (e.g., gas, bio-oil, or hydrogen) and the rest made to biochar (typically about 50% of biomass). This biochar can then be land-applied to soil as a carbon sink because of its recalcitrant nature (Lehmann, 2007a,b). Life cycle analyses have shown that properly implemented bioenergy-biochar systems could be both carbon-negative (i.e., removing CO_2 from the atmosphere) and economically viable (Gaunt and Lehmann, 2008; Roberts et al., 2010). Although a limited number of studies have shown that biochar land application offers multiple environmental benefits, more research on the environmental benefits and risks is needed before recommending large-scale adoption (Lehmann, 2007b).

Once in the field, biochar (BC) could move laterally through soil erosion and surface runoff to recipient surface water and vertically to deeper soil depth or

groundwater aquifers (Rumpel et al., 2006; Hockaday et al., 2007; Guggenberger et al., 2008; Major et al., 2010). By analyzing BC concentrations at various soil depths its downward migration has been observed to occur to soil depths ranging from 10 to 140 cm in studies on an Australian Ustropept soil (Skjemstad et al., 1999), a temperate mixed-grass savanna at the U.S. southern Great Plains (Dai et al., 2005), three German soils (Brodowski et al., 2007), four Swiss peatland soils (Leifeld et al., 2007). Whereas the soil analyses could measure BC stored in soil at the end of its transport, more studies on BC transport flux are needed. Major et al. (2010) directly measured the BC flux in dissolved or particulate forms carried by saturated flow at the field-plot scale and found that BC rapidly percolated to 30 cm in a Colombian savanna sandy Oxisol following its land application. Meanwhile, Major et al. (2010) also hypothesized that the largest BC flux unaccounted in their mass balance was exported by surface runoff. By measuring the BC concentrations in a stream draining a discontinuous permafrost catchment in Russia, Guggenberger et al. (2008) suggested that BC export in dissolved and colloidal phase was an important pathway. Similarly, significant amount of BC was found in the small mountainous Santa Clara River (Masiello and Druffel, 2001) and in the Mississippi River (Mitra et al., 2002). The contribution of fluvial BC to the ocean has also been demonstrated (Mitra et al., 2002; Mannino and Harvey, 2004). Additionally, Hockaday et al. (2006, 2007) reported that the BC in soil charcoal extracts, soil pore water, groundwater, and stream water in the same watershed shared similar molecular formula, implying that they may be from the same BC source. Therefore, it is clear that BC can be mobilized through various pathways to groundwater and surface waters.

The transport of BC in soil is important in terms of BC stability, an important property for BC as a carbon sink, because at various soil depth microbial activity, nutrient and oxygen supply, and etc. are different, thus affecting the decomposability

of BC (Leifeld et al., 2007). Additionally, other than being a passive player, BC also actively interacts with the host soil matrix and soil microbial community, which in turn affects the stability of BC and other types of soil organic matter (Pietikäinen et al., 2000; Brodowski et al., 2005, 2007; Czimczik and Massiello, 2007; Hockaday et al., 2007; Wardle et al., 2008; Lehmann and Sohi, 2008). The BC associated with soil mineral phase may be protected from degradation (Brodowski et al., 2005; Czimczik and Massiello, 2007), whereas porous BC particles can harbor microorganisms and increase microbial activity (Pietikäinen et al., 2000). Thus, the interactions among BC, microorganisms, and soil suggest that the transport of BC is related to its stability, which is critical for employing biochar land application as a carbon sequestration technique (Lehmann et al., 2006, 2007b; Major et al., 2010). Importantly, BC has recently been shown to sorb heavy metals and organic pollutants (Chen et al., 2008; Cao et al., 2009), and thus may serve as vehicle for facilitated transport of these compounds. Nonetheless, to date, the knowledge on the transport of BC in the landscape is still limited (Lehmann et al., 2006; Major et al., 2010).

Moreover, studies examining environmental factors that govern the BC transport are sparse, thus actual mechanisms for the movement of BC have not been established (Major et al., 2010). For this reason, previous discussions of past BC transport studies rarely considered soil properties including pH, ionic strength, and etc. Here, we focused on studying the factors influencing the transport of BC particles because they can be transported rapidly (Major et al., 2010) and the colloidal BC flux is an important component of their mobility in the environment (Guggenberger et al., 2008). Generally, the transport of colloids (i.e., particle smaller than 10 μm, including soil mineral fragments, natural organic matter, microorganisms, etc.) is greatly dependent on pH, ionic strength, and particle size (McDowell-Boyer et al., 1986; DeNovio et al., 2004). Since in the environment soil pH ranges from extremely acid (<4.5) to highly

alkaline (e.g., 10) (USDA, 1954; Sparks, 2003), stream pH varies from 2.6 to 9.8 (DeNiCola, 2000; Guggenberger et al., 2008), soil water ionic strength changes rapidly during rain water infiltration, irrigation, and drainage, and the BC particles in soils have a wide size distribution (< 53 μm) with highly irregular shapes (Skjemstad et al., 1996; Brodowski et al., 2007), it is imperative to examine the effect of pH, ionic strength, and particle size on the transport of BC particles.

Therefore, the objectives of this study were to elucidate factors influencing the transport of BC particles, including pH, ionic strength, and particle size, through column breakthrough experiments under both saturated and unsaturated conditions. The breakthrough curves (BTCs) were fitted to mathematical models to estimate key transport parameters (e.g., deposition rate coefficients) and their relationship to tested system variables. The particle retention was then explained by the Derjaguin-Landau-Vervey-Overbeek theory of colloidal interactions. Particle size in the column influents and effluents was characterized by microscopic methods to establish a critical ratio of particle to median grain diameter that permits the particle passage through the media.

Materials and Methods

Column experiments

The biochar (BC) was made from a mixture of hardwoods by fast pyrolysis at 450 °C with a retention time less than 5 seconds (Dynamotive, Vancouver, Canada). Selected BC properties are summarized in Table 5.1. BC powder was passed through a 75 μm sieve to obtain a size fraction (<75 μm) similar to that found in soils (Skjemstad et al., 1996). The sieved particles were then used in column experiments. To obtain 500 mg L^{-1} suspensions sieved and air-dried BC particles (50 mg) were dispersed into 100 mL of three pH buffer solutions with pH maintained at 4 (potassium hydrogen phthalate), 7 (sodium dihydrogen phosphate: disodium hydrogen

phosphate, molar ratio 1:0.6), and 10 (sodium bicarbonate: sodium carbonate, molar ratio 1:1) and ionic strength (IS) at 10 mM or 100 mM. The BC addition did not change the pH of the buffer solutions. The pH buffered solutions free of BC particles were used as background influents in column experiments conducted in duplicates for each treatment (Table 5.2).

Table 5.1. Properties of the biochar used in this study.

		Properties
Bulk density (g cm^{-3})		0.25 – 0.30
Moisture content (% by weight)		29.1 ± 4.8
Organic matter (% by weight)		51.0 ± 1.4
pH in water		7.2 ± 0.2
Morgan extractable	P	34 ± 4
constituents (mg kg^{-1})	K	6028 ± 672
	Mg	274 ± 22
	Ca	2346 ± 57
	Fe	70 ± 35
	Mn	48 ± 8
	Zn	3.4 ± 0.7
	Al	0
	NO_3	0
Fraction < 75 µm (% by weight)		40

Angular translucent sand with d_{10} = 0.27 mm, d_{50} = 0.40 mm, d_{90} = 0.53 mm was used as a model porous media (Size 2, AGSCO Corporation, Hasbrouck Heights, NJ), consisting of 99.5% silicon oxide (S_iO_2) and trace amount of aluminum oxide, iron oxide, etc. The sand was washed with deionized (DI) water to remove dust, dried, and stored in a closed container.

A transparent acrylic column of 10-cm-long (L) and 2×2-cm-wide was wet-packed with the sand to a porosity (θ_0) of 0.39 to 0.40 $cm^3\,cm^{-3}$. The experimental procedure has been previously used in studying polystyrene colloids (Morales et al., 2009; Zhang et al., 2010). Briefly, the column experiments were conducted at a steady state inflow and outflow rate (q) of 0.3 mL min^{-1} (i.e., Darcy velocity U = 0.075 cm min^{-1}) for unsaturated experiments and 0.56 mL min^{-1} (U = 0.14 cm min^{-1}) for saturated

experiments, controlled by a dual-channel peristaltic pump (MasterFlex® C/L, Cole-Parmer, Vernon Hills, IL). Prior to injection of a 9 mL BC pulse input (C_0 = 500 mg L^{-1}), the columns were flushed with the BC-free background influents to stabilize the background effluent absorbance. Immediately before the pulse injection the input BC suspension was briefly sonicated for 5 min to disperse the particles. During the injection of BC input pulse, the BC suspension was stirred periodically to prevent the particle settling. After the injection of BC pulse, the inflow was immediately switched back to the BC-free background influent until the effluent absorbance returned to the background absorbance level. Effluent samples were collected at either 5 min or 3 min intervals for the unsaturated and saturated experiments, respectively. In separate column experiments, a pulse of bromide solution in DI water (100 mg L^{-1}) was applied instead of the BC to define the water flow in the columns. At the end of the column experiments, the volumetric moisture content (θ) was measured by determining water mass in the columns and using water density of 1.0 g cm^{-3}. Biochar particle concentration was measured by a spectrophotometer at the wavelength of 550 nm (SPECTRONIC 501, Milton Roy, Ivyland, PA) and the calibration curves had a linearity range of 0 to 500 mg L^{-1} (r^2 = 0.9997). The particle concentration (C) was determined from sample absorbance after subtracting the background effluent value. The bromide concentrations was measured via ion chromatography (IC) (Dionex ICS-2000 with Ion Pac® AS18 column, Dionex, Sunnyvale, CA). The normalized effluent concentrations (C/C_0) are plotted against pore volumes to obtain the breakthrough curves (BTCs). The experimental parameters, including experimental treatments, θ, degree of water saturation (θ/θ_0), and pore water velocity ($v = U/\theta$), are listed in Table 5.2.

Table 5.2. Summary of bromide and biochar particle breakthroughs in saturated and unsaturated column experiments [a]

Experiment	Measured parameters				Modeled parameters [b]				
Saturated	θ (cm^3 cm^{-3})	S_w	v (cm min^{-1})	M_{ER}	D (cm^2 min^{-1})	k_e (L kg^{-1})	k_d (min^{-1})		R^2
Bromide-A	0.39	1.0	0.36	1.00	0.032	–	–		0.967
Bromide-B	0.39	1.0	0.35	0.948	0.027	–	–		0.985
pH4IS10-A	0.38	1.0	0.39	0.049	0.087	0.034	0.125		0.995
pH4IS10-B	0.39	1.0	0.35	0.039	0.066	0.010	0.119		0.994
pH7IS10-A	0.39	1.0	0.36	0.136	0.048	0.017	0.065		0.998
pH7IS10-B	0.39	1.0	0.35	0.137	0.029	0.016	0.064		0.998
pH7IS100-A	0.39	1.0	0.35	0.100	0.048	0.010	0.085		0.995
pH7IS100-B	0.39	1.0	0.35	0.103	0.080	0.032	0.084		0.992
pH10IS10-A	0.39	1.0	0.38	0.296	0.082	0.025	0.049		0.994
pH10IS10-B	0.37	0.94	0.38	0.283	0.083	-0.026	0.048		0.998
Unsaturated						θ_m (cm^3 cm^{-3})	k_{im} (min^{-1})	α (min^{-1})	
Bromide-A	0.22	0.56	0.34	1.04	0.072	0.13	–	0	0.998
Bromide-B	0.22	0.54	0.35	1.01	0.084	0.11	–	0	0.997
pH4IS10-A	0.23	0.57	0.33	0.010	0.078	0.14	0.360	0.0133	0.928
pH4IS10-B	0.21	0.51	0.36	0.014	0.078	0.09	0.290	0.0113	0.895
pH7IS10-A	0.21	0.53	0.35	0.099	0.078	0.13	0.222	0.0065	0.935
pH7IS10-B	0.21	0.53	0.35	0.098	0.078	0.16	0.205	0.0075	0.988
pH7IS100-A	0.17	0.44	0.44	0.021	0.078	0.06	0.325	0.0300	0.944
pH7IS100-B	0.22	0.56	0.34	0.029	0.078	0.10	0.305	0.0126	0.949
pH10IS10-A	0.24	0.59	0.32	0.172	0.078	0.14	0.080	0.0024	0.993
pH10IS10-B	0.21	0.53	0.36	0.188	0.078	0.11	0.070	0.0037	0.993

[a] θ = total volumetric water content; S_w = average degree of water saturation; v = average pore water velocity; M_{ER} = mass recovery in effluents; D = hydrodynamic dispersion coefficient; k_e = partition coefficient at linear equilibrium deposition site; k_d = the first-order particle deposition rate coefficient; θ_m = volumetric mobile water content; k_{im} = the first-order particle deposition rate coefficient in the immobile water region; α = the first-order mass transfer coefficient of the particle exchange rate between the mobile and immobile regions.

[b] the kinetic and equilibrium deposition model (KEDM) was used for the saturated experiments and the mobile and immobile model (MIMM) used for the unsaturated experiments. In the MIMM model the deposition rate coefficient in the mobile region was set to be equal to the values from the saturated experiments.

Modeling

The transport of particles including colloids through porous media at a steady state flow rate is governed by the convection-dispersion equation with terms accounting for particle deposition and release (Cherrey et al., 2003; Chen et al., 2007; Smith et al, 2008). Here, the deposition term groups all particle retention processes, including attachment, mechanical filtration, and straining (McDowell-Boyer et al., 1986;

DeNovio et al., 2004; Bradford et al., 2006). Attachment involves the collision of particle with and subsequent retention at the grain surface through diffusion, interception, and sedimentation, thus colloidal interactions and hydrodynamics are among the main determinants. Mechanical filtration occurs at the soil surface when particles or aggregates are larger than all of the soil pores, while straining refers to particle retention at the intersection of multiple interfaces in the soil pore, i.e., the grain-grain contacts, water film, and the air-water-solid (AWS) interfaces, thus controlled by both physical and chemical factors (Bradford et al., 2007). The conservative bromide tracer does not experience any retention, thus it can be used to define water flow in the columns.

In saturated media, we assumed that there are two types of particle deposition sites, including a kinetic irreversible deposition site and a linear reversible equilibrium deposition site. This model is from here on referred to as the kinetic and equilibrium deposition model (KEDM). The governing equation is

$$\frac{\partial C}{\partial t} = D\frac{\partial^2 C}{\partial z^2} - v\frac{\partial C}{\partial z} - \frac{\rho_b}{\theta}\left(\frac{\partial S_1}{\partial t} + \frac{\partial S_2}{\partial t}\right) \qquad (1)$$

where C (mg L^{-1}) is the particle concentration in the liquid phase, t (min) is the elapsed time, D (cm^2 min^{-1}) is the longitudinal hydrodynamic dispersion coefficient, z (cm) is the travel distance, v (cm min^{-1}) is the pore water velocity, ρ_b (g cm^{-3}) is the bulk density of packed media, θ (cm^3 cm^{-3}) is the moisture content in the media (i.e., the porosity [θ_0] under saturated conditions), and S_1 (mg kg^{-1}) and S_2 (mg kg^{-1}) are the deposited particle concentrations in the solid phase by the two deposition sites. The particle deposition at the equilibrium site follows a linear isotherm

$$S_1 = k_e C \qquad (2)$$

where k_e (L kg^{-1}) is the equilibrium partition coefficient. Thus, the particle deposition rate is determined as

$$\frac{\partial S_1}{\partial t} = k_e \frac{\partial C}{\partial t} \qquad (3)$$

We further assumed a first-order deposition rate coefficient (k_d) for the kinetic site. Then, the kinetic deposition rate becomes

$$\frac{\partial S_2}{\partial t} = \frac{\theta}{\rho_b} k_d C \qquad (4)$$

We also tested other two types of particle transport models that include a release term (Smith et al., 2008) or exclusively the deposition term (Chen et al., 2007). Their governing equations and comparison with the KEDM model are presented in Appendix S1 (Figure 5.S1). The KEDM model gave the best fit, thus it was used.

In unsaturated media, we assumed that there were only the irreversible kinetic deposition sites, an approach that is commonly used (Cherrey et al., 2003; Chen et al., 2007). From the fitting of bromide BTCs, it was shown that water separated into the mobile and immobile regions in the unsaturated columns, which agreed with other studies (Cherrey et al., 2003; Gao and Saiers, 2006; Chen et al., 2007). The immobile water region usually expands with decreasing water content, and is minimal in saturated media (Gao and Saiers, 2006; Chen et al., 2007). Thus, the particle deposition must also occur in these two regions. In the past, the assumption of colloid deposition either in the mobile region (Cherrey et al., 2003) or in the immobile region (Chen et al., 2007) has been made. Our experiments allowed us to independently estimate the deposition rate coefficients in the mobile region (k_m) from the saturated experiments ($k_m = k_d$) because the pore water velocities and chemical conditions were matched in these two experimental sets, and similar colloidal interactions and hydrodynamics (thus the deposition rate coefficients) in the mobile regions may be assumed. This model is the mobile-immobile-two-region model (MIMM) with the governing equation as

$$\frac{\theta_m}{\theta}\frac{\partial C_m}{\partial t} = D\frac{\partial^2 C_m}{\partial z^2} - v\frac{\partial C_m}{\partial z} - \frac{\alpha}{\theta}\left(C_m - C_{im}\right) - \frac{\theta_m}{\theta} k_m C_m \qquad (5)$$

$$\theta_{im}\frac{\partial C_{im}}{\partial t} = \alpha\left(C_m - C_{im}\right) - \theta_{im}k_{im}C_{im} \qquad (6)$$

where C_m and C_{im} (mg L^{-1}) are the particle concentrations in the mobile and immobile water regions, θ_m and θ_{im} (cm^3 cm^{-3}) are the mobile and immobile volumetric water content ($\theta = \theta_m + \theta_{im}$), α (min^{-1}) is the first-order mass transfer coefficient of the particle exchange between the mobile and immobile regions, and k_m and k_{im} (min^{-1}) are the particle deposition rate coefficients in the mobile and immobile regions.

The fitting of the KEDM and MIMM models were implemented in CXTFIT 2.1 (Toride et al., 1995) using the third-type boundary condition and a pulse input. For the bromide all the retention terms in the models were equal to 0 (i.e., k_e, k_d, k_m, and $k_{im} = 0$) and the governing equation was reduced to the convection-dispersion equation. During the fitting of the particle BTCs to the KEDM, the parameters D, k_d, and k_e were estimated. In unsaturated experiments, k_m was set equal to k_d due to similar colloidal interactions and hydrodynamics (thus the deposition rate coefficients). The dispersion coefficients (D) of bromide was used in this case because the model did not gave a good fit when including four fitting parameters (i.e., k_{im}, α, θ_m, and D). The parameters k_{im}, α, and θ_m were then fitted by the MIMM.

Particle size measurement

A digital bright field microscope (BFM) (KH-7700, Hirox-USA, River Edge, NJ) with a resolution of 0.278 µm/pixel was used to measure particle size in the influent and effluent from the saturated experiments (pH7IS10 and pH10IS10), since these experiments eluted more BC particles, as shown in the result section. Briefly, a liquid sample of 10 µL was placed on a glass slide and then covered with a cover slide. Microscopic images were taken randomly at the 25 locations per sample. A total 50 images were taken for the influent samples and 25 images were taken for the effluent samples. Images were analyzed for particle size using a marco routine developed in ImageJ 1.41o (Wayne Rasband, National Institutes of Health, USA). The image was

first converted to an 8-bit image, the background subtracted using a rolling radius of 150 pixels, the brightness/contrast adjusted, and finally the threshold was adjusted. The particle analyses on the adjusted images allowed counting of the number of identified particles and measurement of other parameters, including particle area (A_p), particle perimeter (P), Feret's diameter (d_F, the longest distance between any two points along the selected particle boundary), major axis of the best fitting ellipse over particle (X_1), minor axis of the fitting ellipse (X_2), and aspect ratio ($AR = X_1/X_2$). The particle size distribution was constructed against d_F, based on either the number of particles or the total area of particles in a particle size fraction. Here, the particle area was considered as a surrogate for its mass (Zevi et al., 2006, 2009), which allowed the approximate construction of the particle size distribution by mass. This construction using particle area only gave a coarse approximation because of the lacking of third dimension in the measurement.

To examine the lower limit of particle size, the influent and effluent particles in the saturated experiment of pH10IS10 were imaged by transmission electron microscopy (TEM) (FEI Tecnai T-12 TWIN, Hillsboro, Oregon, USA). The smallest particle size was measured in ImageJ, and the existence of these small particles in the bulk solution were confirmed by dynamic light scattering (Zetasizer Nano-ZS, Malvern Instruments Ltd., Malvern, Worcestershire, United Kingdom) after filtering through 0.1 μm mixed cellulose membrane (Millipore, Burlington, MA). Dynamic light scattering was not a suitable method for measuring the BC size distribution because the BC suspension was highly polydispersed. However, the technique can be used to confirm the existence of submicron particles after filtering out the particles larger than 0.1 μm.

DLVO interactions

In additional to mechanical filtration of large particles, the breakthrough of BC particles is also expected to depend on colloidal interactions between BC colloids and

various interfaces in the soil pores, including the solid-water interface (SWI), the air-water interface (AWI), and the air-water-solid (AWS) interfaces (DeNovio et al., 2004; Bradford et al., 2008; Zevi et al., 2009). Thus, we calculated the Derjaguin-Landau-Verwey-Overbeek (DLVO) energy (Φ) as the sum of Lifshitz-van der Waals (Φ^{LVW}), electric double layer (Φ^{EDL}), and Born repulsion (Φ^{BNR}) interactions for a BC colloid interacting with SWI, AWI, or another BC colloid (Zhang et al., 2010). The negative DLVO energy at certain separation distances (e.g., primary energy minimum or secondary energy minimum) indicates an attractive force that contributes to colloid aggregation or attachment, whereas the positive Φ suggests a repulsive force that promotes colloid stability or mobility. To calculate the DLVO energy, the ζ-potentials of the sand surface and the BC colloids were determined. Quartz fragments were liberated from the sand by sonication in DI water for 30 min (Zevi et al., 2009; Zhang et al., 2010). The quartz suspension was filtered through 0.45 μm filter membrane and the filtrates diluted into the select pH buffered solutions for electrophoretic mobility (EM) measurements by the Zetasizer. Similarly, the BC fragments were liberated from the BC suspensions in the pH buffered solutions, and the filtrates were used in the EM measurements. The ζ-potentials of the sand surface and BC particle were calculated from the EM values using the Smoluchowski equation and listed in Table 5.3.

A much idealized DLVO approach was used by assuming BC colloids as smooth spheres because the equations for rough and irregular surfaces are currently not available. In addition, BC particle of 1 μm in diameter was selected to calculate the DLVO energies. Although the approach was idealized, the energy calculations still captured the qualitative trends with pH and ionic strength. The primary energy minimum (Φ_{1min}), the primary energy barrier (Φ_{max}), and the secondary energy

minimum (Φ_{2min}) were identified in the DLVO energy profiles. The detailed equations for DLVO energy are presented in Appendix S2.

Table 5.3. Properties of background influents and electrophoretic mobility (EM) and ζ-potentials of quartz sand and biochar colloids.

pH	IS (mM)	Quartz sand		Biochar	
		EM (μm cm s^{-1} V^{-1})	ζ (mV)	EM (μm cm s^{-1} V^{-1})	ζ (mV)
4.2 ± 0.2	10	-2.86 ± 0.10	-36.4 ± 1.3	-0.72 ± 0.20	-9.2 ± 2.6
6.8 ± 0.1	10	-3.62 ± 0.22	-46.1 ± 2.8	-3.04 ± 0.18	-38.7 ± 2.4
6.7 ± 0.1	100	-2.47 ± 0.28	-31.5 ± 3.5	-1.57 ± 0.16	-20.0 ± 2.0
10.0 ± 0.1	10	-3.86 ± 0.11	-49.3 ± 1.4	-4.80 ± 0.13	-61.2 ± 1.7

Results

Column experiments and modeling

As shown in Table 5.2, the particle effluent mass recoveries decreased with lowering pH and increasing ionic strength. For example, under both saturated and unsaturated conditions the effluent mass recoveries decreased respectively by a factor of 6.6 or 15 when pH decreased from 10 to 4 at IS = 10 mM, and by a factor of 1.4 or 3.9 when ionic strength increased from 10 mM to 100 mM at pH = 7. The percentage of particles eluted in saturated experiments was greater than unsaturated experiments by 38% to 302% under otherwise same experimental conditions (Table 5.2).

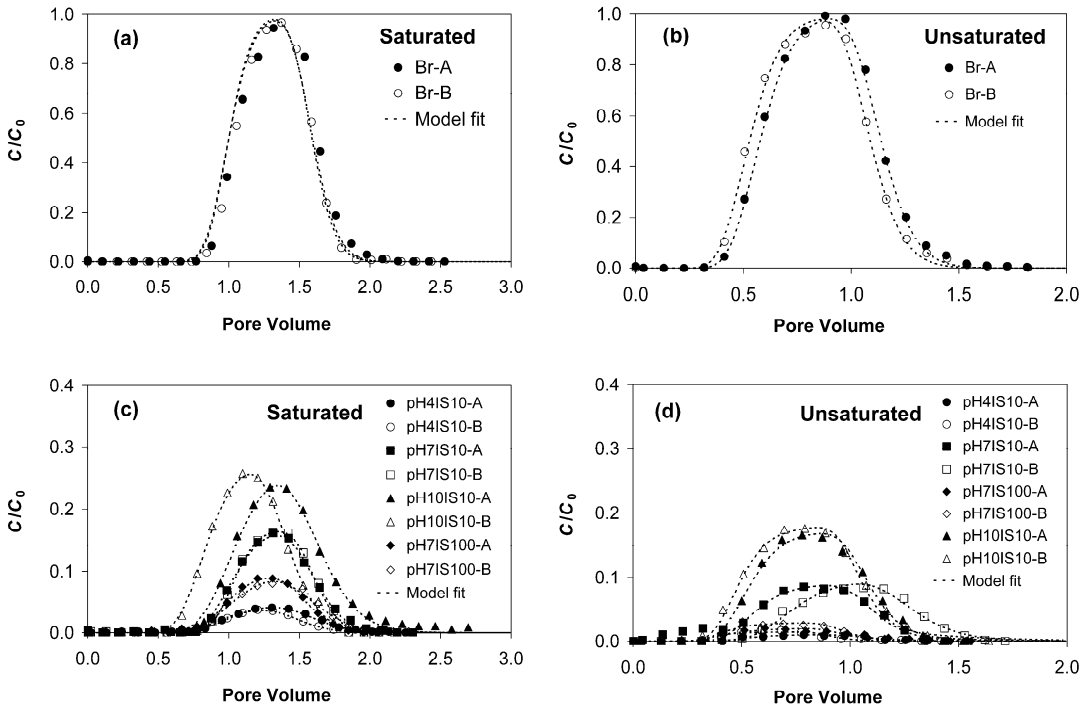

Figure 5.1. Measured and fitted breakthrough curves for bromide and biochar: (a) Bromide in saturated media; (b) Bromide in unsaturated media; (c) Biochar in saturated media; (d) Biochar in unsaturated media.

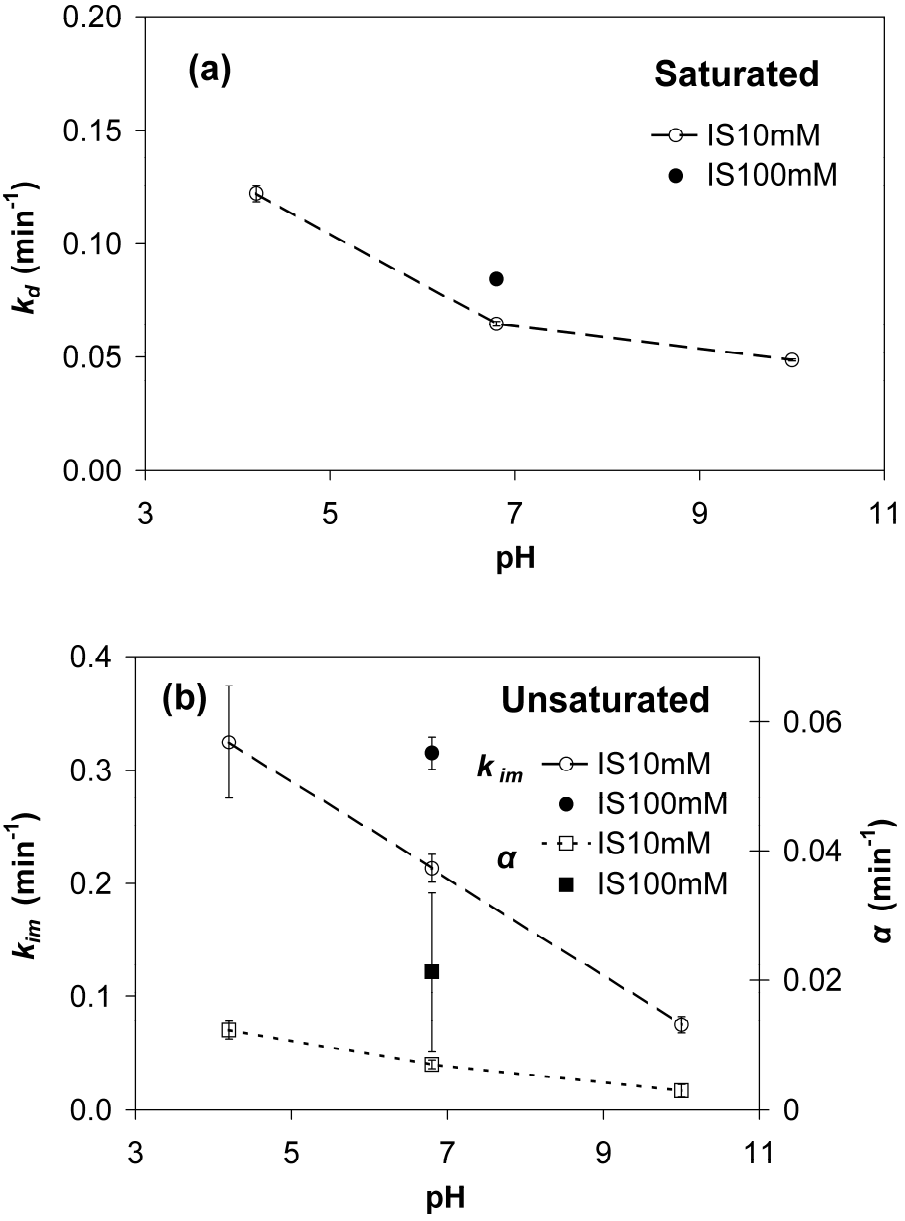

Figure 5.2. Deposition rate coefficients (k_d and k_{im}) and biochar mass transfer coefficients (α) between the mobile and immobile regions as function of pH and ionic strength: (a) saturated media; (b) unsaturated media. Error bar = standard deviation of two tests.

For the conservative bromide tracer, the convection-dispersion equation fitted the BTCs in saturated media well ($R^2 > 0.967$, Table 5.2, Figure 5.1), whereas the two-region model (MIMM) had to be used to fit the BTCs in unsaturated media ($R^2 > 0.997$), which agreed with other studies (Cherrey et al, 2003; Chen et al., 2007). For the BC particle transport, the KEDM fitted the BTCs very well ($R^2 > 0.992$) in saturated experiments, and the MIMM fitted the BTCs satisfactorily ($R^2 > 0.892$) in unsaturated experiments. The lower R^2 values for the experiment pH4IS10 and pH7IS100 could be a result of the fact that the effluent particle concentrations were too low to form well-shaped BTCs.

The estimated deposition rate coefficients (k_d, k_m, and k_{im}) increased by lowering pH and increasing ionic strength (Figure 5.2). For instance, k_d increased by a factor of 2.5 and k_{im} by a factor of 4.3 when pH decreased from 10 to 4, whereas k_d increased by a factor of 1.7 and k_{im} by a factor of 4.2 when ionic strength changed from 10 mM to 100 mM (Table 5.2). The deposition rate coefficients were greater under unsaturated conditions than under saturated conditions. Intriguingly, the mass transfer coefficients (α) of particle exchange between the mobile and immobile regions also showed a similar trend as k_{im} (Figure 5.2b).

Colloidal interactions

The DLVO energies of BC colloid interacting with the sand surface (SWI) and another colloid under select experimental conditions are summarized in Table 5.4. The energy profiles including the Colloid-AWI interaction profile are presented in Appendix S2 (Figure 5.S2). For Colloid-SWI interactions, the primary energy minimum (Φ_{1min}) existed at pH4IS10 and pH7IS100, but not at pH7IS10 and pH10IS100. The heights of the primary energy barrier (Φ_{max}) increased with pH at IS = 10 mM, but decreased with ionic strength at pH = 7. The depth of the secondary energy minimum (Φ_{2min}) was also greater at the lower pH and higher ionic strength.

For Colloid-Colloid interactions, Φ_{1min} existed for pH4IS10 and pH7IS100, and there was no Φ_{max} and Φ_{2min} because the remainder of the energy profile was negative (Figure 5.S2). For pH7IS10 and pH10IS10, there was no Φ_{1min}, whereas Φ_{max} were very high and Φ_{2min} were shallow (Table 5.4). These energy profiles suggested that BC colloid aggregation and attachment to the sand would be highly favorable under pH4IS10 and pH7IS100 conditions, and much less favorable at pH7IS10 and pH10IS10.

Table 5.4. Total DLVO interaction energy parameters for 1 µm biochar colloid interacting with another colloid or the solid-water interface (SWI) as function of pH and ionic strength [a].

pH	IS (mM)	Colloid-SWI interaction			Colloid-Colloid interaction		
		Φ_{1min} (kT)	Φ_{max} (kT)	Φ_{2min} (kT)	Φ_{1min} (kT)	Φ_{max} (kT)	Φ_{2min} (kT)
4.2 ± 0.2	10	-661	29.2	-8.2	-108	n/a (<0)[c]	n/a (<0)
6.8 ± 0.1	10	n/a (>0)[b]	879	-5.8	n/a (>0)	1.4×10^9	-8.7
6.7 ± 0.1	100	-195	23.7	-33.4	-91.1	n/a (<0)	n/a (<0)
10.0 ± 0.1	10	n/a (>0)	1650	-5.3	n/a (>0)	1.4×10^9	-7.2

[a] Φ_{1min} = the depth of the primary energy minimum; Φ_{max} = the height of the primary energy barrier; Φ_{2min} = the depth of the secondary energy minimum; k = Boltzmann constant; and T = temperature in Kelvin

[b] n/a (>0) means that the negative energy minimum is not available

[c] n/a (<0) means that the energy profile is always negative after the primary energy minimum

Particle size measurement

Representative BFM and TEM images of the BC particles in the influents and effluents are shown in Figure 5.3. The particle analyses showed that BC particles had very irregular shapes and a wide size distribution (Table 5.5, Figure 5.3, and Figure 5.4). Although the particles smaller than 10 µm were dominant in number in both influents and effluents, their percentage by mass was small in the influents and became more significant in the effluents (Figure 5.4). The largest effluent Feret's diameter (d_F), major axis (X_1), and minor axis (X_2) were 21.4, 19.8, and 8.5 µm in the

effluents (Table 5.2). Other larger particles present in the influent were filtered out of suspension during passage through the media (Figure 5.4). The smallest measured BC particles were 2.4 ± 0.5 nm in the influent and 2.2 ± 0.6 nm in the effluent, as estimated from TEM images (Figure 5.3). The existence of these BC nanoparticles in the bulk solution was confirmed by dynamic light scattering, measuring the particles of 1.4 ± 0.6 nm and 1.3 ± 0.5 nm in the influent and effluents. Because the irregular shape of BC particles, in order to obtain a representative estimation for the ratio of the largest effluent particle to mean grain diameter it was determined based on d_F, X_1, and X_2, which was 0.054 (d_F/d_{50}), 0.050 (X_1/d_{50}), and 0.021 (X_2/d_{50}). Since d_F/d_{50} is the upper limit of the ratio, it can be said that particles with the size smaller than 5.4% of the median grain diameter may pass through the media, while other larger particles will be removed by mechanical filtration or straining.

Table 5.5. Summary of biochar particle size in the influent and effluent [a].

Conditions			A_p (μm^2)	P (μm)	d_F (μm)	X_1 (μm)	X_2 (μm)	AR
pH7IS10	Influent	Max	4300	615	159	151	43.9	10.0
		Min	0.2	1.2	0.6	0.6	0.3	1.0
		Mean	22.7	10.1	3.4	3.0	1.5	2.0
		(Stdev)	(155)	(30.6)	(8.5)	(7.7)	(3.4)	(0.8)
	Effluent	Max	123	67.3	20.3	18.3	8.5	5.2
		Min	0.1	1.1	0.5	0.4	0.2	1.0
		Mean	2.0	4.5	1.7	1.5	0.8	2.0
		(Stdev)	(9.9)	(6.6)	(2.0)	(1.8)	(0.8)	(0.7)
pH10IS10	Influent	Max	2500	489	109	110	40.8	11.8
		Min	0.2	1.2	0.6	0.6	0.3	1.0
		Mean	18.9	10.3	3.4	3.1	1.5	2.0
		(Stdev)	(110)	(29.2)	(8.1)	(7.4)	(3.1)	(0.8)
	Effluent	Max	86.9	56.8	21.4	19.8	6.4	7.9
		Min	0.2	1.2	0.6	0.6	0.3	1.0
		Mean	3.1	6.4	2.5	2.2	1.0	2.2
		(Stdev)	(7.5)	(7.3)	(2.5)	(2.2)	(0.9)	(1.0)

[a] A_p is the two dimensional area of particle; P = the perimeter of particle; d_F = Feret's diameter; X_1 = the major axis; X_2 = the minor axis; AR = the aspect ratio (X_1/X_2)

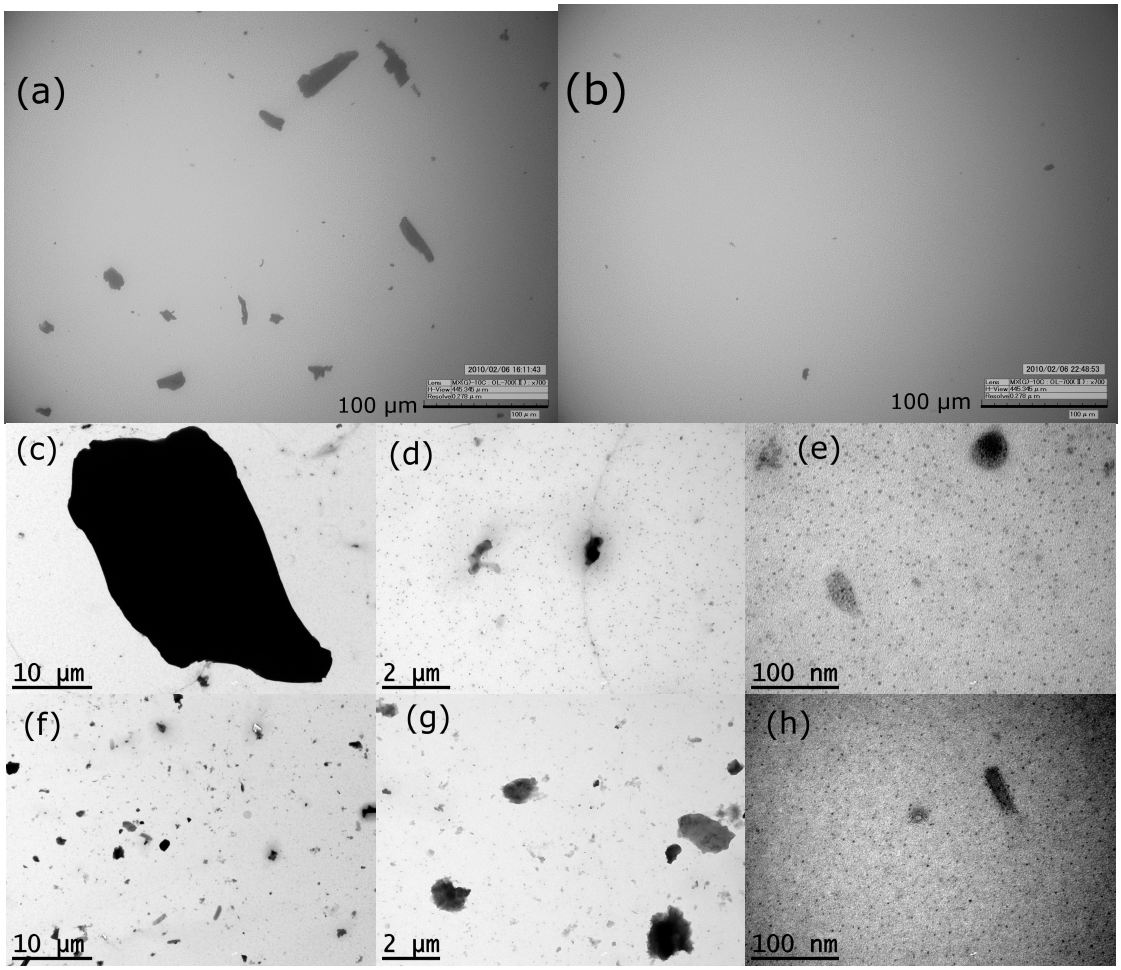

Figure 5.3. Microscopic images of biochar particles in the column influent and effluent under pH = 10 and IS = 10 mM, taken by bright field microscopy (a, b) and transmission electron microscopy (c, d, e, f, g, h): (a) biochar in the influent; (b) biochar in the effluent; (c, d, e) biochar in the influent; (f, g, h) biochar in the effluent.

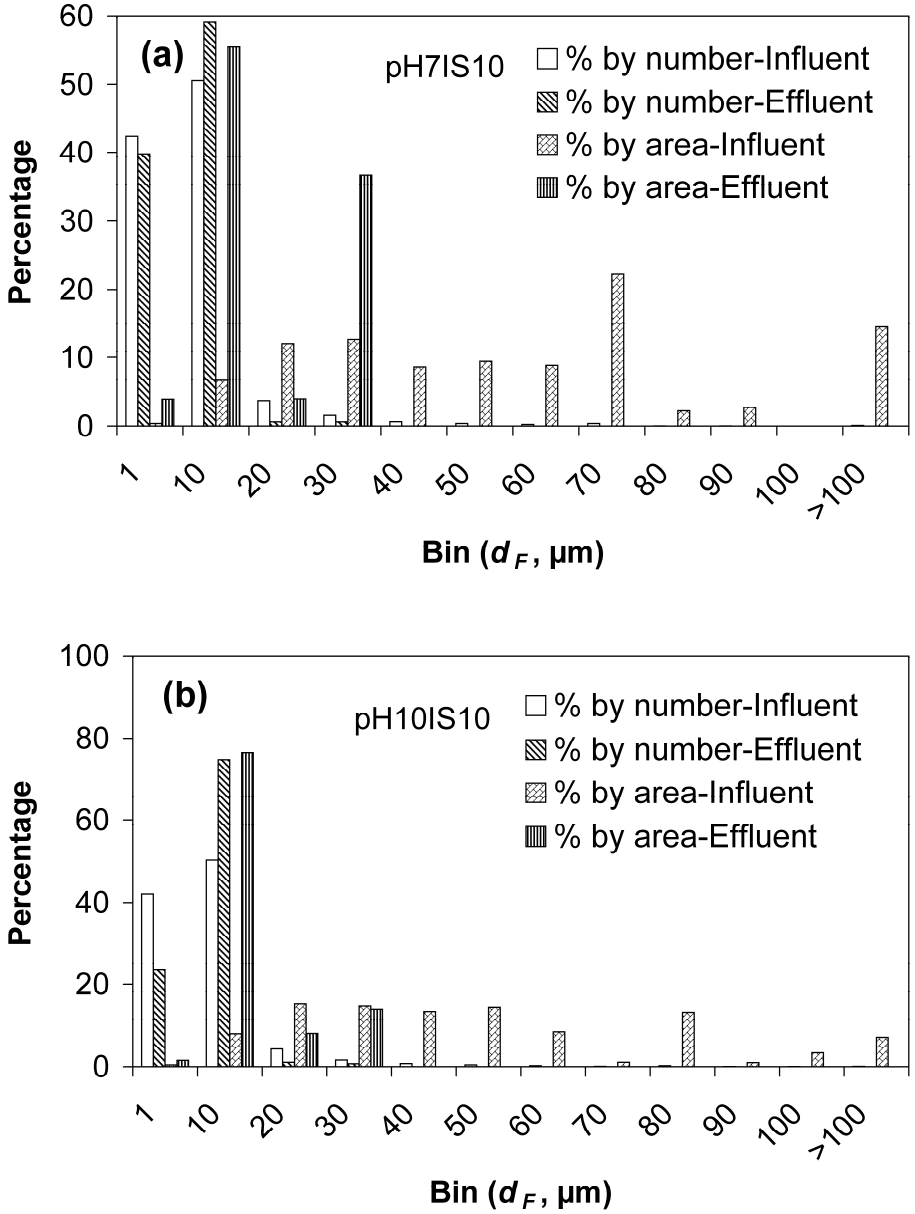

Figure 5.4. Particle size distribution in the column influents and effluents: (a) pH = 7 and IS = 10 mM; (b) pH = 10 and IS = 10 mM.

Discussion

Biochar particle transport and retention

The transport and retention of BC particles were strongly dependent on pH and ionic strength, which agreed with the studies on other types of colloids (DeNovio et al., 2004; Bradford et al., 2008). At the lower solution pH, the BC particles were less negatively charged (Table 5.3), thus reducing electrostatic repulsion, whereas greater ionic strength decreased the electric double layer thickness and weakened electrostatic repulsion (Figure 5.S2).

The BC particles had a wide size distribution from a few tens of microns to a few nanometers, similar to the BC particles observed in the field (Skjemstad et al., 1996; Lehmann et al., 2007b). Thus, while the mechanisms of mechanical filtration, attachment, and straining (Bradford et al., 2006) all likely contribute to the BC retention, the transport of smaller particles was most likely affected by colloidal interactions that lead to attachment or aggregation. It was not possible to discern the exact contribution of each retention mechanism to the retention of each particle size class because accurate measurement of effluent particle mass based on the size class is extremely difficult, considering the wide size distribution and irregular particle shapes. Nonetheless, in principle, it was expected that the larger particles ($d_F > 21.4$ μm) were to a greater extent retained by mechanical filtration, whereas the transport of the smaller ones ($d_F < 21.4$ μm) was clearly dependent on attachment, as influenced by solution chemistry. For straining to occur in uniform sand it has been estimated from geometric relations that the ratio of particle to median grain diameter needs to be greater than 0.18, however, ratios as low as 0.003 have also been previously observed (Bradford et al., 2006). Here, the ratio of the largest effluent particle to median grain diameter ranged from 0.021 to 0.054, indicating straining could be an important process for the BC retention. Additionally, straining is coupled with colloidal

interactions in that straining sites (e.g., small soil pores, wedge-shaped pore spaces, etc.) are optimum locations for colloid attachment due to reduced flow drag force, and colloidal interactions enhance straining (Bradford et al., 2006, 2007).

More evidence supporting the effect of solution chemistry on the BC retention is shown in the trends of deposition rate coefficients with pH and ionic strength (Figure 5.2). These trends quantitatively agreed with DLVO interaction energy profiles. Interestingly, it was noted that greater attractive colloidal interactions resulted in greater particle mass transfer between the mobile and immobile regions in unsaturated media (Figure 5.2b). When chemical interactions are more attractive, there would be a greater number of particles in the proximity of the sand surface, which could be transported to the immobile regions (i.e., the corner of wedge-shaped soil pore space) by the funneling flow (Bradford et al., 2006; Torkzaban et al., 2008; Zevi et al., 2009).

As expected, the BC particle retention was significantly greater in unsaturated experiments than in saturated experiments (Cherrey et al., 2003; Bradford et al., 2006). This effect is likely a result of the flow restricted to smaller soil pore spaces and the expansion of immobile water region at lower moisture content, thus resulting in greater deposition rates (Cherrey et al., 2003; Bradford et al., 2006; Gao et al., 2006; Zhang et al., 2010). Although it is difficult to assess the degree to which this enhancement of retention will affect particles of various sizes, it is anticipated that it will preferentially increase the retention of larger particles because water flow is restricted to smaller soil pore spaces, which allows the retention of larger particles but the passage of smaller ones (Bradford et al., 2006).

For the tested biochar, the size fraction (< 75 μm) used in this study accounted for approximately 40% (by weight) of the total BC powder. The greatest effluent recoveries occurred in the saturated experiments of pH10IS10 and about 29% of the input mass (approximately 12% of the total original mass) was eluted. The transport

of BC was smallest at pH of 4 (less than 2% of the total mass). Although our result is directly applicable to coarse sandy soils or sediments, the fraction transported in finer textured soils would likely be different.

Implications

The results of this study suggest that the BC transport by soil matrix flow in the field is expected to heavily depend on soil water chemistry (i.e., pH and ionic strength) and particle size. Attachment or sorption of BC to soil minerals equally depends on soil pH, as the positive charge of variable-charge iron or alumina oxides may significantly decrease at high pH (e.g., 9.7) (Kosmulski, 2001) and may partially explain the observed difference in leaching at different soil pH. Guggenberger et al. (2008) observed that the lowest BC concentrations in the stream they monitored occurred during the summer low flow period when stream pH was 9.7. They implied that it could have been due to the sorption of BC to the mineral soil, but did not explicitly consider soil pH. Thus, there is an evident need to consider the chemistry of soil and soil water when interpreting the mobility and transport of BC in the field. The BC particle size also played a role, as particles larger than 5.4% of median grain diameter were not eluted. However, only a few studies considered the particle size when studying the BC mobility. Skjemstad et al. (1999) suggested that the BC accumulation in deeper soil depth might be because of its fine particle size. Brodowski et al. (2007) conjectured that the BC movement down the soil profile may be due to leaching of smaller BC particles. Nonetheless, the ratio of particle to median grain diameter needs to be considered in combination with soil water chemistry because of the complex interplay of physical and chemical mechanisms in colloid retention (Bradford et al., 2006; Bradford et al., 2007).

Additionally, as observed in other studies (Cherrey et al., 2003; Bradford et al., 2006), the transport of BC particles decreased by lowering water content, thus

suggesting that saturated flow transported more BC particles than unsaturated flow. Also, in the artificially drained agricultural field the subsurface transport of particles may be facilitated by tile drains (Sims et al., 1998; Laubel et al., 1999; Schelde et al., 2006). Although soil moisture content in most agricultural soils is usually at field capacity or less, saturated conditions often occur in undulating landscapes containing glaciated soils with relatively permeable shallow top soil underlain by a dense slowly permeable fragipan (e.g., the northeastern U.S.). The areas prone to saturation are known as variable source areas (VSAs) because the extent of saturation varies with rainfall and other factors (Walter et al., 2000). In New York City watershed Walter et al. (2000) estimated that VSAs could be 10% of total watershed area and generate 20% of total annual runoff. Thus, when the BC is applied in the VSAs of agricultural field, both surface overland flow and saturated subsurface flow (facilitated by tile drainage) may export a significant amount of BC if the areas are close to field ditch or natural waterways.

Although this study was conducted in a model system within a short-term, its results could be well linked with field-scale phenomena. BC mobilization and transport in the field most likely occur during a rainfall or irrigation event that takes place in a short time (Laubel et al., 1999; DeNovio et al., 2004; Schelde et al., 2006). Thus, this study helps understand the effect of soil water chemistry on the BC mobility, in addition to the water flux. Additionally, the BC transport in the field would be facilitated by a number of other factors, including macropore or preferential flow (McDowell-Boyer et al., 1986; Laudel et al., 1999; Schelde et al., 2006; Major et al., 2010), bioturbation (Carcaillet et al., 2001; Brodowski et al., 2007), or tillage (Skjemstad et al., 1999), which warrant further studies.

Conclusions

The findings of this study suggest that soil properties (e.g., soil pH, total salt concentrations) need to be considered for assessing the BC mobility in the field, because BC particle retention increased with lowering pH and increasing ionic strength. As the ratio of particle to median grain diameter was an important factor, BC particle size and soil texture also warrant serious consideration. Additionally, because the greater amount of BC was transported under saturated conditions, compared with unsaturated conditions, local hydrology (e.g., soil water saturation) is an important driver of the BC transport. The long-term vertical transport of BC is likely a cumulative result of the BC movement due to the reoccurring transport by water infiltration and drainage (e.g., soil matrix flow, macropore or preferential flow), and physical mixing by earth worms or tillage.

Acknowledgement

The funding for this research was primarily provided by USDA-NRI, BARD, and NSF with additional funding from USDA Hatch. The authors like to thank Dr. Yuanming Zhang at Cornell Center for Materials Research for help on transmission electron microscopy and dynamic light scattering measurements and Dr. Bin Gao at University of Florida for sharing the KDRM Matlab code.

APPENDIX

S1. Modeling

Here, we presented the other two models for the particle transport in saturated media and compared them with the KEDM model. The governing equation for the model with a kinetic deposition and release terms (i.e., KDRM) is

$$\frac{\partial C}{\partial t} = D\frac{\partial^2 C}{\partial z^2} - v\frac{\partial C}{\partial z} - \frac{\rho_b}{\theta}\frac{\partial S}{\partial t} \qquad \text{(A1.1)}$$

$$\frac{\partial S}{\partial t} = \frac{\theta}{\rho_b}k_d C - k_r S \qquad \text{(A1.2)}$$

where k_r (min^{-1}) is the first-order release coefficient and S (mg kg^{-1}) is the deposited particle concentration in the solid phase. For the model with only the deposition term (i.e., KDM), the governing equation becomes

$$\frac{\partial C}{\partial t} = D\frac{\partial^2 C}{\partial z^2} - v\frac{\partial C}{\partial z} - k_d C \qquad \text{(A1.3)}$$

The KDM model was implemented in CXTFIT 2.1 and the KDRM model in Matlab (The Mathworks, Natick, MA). The dispersion coefficient (D) of bromide was used when fitting the KDRM, whereas it was estimated as a fitting parameter in the KDM. We also used the D values from the KEDM when fitting the KDRM and found that the estimates of k_d were insensitive to the choice of the D values (Figure 5.S1a). This insensitivity to D is simply because these experiments had a high Peclet number (Pe = vL/D, $43 < Pe < 121$). When Pe is high (e.g., Pe > 50), the dispersion term in eq. A1.1 becomes negligible, and the k_d estimation is minimally related to D (Kretzschmar et al., 1997; Akbour et al., 2002). Compared with the KDM and KDRM models, the KEDM gave the overall best fit ($R^2 > 0.992$), although the k_d estimates from all three models (KEDM, KDM, and KDRM) differed by less than 7% (Figure 5.S1a). Due to the explicit release term in the KDRM and its absence in the KDM, the experimental BTCs tails were overestimated by the KDRM and underestimated by the KDM in

seven out of eight cases as exemplified in Figure 5.S1b. Thus, the KEDM was selected.

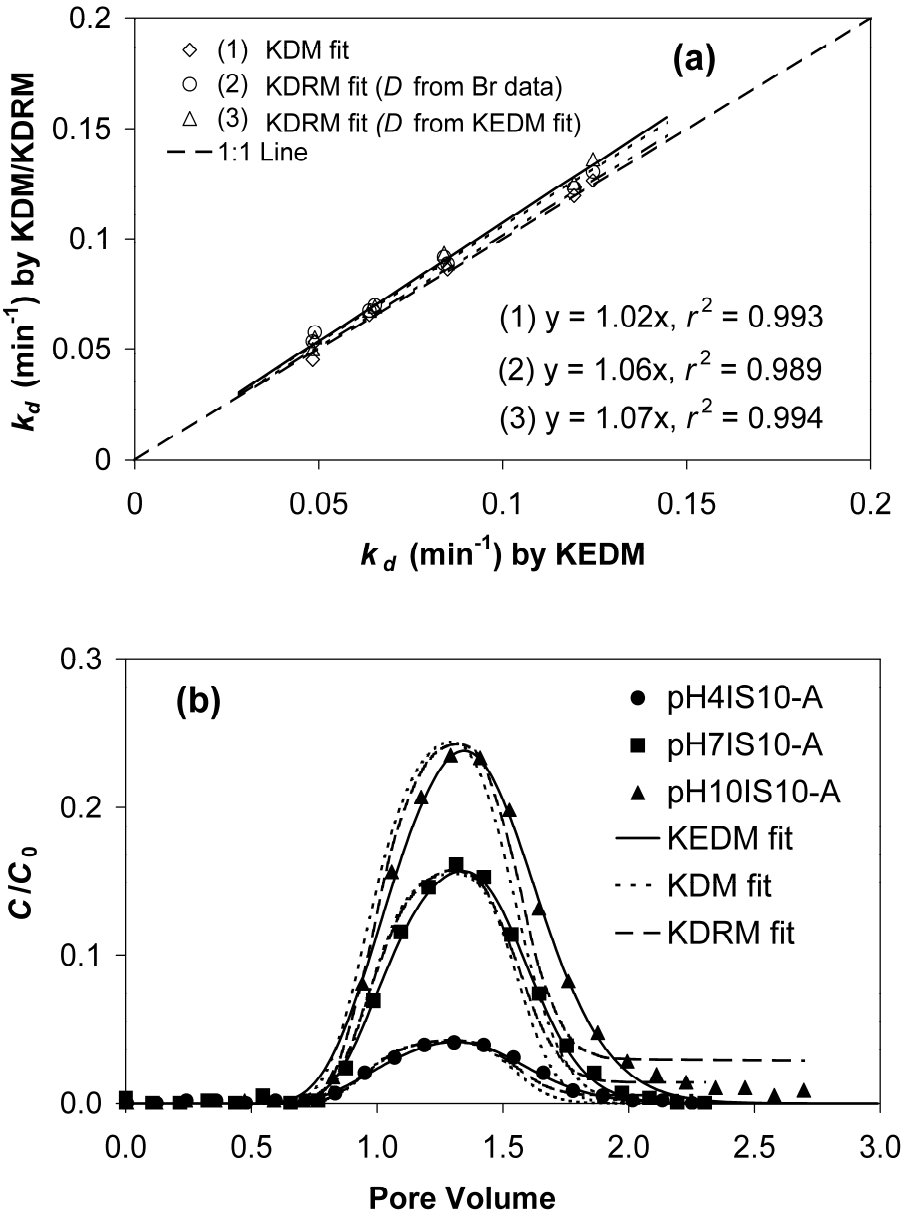

Figure 5.S1. Comparison among the kinetic and equilibrium deposition model (KEDM), the kinetic deposition model (KDM), and the kinetic deposition and release model (KDRM) for biochar transport in saturated media: (a) comparison of deposition rate coefficient (k_d); (b) Comparison of fitted breakthrough curves.

S2. DLVO Calculations

Here, we presented the detailed equations for the DLVO energy calculations. The total DLVO interaction energy (Φ) is determined as a function of separation distance (x)

$$\Phi(x) = \Phi^{LVW}(x) + \Phi^{EDL}(x) + \Phi^{BNR}(x) \qquad \text{(A2.1)}$$

For Colloid-Colloid interaction, the non-retarded Lifshitz-van der Waals interaction energy [$\Phi^{LVW}(x)$] can be calculated as (Hamaker et al., 1937)

$$\Phi^{LVW}(x) = -\frac{A}{12}\left\{\frac{y}{r^2+ry+r} + \frac{y}{r^2+ry+r+y} + 2\ln\left(\frac{r^2+ry+r}{r^2+ry+r+y}\right)\right\} \qquad \text{(A2.2)}$$

where $y = 1$ for the ratio of the radii of two identical spheres, $r = x/(2a_c)$ and a_c is the sphere radius, and A is the Hamaker constant. For Colloid-SWI and Colloid-AWI interactions, the expression is (Norde and Lyklema, 1989)

$$\Phi^{LVW}(x) = -\frac{A}{6}\left\{\frac{2a_c(x+a_c)}{x(x+2a_c)} - \ln\left(\frac{x+2a_c}{x}\right)\right\} \qquad \text{(A2.3)}$$

We used the Hamaker constant of polystyrene to approximate the values of BC. The Hamaker constant is 1.3×10^{-20} J for colloid-water-colloid interaction, 8.9×10^{-21} J for colloid-water-sand interaction, and -1.6×10^{-20} J for colloid-water-air interaction (Zevi et al., 2009).

Assuming constant surface potentials, $\Phi^{EDL}(x)$ of Colloid-SWI or Colloid-AWI interactions is (Hogg et al, 1966; Hoek and Agarwal, 2006)

$$\Phi^{EDL}(x) = \pi\varepsilon\varepsilon_0 a_c\left\{2\psi_1\psi_2\ln\left[\frac{1+\exp(-\kappa x)}{1-\exp(-\kappa x)}\right] + (\psi_1^2+\psi_2^2)\ln[1-\exp(-2\kappa x)]\right\} \qquad \text{(A2.4)}$$

where ε is the dielectric constant of water (80.1 at 293.15 K), ε_0 is the vacuum permittivity (8.854×10^{-12} C^2 N^{-1} m^{-2}), ψ_1 and ψ_2 are the surface potentials of the colloid, and the sand or AWI. κ is the reciprocal electric double layer thickness (κ^{-1}).

$$\kappa^{-1} = \left(\frac{\varepsilon\varepsilon_0 kT}{2000 N_A I e^2}\right)^{1/2} \qquad \text{(A2.5)}$$

where k is Boltzmann constant (1.381×10^{-23} J K^{-1}), T is temperature in Kelvin, N_A is Avogadro constant (6.022×10^{23}), I is ionic strength (mole L^{-1}), and e is the elementary charge (1.602×10^{-19} C). $\Phi^{EDL}(x)$ between two identical colloids is

$$\Phi^{EDL}(x) = \pi\varepsilon\varepsilon_0 a_c \left\{ \psi_1^2 \ln\left[\frac{1+\exp(-\kappa x)}{1-\exp(-\kappa x)}\right] + \psi_1^2 \ln\left[1-\exp(-2\kappa x)\right] \right\} \qquad \text{(A2.6)}$$

Here, we used the measured ζ-potential (Table 5.3) in place of the surface potential (van Oss, 1994). The ζ-potential of AWI was estimated to be -20 mV at pH = 4 and IS = 10 mM, -30 mV at pH = 7 and IS = 10 mM, -25 mV at pH = 7 and IS = 100 mM, and -40 mV at pH = 10 and IS = 10 mM (Schäfer et al, 1998; Xu et al., 2007).

The Born repulsion (Φ^{BNR}) results from the overlap of the atoms' electron clouds and is of short-range. Φ^{BNR} for Colloid-SWI or Colloid-AWI interactions is (Ruckenstein and Prieve, 1976)

$$\Phi^{BNR}(x) = \frac{A\sigma^6}{7560}\left[\frac{8a_c + x}{(2a_c + x)^7} + \frac{6a_c - x}{x^7}\right] \qquad \text{(A2.7)}$$

where σ is the collision diameter (0.5 nm). $\Phi^{BNR}(x)$ for Colloid-Colloid interaction is (Feke et al., 1984)

$$\Phi^{BNR}(x) = 4A\left(\frac{\sigma}{a_c}\right)^6 \frac{4!}{10!}\left[\frac{(x/a_c)^2 - 14x/a_c + 54}{(x/a_c - 2)^7} + \frac{-2(x/a_c)^2 + 60}{(x/a_c)^7} + \frac{(x/a_c)^2 + 14x/a_c + 54}{(x/a_c + 2)^7}\right] \qquad \text{(A2.8)}$$

The DLVO energy profiles for three types of colloidal interactions were presented at Figure 5.S2. In addition to the discussion in the main text, there was a great repulsive energy barrier between colloid and the air-water interface. There was no secondary energy minimum Φ_{2min} up to separation distance of 2000 nm. The negative primary energy for Colloid-AWI interaction stems from its negative Hamaker constant, which resulted in the negative Born repulsion. This Φ_{1min} is irrelevant here because the colloids could hardly pass over the high energy barrier to reach this minimum.

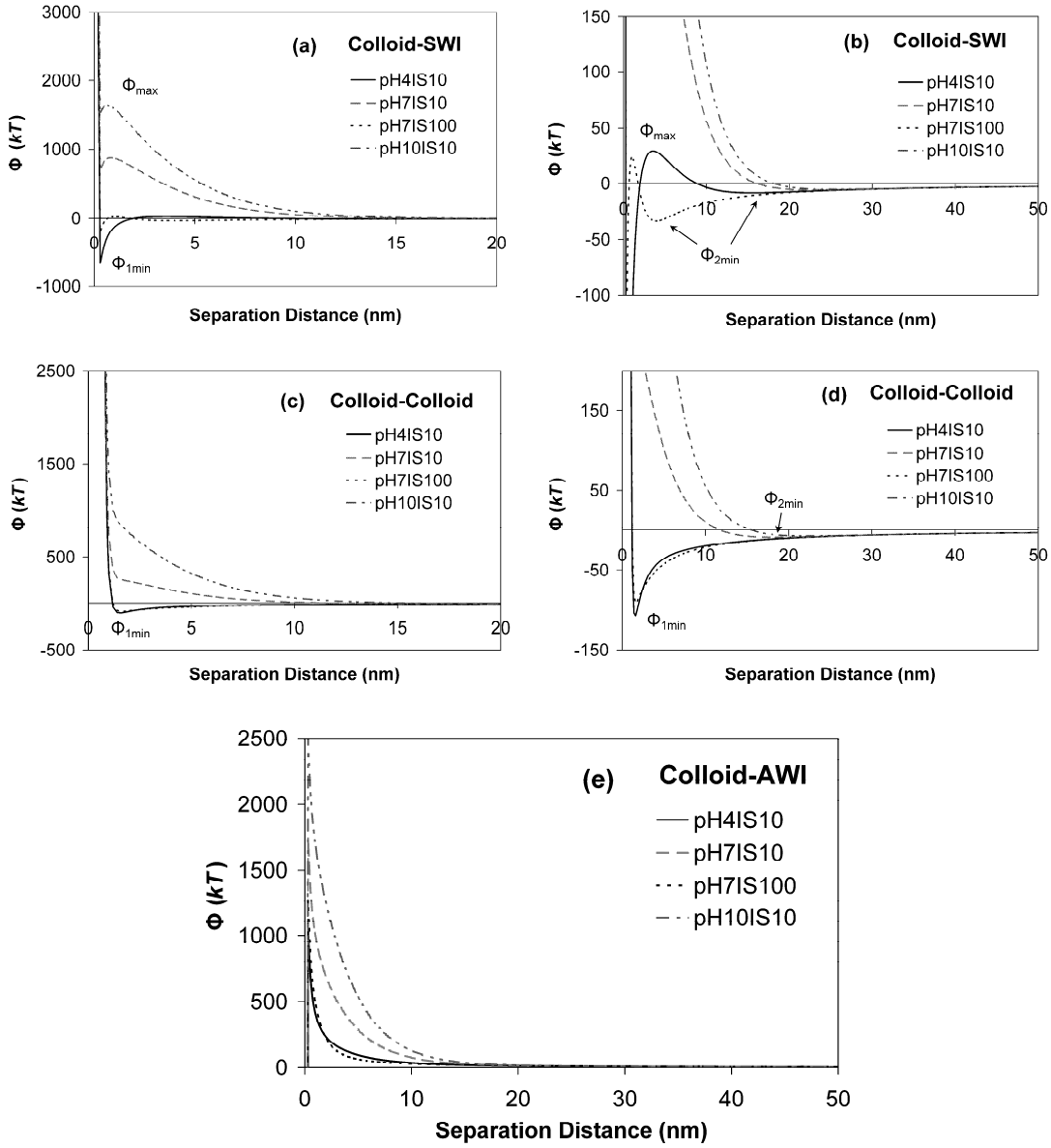

Figure 5.S2. DLVO interaction energy (Φ) of a 1 µm biochar colloid interacting the solid-water interface (SWI), another colloid, and the air-water interface (AWI): (a) Primary energy minimum (Φ_{1min}) and primary energy barrier (Φ_{max}) of Colloid-SWI interactions; (b) Secondary energy minimum (Φ_{2min}) of Colloid-SWI interactions; (c) Φ_{1min} and Φ_{max} of Colloid-Colloid interactions; (d) Φ_{2min} of Colloid-Colloid interactions; (e) Colloid-AWI interactions.

APPENDIX REFERENCES

Akbour, R.A., J. Douch, M. Hamdani, and P. Schmitz. 2002. Transport of kaolinite colloids through quartz sand: Influence of humic acid, Ca2+, and trace metals. *J. Colloid Interface Sci.* 253: 1–8.

Feke, D.L., N.D. Prabhu, Jr.J.A. Mann, and J.A. Mann III. 1984. A formulation of the short-range repulsion between spherical colloidal particles. *J. Phys. Chem.* 88(23): 5735–5739.

Hamaker, H.C. 1937. The London-van der Waals attraction between spherical particles. *Physica* 4: 1058–1072.

Hoek, E.M.V., and G.K. Agarwal. 2006. Extended DLVO interactions between spherical particles and rough surfaces. *J. Colloid Interface Sci.* 298: 50–58.

Hogg, R., T.W. Healy, and D.W. Fuerstenau. 1966. Mutual coagulation of colloidal dispersions. *Trans. Faraday Soc.* 62: 1638–1651.

Kretzschmar, R., K. Barmettler, D. Grolimund, Y.-D. Yan, M. Borkovee, and H. Sticher. 1997. Experimental determination of colloid deposition rates and collision efficiencies in natural porous media. *Water Resour. Res.* 33(5): 1129–1137.

Norde, W., and J. Lyklema. 1989. Protein adsorption and bacterial adhesion to solid-surfaces—A colloid-chemical approach. *Colloids Surf.* 38: 1–13.

Ruckenstein, E., and D.C. Prieve. 1976. Adsorption and desoprtion of particles and their chromatographic separation. *AIChE J.* 22(2): 276–283.

Schäfer, A., H. Harms, and A.J.B. Zehnder. 1998. Bacterial accumulation at the air-water interface. *Environ. Sci. Technol.* 32(23): 3704–3712.

Xu, R., C. Wu, and H. Xu. 2007. Particle size and zeta potential of carbon black in liquid media. *Carbon* 45: 2806–2809.

van Oss, C.J. 1994. Interfacial forces in aqueous media. Marcel Dekker, New York, NY.

Zevi, Y., A. Dathe, B. Gao, W. Zhang, B.K. Brian, and T.S. Steenhuis. 2009. Transport and retention of colloidal particles in partially saturated porous media: effect of ionic strength. Water Resour. Res. 45: W12403, doi:10.1029/2008WR007322.

REFERENCES

Bradford, S.A., J., Šimůnek, M. Bettahar, M.T. van Genuchten, and S.R. Yates. 2006. Significance of straining in colloid deposition: Evidence and implications. *Water Resour. Res.* 42: W12S15, doi:10.1029/2005WR004791.

Bradford, S.A., S. Torkzaban, and S.L. Walker. 2007. Coupling of physical and chemical mechanisms of colloid straining in saturated porous media. *Water Res.* 41: 3012–3024.

Bradford, S.A., and S. Torkzaban. 2008. Colloid transport and retention in unsaturated porous media: A review of interface-, collector-, and pore-scale processes and models. *Vadose Zone J.* 7(2): 667–681.

Brodowski, S., W. Amelung, L. Haumaier, C. Abetz, and W. Zech. 2005. Morphological and chemical properties of black carbon in physical soil fractions as revealed by scanning electron microscopy and energy-dispersive X-ray spectroscopy. *Geoderma* 128: 116–129.

Brodowski, S., W. Amelung, L. Haumaier, W. Zech. 2007. Black carbon contribution to stable humus in German arable soils. *Geoderma* 139: 220–228.

Cao, X., L. Ma, B. Gao, and W. Harris. 2009. Dariy-manure derived biochar effectively sorbs lead and atrazine. *Environ. Sci. Technol.* 43(9): 3285–3291.

Chen, B., D. Zhou, and L. Zhu. 2008. Transitional adsorption and partition of nonpolar and polar aromatic contaminants by biochars of pine needles with different pyrolytic temperatures. *Environ. Sci. Technol.* 42(14): 5137–5143.

Chen, G., T. Abichou, K. Tawfiq, and P.K. Subramaniam. 2007. Impact of surface charge density on colloid deposition in unsaturated porous media. *Colloids Surf. A: Physicochem. Eng. Aspects* 302: 342–348.

Cherrey, K.D., M. Flury, and J.B. Harsh. 2003. Nitrate and colloid transport through coarse Hanford sediments under steady state, variably saturated flow. *Water Resour. Res.* 39(6): 1165, doi:10.1029/2002WR001944.

Carcaillet, C. 2001. Are Holocene wood-charcoal fragments stratified in alpine and subalpine soils? Evidence from the Alps based on AMS 14C dates. *The Holocene* 11(2): 231–242.

Czimczik, C.I., M.W.I. Schmidt, and E.-D. Schulze. 2005. Effects of increasing fire frequency on black carbon and organic matter in Podzols of Siberian Scots pine forests. *Eur. J. Soil Sci.* 56: 417–428.

Czimczik, C.I., and C.A. Masiello. 2007. Controls on black carbon storage in soils. *Global Biogeochem. Cy.* 21: GB3005, doi:10.1029/2006GB002798.

Dai, X., T.W. Boutton, B. Glaser, R.J. Ansley, and W. Zech. 2005. Black carbon in a temperate mixed-grass savanna. *Soil Biol. Biochem.* 37: 1879–1881.

DeNicola, D.M. 2000. A review of diatoms found in highly acidic environments. *Hydrobiologia* 433: 111–122.

DeNovio, N.M., J.E. Saiers, and J.N. Ryan. 2004. Colloid movement in unsaturated porous media: Recent advances and future directions. *Vadose Zone J.* 3: 338–351.

Fraiser, B. 2010. High-tech charcoal fights climate change. *Environ. Sci. Technol.* 44(2): 548–549.

Gao, B., and J.E. Saiers. 2006. Pore-scale mechanisms of colloid deposition and mobilization during steady and transient flow through unsaturated granular media. Water Resour. Res. 42: W01410, doi:10.1029/2005WR004233.

Gaunt, J.L., and J. Lehmann. 2008. Energy balance and emissions associated with biochar sequestration and pyrolysis bioenergy production. *Environ. Sci. Technol.* 42(11): 4152–4158.

Guggenberger, G., A. Rodionov, O. Shibistova, M. Grabe, O.A. Kasansky, H. Fuchs, N. Mikheyeva, G. Zrazhevskaya, and H. Flessa. 2008. Storage and mobility of black carbon in permafrost soils of the forest tundra ecotone in Northern Siberia. *Global Change Biology* 14: 1367–1381.

Hockaday, W.C., A.M. Grannas, S. Kim, and P.G. Hatcher. 2006. Direct molecular evidence for the degradation and mobility of black carbon in soils from ulatrahigh-resolution mass spectral analysis of dissolved organic matter from a fire-impacted forest soil. *Org. Geochem.* 37(4): 501–510.

Hockaday, W.C., A.M. Grannas, S. Kim, and P.G. Hatcher. 2007. The transformation and mobility of charcoal in a fire-impacted watershed. *Geochim. Cosmochim. Ac.* 71: 3432–3445.

Kosmulski, M. 2001. Chemical properties of material surfaces. Marcel Dekker, New York, NY.

Laubel, A., O.H. Jacobsen, B.K. Kronvang, R. Grant, and H.E. Anderson. 1999. Subsurface drainage loss of particles and phosphorus from field plot experiments and a tile-drained catchment. *J. Environ. Qual.* 28: 576-584.

Lehmann, J., J. Gaunt, and M. Rondon. 2006. Bio-char sequestration in terrestrial ecosystems – A review. *Mitigation and Adaptation Strategies for Global Change* 11: 403–427.

Lehmann, J. 2007a. A handful of carbon. *Nature* 447: 143–144.

Lehmann, J. 2007b. Bio-energy in the black. *Front. Ecol. Environ.* 5(7): 381–387.

Lehmann, J., and S. Sohi. 2008. Comment on "Fire-derived charcoal causes loss of forest humus'. *Science* 321: 1295c.

Leifeld, J., S. Fenner, and M. Müller. 2007. Mobility of black carbon in drained peatland soils. *Biogeosciences* 4: 425–432.

Major, J., J. Lehmann, M. Rondon, and C. Goodale. 2010. Fate of soil-applied black carbon: downward migration, leaching, and soil respiration. *Global Change Biology* 16(4): 1366–1379.

Mannino, A., and H.R. Harvey. 2004. Black carbon in estuarine and coastal ocean dissolved organic matter. *Limnol. Oceanogr.* 49(3): 735-740.

Marris, E. 2006. Putting the carbon back: Black is the new green. *Nature* 442: 624–626.

Masiello, C.A., and E.R.M. Druffel. 2001. Carbon isotope geochemistry of the Santa Clara River. *Global Biogeochem. Cy.* 15(2): 407–416.

McDowell-Boyer, L.M., J.R. Hunt, and N. Sitar. 1986. Particle transport through porous media. *Water Resour. Res.* 22(13): 1901–1921.

Mitra, S., T.S. Bianchi, B.A. McKee, and M. Sutula. 2002. Black carbon from the Mississippi River: Quantities, sources, and potential implications for the global carbon cycle. *Environ. Sci. Technol.* 36 (11): 2296–2302.

Morales, V.L., B. Gao, and T.S. Steenhuis. 2009. Grain surface-roughness effects on colloid retention in the vadose zone. *Vadose Zone J.* 8(1): 11–20.

Pietikäinen, J., O. Kiikkilä, and H. Fritze. 2000. Charcoal as a habitat for microbes and its effect on the microbial community of the underlying humus. *Oikos* 89: 231–242.

Renner, R. 2007. Rethinking biochar. *Environ. Sci. Technol.* 41(17): 5932–5933.

Roberts, K.G., B.A. Gloy, S. Joseph, N.R. Scott, and J. Lehmann. 2010. Life cycle assessment of biochar systems: Estimating the energetic, economic, and climate change potential. *Environ. Sci. Technol.* 44(2): 827–833.

Rumpel, C., V. Chaplot, O. Planchon, J. Bernadou, C. Valentin, and A. Mariotti. 2006. Preferential erosion of black carbon on steep slopes with slash and burn agriculture. *Catena* 65: 30–40.

Schelde, K., L.W. de Jonge, C. Kjaergaard, M. Laegdsmand, and G.H. Rubaek. 2006. Effects of manure application and plowing on transport of colloids and phosphorus to tile drains. *Vadose Zone J.* 5: 445–458.

Sims, J.T., R.R. Simard, and B.C. Joern. 1998. Phosphorus loss in agricultural drainage: historical perspective and current research. *J. Environ. Qual.* 27: 277-293.

Sparks, D.L. 2003. Environmental Soil Chemistry. Academic Press. San Diego, CA.

Skjemstad, J.O., P. Clarke, J.A. Taylor, J.M. Oades, and S.G. McClure. 1996. The chemistry and nature of protected carbon in soil. *Aust. J. Soil Res.* 34: 251–271.

Skjemstad, J.O., J.A. Taylor, L.J. Janik, and S.P. Marvanek. 1999. Soil organic carbon dynamics under long-term sugarcane monoculture. *Aust. J. Soil Res.* 37: 151–164.

Smith, J., B. Gao, H. Funabashi, T.N. Tran, D. Luo, B.A. Ahner, T.S. Steenhuis, A.G. Hay, and M.T. Walter. 2008. Pore-scale quantification of colloid transport in saturated porous media. *Environ. Sci. Techno.* 42(2): 517–523.

Toride, N., F.J. Leij, and M.T. van Genuchten. 1995. The CXTFIT code for estimating transport parameters from laboratory or field tracer experiments, version 2.1, Res. Rep. 137, U.S. Salinity Lab., Riverside, CA.

Torkzaban, S., S.S. Tazehkand, S.L. Walker, and S.A. Bradford. 2008. Transport and fate of bacteria in porous media: Coupled effects of chemical conditions and pore space geometry. Water Resour. Res. 44: W04403, doi:10.1029/2007WR006541.

USDA. 1954. Diagnosis and improvement of saline and alkali soils. Ed.: L.A. Richards, Agriculture Handbook No. 60, U.S. Department of Agriculture, Washington, D.C.

Wardle, D.A., M.-C. Nilsson, and O. Zackrisson. 2008. Fire-derived charcoal causes loss of forest humus. *Science* 320: 629.

Walter, M.T., M.F. Walter, E.S. Brooks, T.S. Steenhuis, J. Boll, and K.R. Weiler. 2000. Hydrologically sensitive areas: variable source area hydrology implications for water quality risk assessment. *J. Soil and Water Conserv.* 3: 277-284.

Zevi, Y., A. Dathe, B. Gao, B.K. Richards, and T.S. Steenhuis. 2006. Quantifying colloid retention in partially saturated porous media. *Water Resour. Res.* 42: W12S03, doi:10.1029/2006WR004929.

Zevi, Y., A. Dathe, B. Gao, W. Zhang, B.K. Brian, and T.S. Steenhuis. 2009. Transport and retention of colloidal particles in partially saturated porous media: effect of ionic strength. *Water Resour. Res.* 45: W12403, doi:10.1029/2008WR007322.

Zhang, W., V.L. Morales, M.E. Cakmak, A.E. Salvucci, L.D. Geohring, A.G. Hay, J.-Y. Parlange, and T.S. Steenhuis. 2010. Colloid transport and retention in unsaturated porous media: Effect of colloid input concentration. *Environ. Sci. Technol.* (in press).

CHAPTER 6

CONCLUSIONS AND FUTURE WORK

In this dissertation the fate and transport of phosphorus (P), colloids, and biochar in soil environment was investigated using several experimentation and modeling techniques. For the studies on P transport, soil P sorption process of New York soils that have heavily received P applications were examined using batch P sorption experiments. For the studies on colloid transport, model colloids (carboxylated polystyrene microspheres) and non-ideal colloidal particles (biochar particles) were investigated. Major conclusions were outlined as follows:

I. The modified Langmuir model is a valid tool for P sorption studies of P-enriched New York soils.

II. Soil redox fluctuations, induced by saturated and unsaturated soil moisture regimes and microbial activity, may increase P sorption capacity of an organic-rich silt loam due to freshly precipitated amorphous iron hydroxides.

III. For the tested carboxylated polystyrene colloids, greater input concentration lead to greater colloid retention and this concentration effect was enhanced at higher ionic strength.

IV. The tested biochar particles exhibited greater mobility at higher pH and lower ionic strength, and saturated flow transported more biochar than unsaturated flow.

Building upon this work, future research will be directed to understanding how the coupling of chemical, biological, hydrological, and geological processes affect the solute transport and further studying the transport of natural and engineered colloids

(including nanomaterials). The study on the environment-relevant solute and particles are extremely important to the quality and sustainability of soil and water resources.

Appendix A: Phosphorus Sorption Data [a]

Test 1			Test 2			Test 1			Test 2		
M (g)	C_i	C	M (g)	C_i	C	M (g)	C_i	C	M (g)	C_i	C
	mg L^{-1}			mg L^{-1}			mg L^{-1}			mg L^{-1}	
Tompkins County site: Soil T1S, air-dried						Tompkins County site: Soil T1D, air-dried					
1.0043	0.00	0.58	1.0065	0.00	0.62	1.0034	0.00	0.06	1.0040	0.00	0.08
1.0026	0.92	0.74	1.0034	0.92	0.71	1.0025	0.92	0.08	1.0023	0.92	0.08
1.0004	4.36	1.11	1.0019	4.36	1.16	1.0048	4.59	0.43	1.0087	4.59	0.40
1.0028	8.93	2.20	1.0047	8.93	2.19	1.0014	9.93	2.19	1.0055	9.93	2.28
1.0029	49.52	24.28	1.0094	49.52	25.24	1.0101	49.31	32.41	1.0039	49.31	32.97
1.0040	97.36	65.28	1.0016	97.36	64.37	1.0060	96.07	75.63	1.0019	96.07	78.02
1.0037	197.25	156.98	1.0026	197.25	158.61	1.0039	198.24	173.06	1.0076	198.24	172.47
Tompkins County site: Soil T2S, air-dried						Tompkins County site: Soil T2D, air-dried					
1.0041	0.00	1.57	1.0013	0.00	1.68	1.0018	0.00	0.079	1.0015	0.00	0.072
1.0046	0.92	2.01	1.0018	0.92	1.87	1.0014	0.97	0.102	1.0045	0.97	0.094
1.0058	4.36	3.00	1.0028	4.36	3.03	1.0022	4.90	0.45	1.0053	4.90	0.47
1.0083	8.93	5.12	1.0022	8.93	4.99	1.0035	9.67	2.28	1.0095	9.67	2.36
1.0058	49.52	33.49	1.0023	49.52	32.80	1.0088	50.90	34.27	1.0016	50.90	34.43
1.0024	97.36	76.17	1.0048	97.36	73.50	1.0028	99.77	78.54	1.0068	99.77	79.33
1.0011	197.25	169.98	1.0017	197.25	167.88	1.0018	200.65	177.87	1.0014	200.65	178.24
Tompkins County site: Soil T4S, air-dried						Tompkins County site: Soil T4D, air-dried					
1.0022	0.00	1.99	1.0024	0.00	1.95	1.0017	0.00	0.049	1.0065	0.00	0.037
1.0059	0.92	2.29	1.0014	0.92	2.23	1.0104	0.92	0.057	1.0058	0.92	0.059
1.0036	4.36	3.99	1.0026	4.36	3.99	1.0028	4.59	0.33	1.0098	4.59	0.32
1.0089	8.93	6.38	1.0033	8.93	6.89	1.0012	9.93	2.51	1.0016	9.93	2.56
1.0024	49.52	39.04	1.0050	49.52	39.67	1.0017	49.31	35.78	1.0062	49.31	35.27
1.0024	97.36	86.58	1.0049	97.36	87.27	1.0096	96.07	82.84	1.0018	96.07	82.44
1.0011	197.25	179.06	1.0063	197.25	182.70	1.0046	198.24	178.78	1.0093	198.24	196.88
Wyoming County site: Soil W1S, air-dried						Wyoming County site: Soil W1D, air-dried					
1.0010	0.00	3.49	1.0019	0.00	3.46	1.0074	0.00	0.52	1.0083	0.00	0.46
1.0057	0.92	3.87	1.0061	0.92	3.96	1.0007	0.92	0.62	1.0048	0.92	0.63
1.0029	4.59	5.62	1.0031	4.59	5.73	1.0029	4.81	1.45	1.0066	4.81	1.44
1.0026	9.93	8.77	1.0038	9.93	8.73	1.0011	9.98	3.50	1.0018	9.98	3.36
1.0077	49.31	38.81	1.0028	49.31	37.62	1.0023	49.52	31.41	1.0044	49.52	32.12
1.0026	96.07	83.55	1.0024	96.07	83.11	1.0047	103.92	82.21	1.0011	103.92	81.01
1.0038	198.24	175.40	1.0068	198.24	178.52	1.0087	208.96	175.79	1.0029	208.96	178.28
Wyoming County site: Soil W2S, air-dried						Wyoming County site: Soil W2D, air-dried					
1.0026	0.00	3.860	1.0042	0.00	3.94	1.0054	0.00	0.14	1.0019	0.00	0.13
1.0053	0.92	4.42	1.0112	0.92	4.36	1.0099	0.92	0.19	1.0024	0.92	0.18
1.0035	4.59	6.22	1.0088	4.59	6.16	1.0015	4.81	0.57	1.0029	4.81	0.58
1.0098	9.93	9.36	1.0027	9.93	9.55	1.0009	9.98	2.13	1.0024	9.98	2.16
1.0073	49.31	40.29	1.0059	49.31	39.85	1.0038	49.52	30.37	1.0058	49.52	30.61
1.0085	96.07	84.52	1.0026	96.07	86.49	1.0062	103.92	80.96	1.0019	103.92	80.22
1.0089	208.96	188.22	1.0086	208.96	189.84	1.0044	208.96	176.86	1.0084	208.96	176.26
Wyoming County site: Soil W4S, air-dried						Wyoming County site: Soil W4D, air-dried					
1.0063	0.00	5.07	1.0010	0	5.34	1.0054	0.00	0.09	1.0059	0.00	0.08
1.0015	0.92	5.75	1.0070	0.9	5.79	1.0035	0.92	0.11	1.0036	0.92	0.11
1.0045	4.81	7.66	1.0089	4.8	7.82	1.0023	4.81	0.64	1.0005	4.81	0.62
1.0078	9.98	10.54	1.0026	10.0	10.67	1.0053	9.98	2.62	1.0074	9.98	2.79
1.0052	49.52	40.91	1.0006	49.5	40.97	1.0064	49.52	35.16	1.0050	49.52	34.99
1.0043	103.92	87.81	1.0089	103.9	91.22	1.0027	103.92	87.59	1.0014	103.92	87.40
1.0024	208.96	190.35	1.0058	209.0	186.44	1.0026	208.96	182.99	1.0088	208.96	190.58

[a] Experiments were conducted in 0.01 M KCl solution unless noted otherwise.

continue

Test 1			Test 2			Test 1			Test 2		
M (g)	C_i	C	M (g)	C_i	C	M (g)	C_i	C	M (g)	C_i	C
	mg L^{-1}			mg L^{-1}			mg L^{-1}			mg L^{-1}	
Delaware County site: Soil D1S, air-dried						Delaware County site: Soil D1D, air-dried					
1.0022	0.00	2.68	1.0019	0.00	2.76	1.0030	0.00	0.09	1.0032	0.00	0.10
1.0063	0.98	2.93	1.0076	0.98	2.96	1.0056	0.98	0.16	1.0036	0.98	0.15
1.0014	4.91	4.56	1.0098	4.91	4.51	1.0059	4.91	1.34	1.0085	4.91	1.33
1.0084	9.82	7.19	1.0020	9.82	7.17	1.0086	9.82	4.18	1.0005	9.82	4.18
1.0040	50.13	36.41	1.0011	50.13	36.11	1.0033	50.13	39.70	1.0033	50.13	39.70
1.0094	98.98	76.10	1.0064	98.98	78.53	0.9962	98.98	86.60	0.9962	98.98	86.60
1.0029	202.07	166.45	1.0018	202.07	167.68	0.9994	202.07	184.28	0.9994	202.07	184.28
Delaware County site: Soil D3S, air-dried						Delaware County site: Soil D3D, air-dried					
1.0024	0.00	0.32	1.0023	0.00	0.32	1.0048	0.00	0.086	1.0063	0.00	0.078
1.0036	0.98	0.39	1.0085	0.98	0.39	1.0018	0.98	0.092	1.0010	0.98	0.090
1.0015	4.91	0.91	1.0033	4.91	0.92	1.0012	4.91	0.74	1.0018	4.91	0.75
1.0031	9.82	2.10	1.0059	9.82	2.04	1.0065	9.82	2.68	1.0049	9.82	2.77
1.0091	50.13	25.43	1.0021	50.13	26.53	1.0033	50.13	35.70	1.0049	50.13	36.20
1.0054	98.98	66.69	1.0061	98.98	66.80	1.0079	98.98	81.78	1.0078	98.98	81.67
1.0038	202.07	153.70	1.0045	202.07	152.66	1.0082	202.07	178.28	1.0034	202.07	177.63
Tompkins County site: Soil T1S (S1), reduced						Tompkins County site: Soil T2S (S2), reduced					
1.0045	0.00	0.30	1.0001	0.00	0.30	1.0049	0.00	1.49	1.0009	0.00	0.81
1.0011	1.37	0.30	1.0035	1.37	0.56	1.0042	1.37	1.07	1.0073	1.37	1.08
1.0061	5.17	0.69	1.0033	5.17	0.45	1.0059	5.17	1.17	1.0083	5.17	1.08
1.0074	10.10	0.72	1.0036	10.10	0.84	1.0035	10.10	2.19	1.0036	10.10	1.74
1.0098	49.36	10.42	1.0038	49.36	9.70	1.0043	49.36	18.68	1.0009	49.36	18.71
1.0015	96.86	43.35	1.0020	96.86	44.53	1.0053	96.86	54.26	1.0007	96.86	57.29
1.0056	193.32	120.31	1.0063	193.32	124.29	1.0033	193.32	143.42	1.0017	193.32	140.14
Tompkins County site: Soil T4S (S4), reduced						Tompkins County site: Soil T2D (D2), reduced					
1.0011	0.00	0.23	1.0029	0.00	0.26	1.0046	0.00	0.07	1.0093	0.00	0.08
1.0056	1.37	0.22	1.0034	1.37	0.33	1.0089	1.35	0.12	1.0042	1.35	0.10
1.0075	5.17	0.39	1.0055	5.17	0.56	1.0081	5.12	0.80	1.0018	5.12	0.65
1.0041	10.10	0.42	1.0011	10.10	0.69	1.0050	10.13	3.31	0.9971	10.13	3.06
1.0062	49.36	16.40	1.0005	49.36	14.93	0.9998	49.02	33.80	1.0081	49.02	31.96
1.0029	96.86	46.87	1.0036	96.86	50.16	1.0067	97.77	77.51	1.0097	97.77	76.99
1.0002	193.32	133.70	1.0051	193.32	135.58	0.9955	194.48	170.29	1.0032	194.48	174.16
Tompkins County site: Soil S2N, air-dried						Tompkins County site: Soil D2N, air-dried					
1.3844	0.00	1.51	1.3818	0.00	1.58	2.4820	0.00	0.11	2.4803	0.00	0.09
1.3780	0.92	1.72	1.3835	0.92	1.79	2.4799	0.92	0.06	2.4925	0.92	0.06
1.3769	4.87	2.71	1.3787	4.87	2.72	2.4839	4.87	0.09	2.4819	4.87	0.10
1.3718	9.73	4.00	1.3798	9.73	3.94	2.4849	9.73	0.21	2.4765	9.73	0.22
1.3705	48.74	24.58	1.3722	48.74	25.21	2.4835	48.74	11.21	2.4815	48.74	11.22
1.3784	97.66	63.59	1.3810	97.66	62.77	2.4911	97.66	43.31	2.4897	97.66	44.46
1.3735	193.41	150.78	1.3729	193.41	149.63	2.4804	193.41	123.76	2.4882	193.41	123.30
Tompkins County site: Soil S2N, field-wet						Tompkins County site: Soil D2N, field-wet					
1.3797	0.00	0.67	1.3632	0.00	0.56	2.3161	0.00	0.03	2.4322	0.00	0.03
1.3473	0.97	0.94	1.3293	0.97	0.74	2.5513	0.97	0.03	2.4398	0.97	0.02
1.3171	5.07	1.27	1.4017	5.07	1.29	2.6073	5.07	0.05	2.4515	5.07	0.05
1.3977	10.14	2.57	1.3380	10.14	2.31	2.4939	10.14	0.13	2.4553	10.14	0.16
1.3735	51.39	25.52	1.3755	51.39	26.26	2.5449	51.39	7.87	2.4647	51.39	9.49
1.4226	101.69	64.18	1.3504	101.69	66.84	2.5116	101.69	31.70	2.4473	101.69	40.38
1.3999	204.53	149.76	1.4134	204.53	154.20	2.5992	204.53	113.42	2.4372	204.53	112.68

continue

Test 1			Test 2			Test 1			Test 2		
M (g)	C_i	C	M (g)	C_i	C	M (g)	C_i	C	M (g)	C_i	C
	mg L^{-1}			mg L^{-1}			mg L^{-1}			mg L^{-1}	
Tompkins County site: Soil SC, air-dried						Tompkins County site: Soil DC, air-dried					
1.5402	0.00	0.19	1.5291	0.00	0.21	1.7322	0.00	0.04	1.7408	0.00	0.05
1.5350	0.92	0.26	1.5404	0.92	0.27	1.7278	0.92	0.05	1.7476	0.92	0.05
1.5280	4.87	0.57	1.5244	4.87	0.62	1.7367	4.87	0.17	1.7457	4.87	0.18
1.5333	9.73	1.24	1.5417	9.73	1.28	1.7358	9.73	0.71	1.7486	9.73	0.74
1.5380	48.74	21.02	1.5308	48.74	20.85	1.7433	48.74	25.25	1.7408	48.74	25.03
1.5424	97.66	59.48	1.5435	97.66	58.38	1.7405	97.66	66.74	1.7378	97.66	68.44
1.5395	193.41	141.76	1.5328	193.41	141.19	1.7257	193.41	155.36	1.7401	193.41	157.09
Tompkins County site: Soil SC, field-wet						Tompkins County site: Soil DC, field-wet					
1.4480	0.00	0.20	1.5550	0.00	0.19	1.7722	0.00	0.03	1.6749	0.00	0.02
1.4473	0.97	0.30	1.4853	0.97	0.20	1.6768	0.97	0.04	1.5826	0.97	0.02
1.6055	5.07	1.15	1.5392	5.07	1.21	1.7621	5.07	0.31	1.8424	5.07	0.26
1.5446	10.14	3.58	1.4981	10.14	3.69	1.6842	10.14	1.84	1.7756	10.14	2.08
1.6035	51.39	31.53	1.5293	51.39	31.99	1.8667	51.39	29.93	1.7692	51.39	31.47
1.6455	101.69	73.37	1.4784	101.69	75.13	1.6436	101.69	75.62	1.6549	101.69	78.89
1.5178	204.53	163.37	1.5046	204.53	165.94	1.7718	204.53	166.80	1.8892	200.26	157.57
Tompkins County site: Soil T2S (S2), air-dried, 1/2 wastewater						Tompkins County site: Soil T2D (D2), air-dried, 1/2 wastewater					
1.0096	0.05	0.79	1.0075	0.05	0.90	1.0042	0.05	0.03	1.0039	0.05	0.03
1.0054	0.06	1.06	0.9991	0.06	1.12	1.0056	0.06	0.03	0.9972	0.06	0.03
1.0056	3.05	1.90	1.0049	3.05	1.81	1.0073	3.05	0.18	1.0000	3.05	0.18
1.0053	7.65	2.92	1.0078	7.65	2.92	0.9960	7.65	1.17	1.0012	7.65	1.13
1.0076	43.90	20.33	1.0098	43.90	20.45	1.0043	43.90	24.94	1.0005	43.90	25.57
1.0078	92.00	50.93	1.0020	92.00	50.15	1.0066	92.00	63.21	0.9995	92.00	63.76
0.9962	182.62	123.63	1.0009	182.62	125.72	0.9976	182.62	151.02	1.0077	182.62	150.25
Tompkins County site: Soil S2), reduced, 1/2 wastewater						Tompkins County site: Soil T2D (D2), reduced, 1/2 wastewater					
0.9937	0.00	0.46	0.9956	0.00	0.50	1.0019	0.00	0.04	1.0012	0.00	0.05
0.9983	1.35	0.99	1.0089	1.35	1.48	1.0075	1.35	0.08	1.0078	1.35	0.10
1.0040	5.12	1.02	1.0014	5.12	1.46	0.9935	5.12	0.32	0.9953	5.12	0.37
1.0096	10.13	2.46	1.0006	10.13	2.13	0.9912	10.13	1.32	1.0048	10.13	1.11
1.0065	49.02	10.30	0.9909	49.02	8.97	1.0063	49.02	8.08	0.9912	49.02	9.79
1.0067	97.77	31.21	1.0088	97.77	31.53	1.0049	97.77	32.73	1.0061	97.77	31.65
1.0096	194.48	94.11	0.9905	194.48	94.51	0.9960	194.48	107.11	0.9928	194.48	109.85

Appendix B: Column Breakthrough Experiments Data [a]

Expt. 1: Carboxylated polystyrene microspheres (CPM), ionic strength (IS) = 0 mM NaCl, C_0 = 10 mg L^{-1}							
Replicate 1, θ = 0.24		Replicate 2, θ = 0.22		Replicate 3, θ = 0.23		Replicate 4, θ = 0.21	
v = 0.32 cm min^{-1}		v = 0.35 cm min^{-1}		v = 0.33 cm min^{-1}		v = 0.35 cm min^{-1}	
Input PV = 0.765		Input PV = 0.747		Input PV = 0.746		Input PV = 0.751	
PV	C/C_0	PV	C/C_0	PV	C/C_0	PV	C/C_0
0.00	0.000	0.00	0.000	0.00	0.000	0.00	0.000
0.04	0.000	0.04	0.000	0.04	0.000	0.04	0.000
0.14	0.000	0.14	0.000	0.14	0.000	0.14	0.000
0.24	0.000	0.23	0.000	0.23	0.000	0.23	0.029
0.33	0.000	0.32	0.034	0.32	0.031	0.33	0.029
0.43	0.138	0.42	0.103	0.42	0.156	0.42	0.088
0.52	0.379	0.51	0.276	0.51	0.375	0.51	0.206
0.62	0.517	0.60	0.414	0.60	0.500	0.61	0.324
0.71	0.621	0.70	0.483	0.70	0.594	0.70	0.412
0.81	0.655	0.79	0.517	0.79	0.625	0.80	0.471
0.91	0.690	0.88	0.517	0.88	0.688	0.89	0.471
1.00	0.724	0.98	0.517	0.98	0.656	0.98	0.471
1.10	0.690	1.07	0.517	1.07	0.656	1.08	0.500
1.19	0.655	1.16	0.448	1.16	0.531	1.17	0.471
1.29	0.448	1.26	0.310	1.26	0.344	1.26	0.382
1.38	0.241	1.35	0.172	1.35	0.219	1.36	0.294
1.48	0.138	1.44	0.103	1.44	0.125	1.45	0.176
1.57	0.069	1.54	0.034	1.54	0.063	1.55	0.118
1.67	0.034	1.63	0.034	1.63	0.063	1.64	0.088
1.77	0.000	1.72	0.000	1.72	0.063	1.73	0.059
1.86	0.000			1.82	0.063	1.83	0.059
1.96	0.000					1.92	0.029
2.05	0.000					2.02	0.029
2.15	0.000					2.11	0.029
2.24	0.000					2.20	0.000

Expt. 4: CPM, IS = 0.1 mM NaCl, C_0 = 10 mg L^{-1}									
Replicate 1, θ = 0.18		Replicate 2, θ = 0.23		Replicate 3, θ = 0.27		Replicate 4, θ = 0.17		Replicate 5, θ = 0.20	
v = 0.44 cm min^{-1}		v = 0.32 cm min^{-1}		v = 0.28 cm min^{-1}		v = 0.45 cm min^{-1}		v = 0.37 cm min^{-1}	
Input PV = 0.792		Input PV = 0.752		Input PV = 0.760		Input PV = 0.752		Input PV = 0.749	
PV	C/C_0	PV	C/C_0	PV	C/C_0	PV	C/C_0	PV	C/C_0
0.00	0.000	0.00	0.000	0.00	0.000	0.00	0.000	0.00	0.000
0.05	0.031	0.04	0.000	0.05	0.000	0.04	0.000	0.04	0.000
0.15	0.031	0.14	0.000	0.14	0.000	0.14	0.000	0.14	0.000
0.25	0.031	0.23	0.000	0.24	0.000	0.23	0.000	0.23	0.000
0.35	0.094	0.33	0.000	0.33	0.000	0.33	0.057	0.33	0.026
0.44	0.156	0.42	0.081	0.43	0.026	0.42	0.171	0.42	0.053
0.54	0.219	0.51	0.189	0.52	0.132	0.51	0.257	0.51	0.211
0.64	0.188	0.61	0.297	0.62	0.263	0.61	0.286	0.61	0.316
0.74	0.250	0.70	0.324	0.71	0.395	0.70	0.343	0.70	0.395
0.84	0.250	0.80	0.351	0.81	0.500	0.80	0.371	0.79	0.421
0.94	0.250	0.89	0.378	0.90	0.526	0.89	0.371	0.89	0.421
1.04	0.250	0.98	0.378	1.00	0.526	0.98	0.371	0.98	0.421
1.14	0.188	1.08	0.405	1.09	0.526	1.08	0.286	1.07	0.421
1.24	0.125	1.17	0.351	1.19	0.526	1.17	0.143	1.17	0.368
1.34	0.063	1.27	0.243	1.28	0.474	1.27	0.086	1.26	0.211
1.43	0.063	1.36	0.162	1.38	0.316	1.36	0.029	1.36	0.079
1.53	0.031	1.45	0.054	1.47	0.158	1.45	0.000	1.45	0.053
1.63	0.031	1.55	0.027	1.57	0.079	1.55	0.000	1.54	0.026
1.73	0.031	1.64	0.000	1.66	0.026	1.64	0.000	1.64	0.000
1.83	0.000	1.74	0.000	1.76	0.000			1.73	0.000
1.93	0.000	1.83	0.0000	1.85	0.000			1.82	0.000
2.03	0.000			1.95	0.000				
2.13	0.000			2.04	0.000				
2.23	0.000								
2.33	0.000								

[a] PV = Pore volumes, θ = volumetric water content, and v = average pore water velocity.

continue

Expt. 7: CPM, IS = 0.5 mM NaCl, C_0 = 10 mg L^{-1}							
Replicate 1, θ = 0.22		Replicate 2, θ = 0.20		Replicate 3, θ = 0.19		Replicate 4, θ = 0.24	
v = 0.34 cm min^{-1}		v = 0.38 cm min^{-1}		v = 0.39 cm min^{-1}		v = 0.32 cm min^{-1}	
Input PV = 0.748		Input PV = 0.752		Input PV = 0.755		Input PV = 0.744	
PV	C/C_0	PV	C/C_0	PV	C/C_0	PV	C/C_0
0.00	0.000	0.00	0.000	0.00	0.000	0.00	0.000
0.04	0.000	0.04	0.000	0.04	0.000	0.04	0.000
0.14	0.000	0.14	0.000	0.14	0.000	0.14	0.000
0.23	0.000	0.23	0.000	0.23	0.000	0.23	0.000
0.32	0.000	0.33	0.000	0.33	0.000	0.32	0.000
0.42	0.069	0.42	0.028	0.42	0.000	0.42	0.000
0.51	0.069	0.51	0.083	0.52	0.054	0.51	0.054
0.60	0.103	0.61	0.111	0.61	0.081	0.60	0.108
0.70	0.103	0.70	0.111	0.70	0.081	0.69	0.135
0.79	0.103	0.80	0.083	0.80	0.108	0.79	0.189
0.89	0.103	0.89	0.083	0.89	0.108	0.88	0.189
0.98	0.103	0.98	0.083	0.99	0.081	0.97	0.189
1.07	0.103	1.08	0.111	1.08	0.081	1.07	0.189
1.17	0.069	1.17	0.056	1.18	0.054	1.16	0.189
1.26	0.069	1.27	0.028	1.27	0.000	1.25	0.135
1.35	0.034	1.36	0.000	1.36	0.000	1.35	0.108
1.45	0.000	1.45	0.000	1.46	0.000	1.44	0.081
1.54	0.000	1.55	0.000	1.55	0.000	1.53	0.027
1.63	0.000	1.64	0.000	1.65	0.000	1.63	0.000
1.73	0.000					1.72	0.000
1.82	0.000					1.81	0.000
1.91	0.000						
2.01	0.000						
2.10	0.000						
2.19	0.000						

Expt. 10: CPM, IS = 1.0 mM NaCl, C_0 = 10 mg L^{-1}						Expt. 14: CPM, IS = 1.0 mM NaCl, C_0 = 10 mg L^{-1}, saturated					
Replicate 1		Replicate 2		Replicate 3		Replicate 1		Replicate 2		Replicate 3	
θ = 0.23		θ = 0.23		θ = 0.20		θ = 0.40		θ = 0.40		θ = 0.40	
v = 0.33 cm min^{-1}		v = 0.33 cm min^{-1}		v = 0.38 cm min^{-1}		v = 0.19 cm min^{-1}		v = 0.19 cm min^{-1}		v = 0.19 cm min^{-1}	
Input PV = 0.746		Input PV = 0.745		Input PV = 0.750		Input PV = 0.756		Input PV = 0.755		Input PV = 0.763	
PV	C/C_0	PV	C/C_0	PV	C/C_0	PV	C/C_0	PV	C/C_0	PV	C/C_0
0.00	0.000	0.00	0.000	0.00	0.000	0.00	0.000	0.00	0.000	0.00	0.000
0.04	0.000	0.04	0.000	0.04	0.000	0.04	0.000	0.04	0.000	0.04	0.000
0.14	0.000	0.14	0.000	0.14	0.000	0.14	0.000	0.14	0.000	0.14	0.000
0.23	0.000	0.23	0.000	0.23	0.000	0.23	0.000	0.23	0.000	0.24	0.000
0.32	0.000	0.32	0.000	0.33	0.000	0.33	0.000	0.33	0.000	0.33	0.000
0.42	0.000	0.42	0.000	0.42	0.028	0.42	0.000	0.42	0.000	0.43	0.000
0.51	0.033	0.51	0.000	0.51	0.028	0.52	0.000	0.52	0.000	0.52	0.000
0.60	0.033	0.60	0.028	0.61	0.083	0.61	0.000	0.61	0.000	0.62	0.000
0.70	0.100	0.70	0.056	0.70	0.111	0.71	0.000	0.71	0.030	0.71	0.000
0.79	0.133	0.79	0.083	0.79	0.139	0.80	0.000	0.80	0.030	0.81	0.025
0.88	0.133	0.88	0.111	0.89	0.139	0.89	0.024	0.89	0.030	0.90	0.025
0.98	0.100	0.97	0.111	0.98	0.167	0.99	0.073	0.99	0.061	1.00	0.075
1.07	0.100	1.07	0.139	1.08	0.139	1.08	0.098	1.08	0.061	1.09	0.100
1.16	0.133	1.16	0.139	1.17	0.111	1.18	0.122	1.18	0.061	1.19	0.100
1.26	0.100	1.25	0.139	1.26	0.111	1.27	0.146	1.27	0.091	1.28	0.100
1.35	0.067	1.35	0.111	1.36	0.083	1.37	0.146	1.37	0.091	1.38	0.125
1.44	0.033	1.44	0.139	1.45	0.056	1.46	0.171	1.46	0.121	1.48	0.100
1.54	0.033	1.53	0.083	1.54	0.028	1.56	0.171	1.56	0.091	1.57	0.100
1.63	0.033	1.63	0.056	1.64	0.028	1.65	0.146	1.65	0.091	1.67	0.075
1.72	0.033	1.72	0.056	1.73	0.028	1.75	0.122	1.74	0.061	1.76	0.075
1.82	0.033	1.81	0.056	1.83	0.028	1.84	0.073	1.84	0.030	1.86	0.075
1.91	0.000	1.91	0.028	1.92	0.028	1.93	0.049	1.93	0.000	1.95	0.025
2.00	0.000	2.00	0.028	2.01	0.028	2.03	0.024	2.03	0.000	2.05	0.025
2.10	0.000	2.09	0.028	2.11	0.000	2.12	0.024	2.12	0.000	2.14	0.000
2.19	0.0000	2.18	0.000	2.20	0.000	2.22	0.000	2.22	0.000	2.24	0.000
						2.31	0.000				

continue

Expt. 2: CPM, IS = 0 mM NaCl, C_0 = 100 mg L^{-1}						Expt. 5: CPM, IS = 0.1 mM NaCl, C_0 = 100 mg L^{-1}					
Replicate 1		Replicate 2		Replicate 3		Replicate 1		Replicate 2		Replicate 3	
θ = 0.20		θ = 0.25		θ = 0.21		θ = 0.25		θ = 0.23		θ = 0.19	
v = 0.38 cm min^{-1}		v = 0.30 cm min^{-1}		v = 0.35 cm min^{-1}		v = 0.30 cm min^{-1}		v = 0.33 cm min^{-1}		v = 0.40 cm min^{-1}	
Input PV = 0.756		Input PV = 0.750		Input PV = 0.754		Input PV = 0.761		Input PV = 0.748		Input PV = 0.747	
PV	C/C_0	PV	C/C_0	PV	C/C_0	PV	C/C_0	PV	C/C_0	PV	C/C_0
0.00	0.000	0.00	0.000	0.00	0.000	0.00	0.000	0.00	0.000	0.00	0.000
0.04	0.000	0.04	0.000	0.04	0.000	0.05	0.000	0.04	0.000	0.04	0.000
0.14	0.000	0.14	0.000	0.14	0.000	0.14	0.000	0.14	0.000	0.14	0.000
0.23	0.000	0.23	0.000	0.23	0.000	0.24	0.000	0.23	0.000	0.23	0.000
0.33	0.010	0.33	0.003	0.33	0.003	0.33	0.000	0.32	0.003	0.32	0.008
0.42	0.135	0.42	0.059	0.42	0.062	0.43	0.020	0.42	0.041	0.42	0.060
0.52	0.344	0.51	0.214	0.52	0.210	0.52	0.099	0.51	0.121	0.51	0.141
0.61	0.479	0.61	0.382	0.61	0.352	0.62	0.222	0.61	0.196	0.60	0.201
0.71	0.569	0.70	0.472	0.70	0.462	0.71	0.281	0.70	0.240	0.70	0.236
0.80	0.614	0.79	0.519	0.80	0.522	0.81	0.318	0.79	0.270	0.79	0.250
0.90	0.653	0.89	0.565	0.89	0.556	0.90	0.330	0.89	0.292	0.88	0.264
0.99	0.685	0.98	0.587	0.99	0.578	1.00	0.344	0.98	0.306	0.98	0.266
1.08	0.682	1.08	0.599	1.08	0.586	1.09	0.344	1.07	0.306	1.07	0.266
1.18	0.585	1.17	0.559	1.18	0.546	1.19	0.330	1.17	0.275	1.16	0.217
1.27	0.357	1.26	0.447	1.27	0.422	1.28	0.264	1.26	0.215	1.26	0.152
1.37	0.154	1.36	0.252	1.36	0.290	1.38	0.168	1.35	0.138	1.35	0.073
1.46	0.090	1.45	0.121	1.46	0.183	1.47	0.085	1.45	0.085	1.45	0.041
1.56	0.029	1.54	0.065	1.55	0.105	1.57	0.040	1.54	0.041	1.54	0.022
1.65	0.006	1.64	0.031	1.65	0.065	1.66	0.017	1.63	0.022	1.63	0.019
1.75	0.003	1.73	0.019	1.74	0.038	1.76	0.009	1.73	0.008	1.73	0.005
1.84	0.003	1.83	0.012	1.83	0.027	1.85	0.003	1.82	0.006	1.82	0.005
1.93	0.003	1.92	0.009	1.93	0.016	1.95	0.000	1.92	0.003	1.91	0.000
2.03	0.003	2.01	0.006	2.02	0.011	2.04	0.000	2.01	0.000	2.01	0.003
2.12	0.003	2.11	0.003	2.12	0.008	2.14	0.000	2.10	0.000		
2.22	0.003	2.20	0.003	2.21	0.003	2.23	0.000	2.20	0.000		

Expt. 8: CPM, IS = 0.5 mM NaCl, C_0 = 100 mg L^{-1}				Expt. 11: CPM, IS = 1.0 mM NaCl, C_0 = 100 mg L^{-1}			
Replicate 1, θ = 0.23		Replicate 2, θ = 0.20		Replicate 1, θ = 0.25		Replicate 2, θ = 0.23	
v = 0.32 cm min^{-1}		v = 0.38 cm min^{-1}		v = 0.30 cm min^{-1}		v = 0.32 cm min^{-1}	
Input PV = 0.750		Input PV = 0.753		Input PV = 0.746		Input PV = 0.744	
PV	C/C_0	PV	C/C_0	PV	C/C_0	PV	C/C_0
0.00	0.000	0.00	0.000	0.00	0.000	0.00	0.000
0.04	0.000	0.04	0.000	0.04	0.000	0.04	0.000
0.14	0.000	0.14	0.000	0.14	0.000	0.14	0.000
0.23	0.000	0.23	0.000	0.23	0.000	0.23	0.000
0.33	0.006	0.33	0.000	0.32	0.000	0.32	0.000
0.42	0.030	0.42	0.006	0.42	0.000	0.42	0.006
0.51	0.058	0.51	0.026	0.51	0.003	0.51	0.013
0.61	0.061	0.61	0.047	0.60	0.016	0.60	0.013
0.70	0.067	0.70	0.052	0.70	0.010	0.69	0.010
0.79	0.067	0.80	0.067	0.79	0.010	0.79	0.013
0.89	0.064	0.89	0.073	0.88	0.007	0.88	0.010
0.98	0.061	0.99	0.076	0.98	0.007	0.97	0.010
1.08	0.055	1.08	0.073	1.07	0.007	1.07	0.006
1.17	0.046	1.17	0.067	1.16	0.007	1.16	0.003
1.26	0.024	1.27	0.044	1.26	0.007	1.25	0.003
1.36	0.009	1.36	0.015	1.35	0.003	1.35	0.003
1.45	0.003	1.46	0.012	1.44	0.007	1.44	0.003
1.54	0.000	1.55	0.000	1.54	0.003	1.53	0.003
1.64	0.000	1.64	0.000	1.63	0.003	1.62	0.006
1.73	0.000			1.72	0.003	1.72	0.003
1.82	0.000			1.82	0.003	1.81	0.006
1.92	0.000			1.91	0.003	1.90	0.006
2.01	0.000			2.00	0.003	2.00	0.006
2.11	0.000			2.10	0.000	2.09	0.003
2.20	0.003			2.19	0.000	2.18	0.006

continue

Expt. 3: CPM, IS = 0 mM NaCl, C_0 = 1000 mg L^{-1}						Expt. 6: CPM, IS = 0.1 mM NaCl, C_0 = 1000 mg L^{-1}					
Replicate 1		Replicate 2		Replicate 3		Replicate 1		Replicate 2		Replicate 3	
θ = 0.29		θ = 0.23		θ = 0.22		θ = 0.22		θ = 0.23		θ = 0.24	
v = 0.26 cm min^{-1}		v = 0.33 cm min^{-1}		v = 0.35 cm min^{-1}		v = 0.33 cm min^{-1}		v = 0.32 cm min^{-1}		v = 0.31 cm min^{-1}	
Input PV = 0.743		Input PV = 0.748		Input PV = 0.744		Input PV = 0.749		Input PV = 0.805		Input PV = 0.750	
PV	C/C_0	PV	C/C_0	PV	C/C_0	PV	C/C_0	PV	C/C_0	PV	C/C_0
0.00	0.000	0.00	0.000	0.00	0.000	0.00	0.000	0.00	0.000	0.00	0.000
0.04	0.000	0.04	0.000	0.04	0.000	0.04	0.000	0.04	0.000	0.04	0.000
0.14	0.000	0.14	0.000	0.14	0.000	0.14	0.000	0.14	0.000	0.14	0.000
0.23	0.000	0.23	0.000	0.23	0.000	0.23	0.000	0.23	0.000	0.23	0.000
0.32	0.000	0.32	0.027	0.32	0.003	0.33	0.002	0.33	0.000	0.33	0.005
0.42	0.000	0.42	0.204	0.42	0.095	0.42	0.044	0.42	0.004	0.42	0.040
0.51	0.026	0.51	0.420	0.51	0.275	0.51	0.142	0.52	0.044	0.51	0.101
0.60	0.146	0.60	0.506	0.60	0.517	0.61	0.209	0.61	0.175	0.61	0.114
0.69	0.308	0.70	0.608	0.69	0.572	0.70	0.238	0.75	0.171	0.70	0.106
0.79	0.426	0.79	0.554	0.79	0.623	0.79	0.252	0.80	0.198	0.79	0.082
0.88	0.528	0.88	0.597	0.88	0.649	0.89	0.254	0.90	0.206	0.89	0.077
0.97	0.575	0.98	0.607	0.97	0.671	0.98	0.253	0.99	0.206	0.98	0.073
1.07	0.655	1.07	0.590	1.07	0.653	1.07	0.247	1.09	0.213	1.08	0.066
1.16	0.607	1.17	0.453	1.16	0.604	1.17	0.221	1.18	0.215	1.17	0.046
1.25	0.613	1.26	0.322	1.25	0.419	1.26	0.167	1.28	0.183	1.26	0.024
1.34	0.588	1.35	0.172	1.35	0.250	1.36	0.100	1.37	0.122	1.36	0.014
1.44	0.430	1.45	0.065	1.44	0.128	1.45	0.039	1.46	0.070	1.45	0.003
1.53	0.299	1.54	0.040	1.53	0.066	1.54	0.019	1.56	0.028	1.54	0.004
1.62	0.151	1.63	0.032	1.62	0.036	1.64	0.010	1.65	0.013	1.64	0.002
1.72	0.081	1.73	0.022	1.72	0.021	1.73	0.006	1.75	0.006	1.73	0.001
1.81	0.045	1.82	0.014	1.81	0.014	1.82	0.004	1.84	0.002	1.83	0.000
1.90	0.028	1.91	0.011	1.90	0.011	1.92	0.003	1.94	0.002		
1.99	0.018	2.01	0.008	2.00	0.008	2.01	0.002	2.03	0.001		
2.09	0.013	2.10	0.007	2.09	0.006	2.10	0.002	2.13	0.001		
2.18	0.010	2.19	0.005	2.18	0.0056	2.20	0.002	2.22	0.002		

Expt. 9: CPM, IS = 0.5 mM, C_0 = 1000 mg L^{-1}				Expt. 12: CPM, IS = 1.0 mM, C_0 = 1000 mg L^{-1}				Expt. 15: CPM, IS = 1.0 mM, C_0 = 1000 mg L^{-1}, saturated			
Replicate 1		Replicate 2		Replicate 1		Replicate 2		Replicate 1		Replicate 2	
θ = 0.28		θ = 0.22		θ = 0.20		θ = 0.24		θ = 0.40		θ = 0.40	
v = 0.27 cm min^{-1}		v = 0.34 cm min^{-1}		v = 0.38 cm min^{-1}		v = 0.31 cm min^{-1}		v = 0.19 cm min^{-1}		v = 0.19 cm min^{-1}	
Input PV = 0.740		Input PV = 0.746		Input PV = 0.753		Input PV = 0.745		Input PV = 0.750		Input PV = 0.759	
PV	C/C_0	PV	C/C_0	PV	C/C_0	PV	C/C_0	PV	C/C_0	PV	C/C_0
0.00	0.000	0.00	0.000	0.00	0.000	0.00	0.000	0.00	0.000	0.00	0.000
0.04	0.000	0.04	0.000	0.04	0.000	0.04	0.000	0.04	0.000	0.04	0.000
0.14	0.001	0.14	0.000	0.14	0.000	0.14	0.000	0.14	0.001	0.14	0.000
0.23	0.000	0.23	0.000	0.23	0.000	0.23	0.000	0.23	0.000	0.23	0.000
0.32	0.000	0.32	0.000	0.33	0.002	0.32	0.000	0.33	0.001	0.33	0.000
0.41	0.004	0.42	0.008	0.42	0.005	0.42	0.003	0.42	0.001	0.42	0.001
0.51	0.021	0.51	0.023	0.51	0.004	0.51	0.011	0.51	0.001	0.52	0.001
0.60	0.029	0.60	0.030	0.61	0.002	0.60	0.011	0.61	0.002	0.61	0.001
0.69	0.025	0.70	0.029	0.70	0.001	0.70	0.007	0.70	0.003	0.71	0.002
0.78	0.016	0.79	0.027	0.80	0.000	0.79	0.004	0.79	0.004	0.80	0.008
0.88	0.010	0.88	0.024	0.89	0.000	0.88	0.002	0.89	0.013	0.90	0.020
0.97	0.007	0.98	0.021	0.99	0.000	0.97	0.001	0.98	0.024	0.99	0.032
1.06	0.006	1.07	0.019	1.08	0.000	1.07	0.000	1.08	0.031	1.09	0.034
1.15	0.006	1.16	0.013	1.17	0.000	1.16	0.000	1.17	0.030	1.18	0.030
1.25	0.004	1.26	0.006	1.27	0.000	1.25	0.000	1.26	0.026	1.28	0.026
1.34	0.004	1.35	0.002	1.36	0.000	1.35	0.000	1.36	0.022	1.37	0.024
1.43	0.003	1.44	0.000	1.46	0.000	1.44	0.000	1.45	0.020	1.47	0.020
1.52	0.002	1.54	0.000	1.55	0.000	1.53	0.000	1.54	0.017	1.56	0.016
1.62	0.002	1.63	0.000	1.64	0.000	1.63	0.000	1.64	0.012	1.66	0.010
1.71	0.002	1.72	0.000					1.73	0.007	1.75	0.002
1.80	0.002	1.82	0.000					1.83	0.002	1.85	0.000
1.89	0.001							1.92	0.000	1.94	0.000
1.99	0.001							2.01	0.000	2.04	0.000
2.08	0.001							2.11	0.000	2.13	0.000
2.17	0.001							2.20	0.000	2.23	0.000

continue

Expt. 13: Bromide, IS = 0 mM NaCl, C_0 = 100 mg L^{-1}					
Replicate 1, θ = 0.26		Replicate 2, θ = 0.17		Replicate 3, θ = 0.21	
v = 0.29 cm min^{-1}		v = 0.43 cm min^{-1}		v = 0.35 cm min^{-1}	
Input PV = 0.757		Input PV = 0.748		Input PV = 0.755	
PV	C/C_0	PV	C/C_0	PV	C/C_0
0.00	0.000	0.00	0.000	0.00	0.000
0.04	0.000	0.04	0.000	0.04	0.000
0.14	0.000	0.14	0.000	0.14	0.000
0.23	0.000	0.23	0.000	0.23	0.000
0.33	0.000	0.32	0.008	0.33	0.000
0.42	0.000	0.42	0.137	0.42	0.000
0.52	0.017	0.51	0.454	0.52	0.041
0.61	0.183	0.60	0.726	0.61	0.237
0.71	0.552	0.70	0.877	0.70	0.565
0.80	0.814	0.79	0.946	0.80	0.812
0.90	0.930	0.89	0.984	0.89	0.922
0.99	0.969	0.98	0.970	0.99	0.963
1.09	0.978	1.07	0.976	1.08	0.988
1.18	0.993	1.17	0.773	1.18	0.991
1.27	0.985	1.26	0.448	1.27	0.921
1.37	0.693	1.35	0.197	1.36	0.560
1.46	0.353	1.45	0.099	1.46	0.254
1.56	0.144	1.54	0.048	1.55	0.105
1.65	0.069	1.63	0.020	1.65	0.051
1.75	0.028	1.73	0.012	1.74	0.015
1.84	0.014	1.82	0.007	1.84	0.011
1.94	0.009	1.91	0.001	1.93	0.007
2.03	0.008	2.01	0.001	2.02	0.001
2.13	0.001	2.10	0.000	2.12	0.001
2.22	0.000	2.19	0.000	2.21	0.000

continue

Biochar (BC), pH = 4, IS = 10 mM, saturated				BC, pH = 7, IS = 10 mM, saturated				BC, pH = 7, IS = 100 mM, saturated			
Replicate 1 θ = 0.38		Replicate 2 θ = 0.39		Replicate 1 θ = 0.39		Replicate 2 θ = 0.39		Replicate 1 θ = 0.39		Replicate 2 θ = 0.39	
v = 0.39 cm min^{-1}		v = 0.36 cm min^{-1}		v = 0.36 cm min^{-1}		v = 0.36 cm min^{-1}		v = 0.35 cm min^{-1}		v = 0.35 cm min^{-1}	
Input PV = 0.596		Input PV = 0.581		Input PV = 0.594		Input PV = 0.581		Input PV = 0.580		Input PV = 0.579	
PV	C/C_0	PV	C/C_0	PV	C/C_0	PV	C/C_0	PV	C/C_0	PV	C/C_0
0.00	0.000	0.00	0.000	0.00	0.000	0.00	0.000	0.00	0.000	0.00	0.000
0.00	0.000	0.02	0.000	0.00	0.003	0.02	0.002	0.02	0.000	0.02	0.002
0.12	0.000	0.13	0.000	0.11	0.000	0.13	0.002	0.13	0.000	0.13	0.002
0.24	0.002	0.24	0.000	0.22	0.000	0.24	0.000	0.24	0.002	0.24	0.000
0.36	0.002	0.35	0.000	0.33	0.002	0.35	0.000	0.34	0.002	0.34	0.002
0.48	0.000	0.45	0.000	0.44	0.000	0.45	0.000	0.45	0.003	0.45	0.002
0.60	0.002	0.56	0.000	0.55	0.005	0.56	0.000	0.56	0.005	0.56	0.003
0.71	0.002	0.67	0.000	0.66	0.000	0.67	0.000	0.67	0.007	0.67	0.002
0.83	0.007	0.77	0.005	0.77	0.002	0.78	0.003	0.77	0.010	0.77	0.007
0.95	0.020	0.88	0.019	0.88	0.023	0.88	0.017	0.88	0.022	0.88	0.024
1.07	0.031	0.99	0.024	0.99	0.069	0.99	0.062	0.99	0.049	0.99	0.048
1.19	0.039	1.10	0.032	1.09	0.116	1.10	0.119	1.10	0.075	1.09	0.063
1.31	0.041	1.20	0.037	1.20	0.146	1.21	0.149	1.20	0.088	1.20	0.077
1.42	0.039	1.31	0.036	1.31	0.161	1.31	0.162	1.31	0.088	1.31	0.080
1.54	0.031	1.42	0.029	1.42	0.152	1.42	0.161	1.42	0.080	1.42	0.080
1.66	0.020	1.53	0.019	1.53	0.114	1.53	0.129	1.52	0.058	1.52	0.071
1.78	0.008	1.63	0.010	1.64	0.074	1.64	0.080	1.63	0.032	1.63	0.048
1.90	0.005	1.74	0.005	1.75	0.039	1.74	0.035	1.74	0.014	1.74	0.026
2.02	0.002	1.85	0.000	1.86	0.020	1.85	0.000	1.85	0.003	1.84	0.012
2.13	0.002	1.96	0.002	1.97	0.007	1.96	0.000	1.95	0.000	1.95	0.005
2.25	0.000	2.06	0.000	2.08	0.003	2.07	0.000	2.06	0.000	2.06	0.003
				2.19	0.000					2.17	0.002
				2.30	0.000					2.27	0.002

BC, pH = 10, IS = 10 mM, saturated				Bromide, C_0 = 100 mg L^{-1}, saturated			
Replicate 1 θ = 0.39		Replicate 2 θ = 0.37		Replicate 1 θ = 0.39		Replicate 2 θ = 0.39	
v = 0.38 cm min^{-1}		v = 0.38 cm min^{-1}		v = 0.36 cm min^{-1}		v = 0.35 cm min^{-1}	
Input PV = 0.590		Input PV = 0.581		Input PV = 0.595		Input PV = 0.589	
PV	C/C_0	PV	C/C_0	PV	C/C_0	PV	C/C_0
0.00	0.000	0.00	0.000	0.00	0.005	0.00	0.001
0.00	0.000	0.02	0.000	0.00	0.000	0.00	0.000
0.12	0.000	0.13	0.000	0.11	0.000	0.10	0.000
0.24	0.002	0.24	0.000	0.22	0.000	0.21	0.000
0.36	0.002	0.35	0.000	0.33	0.000	0.31	0.000
0.47	0.002	0.45	0.000	0.44	0.000	0.42	0.000
0.59	0.002	0.56	0.000	0.55	0.000	0.52	0.000
0.71	0.002	0.67	0.028	0.66	0.000	0.63	0.000
0.82	0.018	0.78	0.096	0.77	0.001	0.74	0.000
0.94	0.081	0.88	0.172	0.88	0.064	0.84	0.035
1.06	0.156	0.99	0.226	0.99	0.341	0.95	0.217
1.18	0.207	1.10	0.258	1.10	0.655	1.06	0.550
1.29	0.235	1.21	0.251	1.21	0.827	1.16	0.815
1.41	0.233	1.31	0.212	1.32	0.945	1.27	0.936
1.53	0.198	1.42	0.135	1.43	1.010	1.37	0.967
1.64	0.132	1.53	0.077	1.54	0.828	1.48	0.859
1.76	0.082	1.64	0.051	1.65	0.446	1.59	0.567
1.88	0.047	1.74	0.018	1.76	0.189	1.69	0.238
1.99	0.028	1.85	0.007	1.87	0.073	1.80	0.057
2.11	0.019	1.96	0.000	1.98	0.029	1.90	0.008
2.23	0.014	2.07	0.000	2.09	0.010	2.01	0.007
2.35	0.011	2.17	0.000	2.20	0.002	2.12	0.010
2.46	0.011			2.31	0.001	2.22	0.000
2.58	0.005			2.42	0.000	2.33	0.000
2.70	0.009			2.53	0.000	2.43	0.000

continue

BC, pH = 4, IS = 10 mM, unsaturated				BC, pH = 7, IS = 10 mM, unsaturated				BC, pH = 7, IS = 100 mM, unsaturated			
Replicate 1 $\theta = 0.23$		Replicate 2 $\theta = 0.21$		Replicate 1 $\theta = 0.21$		Replicate 2 $\theta = 0.21$		Replicate 1 $\theta = 0.17$		Replicate 2 $\theta = 0.22$	
$v = 0.33$ cm min^{-1}		$v = 0.36$ cm min^{-1}		$v = 0.35$cm min^{-1}		$v = 0.35$ cm min^{-1}		$v = 0.44$ cm min^{-1}		$v = 0.34$ cm min^{-1}	
Input PV = 0.562		Input PV = 0.554		Input PV = 0.557		Input PV = 0.559		Input PV = 0.570		Input PV = 0.561	
PV	C/C_0	PV	C/C_0	PV	C/C_0	PV	C/C_0	PV	C/C_0	PV	C/C_0
0.00	0.000	0.00	0.000	0.00	0.000	0.00	0.000	0.00	0.000	0.000	0.000
0.04	0.000	0.04	0.000	0.04	0.002	0.04	0.000	0.04	0.000	0.037	0.000
0.13	0.000	0.13	0.000	0.14	0.010	0.13	0.000	0.13	0.000	0.130	0.000
0.22	0.000	0.22	0.000	0.23	0.015	0.22	0.000	0.23	0.000	0.224	0.002
0.32	0.000	0.31	0.000	0.32	0.020	0.32	0.000	0.32	0.002	0.317	0.002
0.41	0.000	0.41	0.007	0.42	0.018	0.41	0.002	0.42	0.010	0.411	0.010
0.51	0.007	0.50	0.014	0.51	0.028	0.50	0.003	0.51	0.017	0.505	0.031
0.60	0.007	0.59	0.017	0.60	0.057	0.60	0.018	0.61	0.020	0.598	0.026
0.69	0.008	0.68	0.017	0.69	0.079	0.69	0.047	0.70	0.019	0.692	0.027
0.79	0.010	0.77	0.014	0.79	0.085	0.78	0.060	0.80	0.015	0.785	0.026
0.88	0.008	0.87	0.007	0.88	0.082	0.88	0.075	0.89	0.015	0.879	0.024
0.97	0.008	0.96	0.003	0.97	0.079	0.97	0.082	0.99	0.012	0.972	0.015
1.07	0.008	1.05	0.003	1.07	0.062	1.06	0.084	1.08	0.005	1.066	0.010
1.16	0.002	1.14	0.002	1.16	0.040	1.16	0.082	1.18	0.005	1.159	0.003
1.26	0.002	1.24	0.002	1.25	0.017	1.25	0.067	1.27	0.003	1.253	0.002
1.35	0.000	1.33	0.000	1.34	0.002	1.34	0.039	1.37	0.002	1.347	0.000
1.44	0.000	1.42	0.000	1.44	0.000	1.44	0.020	1.46	0.000	1.440	0.000
1.54	0.000					1.53	0.008	1.56	0.000	1.534	0.000
						1.62	0.002				
						1.71	0.000				

BC, pH = 10, IS = 10 mM, unsaturated				Bromide, $C_0 = 100$ mg L^{-1}, unsaturated			
Replicate 1 $\theta = 0.24$		Replicate 2 $\theta = 0.21$		Replicate 1 $\theta = 0.22$		Replicate 2 $\theta = 0.22$	
$v = 0.32$ cm min^{-1}		$v = 0.36$ cm min^{-1}		$v = 0.34$ cm min^{-1}		$v = 0.35$ cm min^{-1}	
Input PV = 0.557		Input PV = 0.565		Input PV = 0.562		Input PV = 0.563	
PV	C/C_0	PV	C/C_0	PV	C/C_0	PV	C/C_0
0.00	0.000	0.00	0.000	0.00	0.007	0.00	0.000
0.04	0.000	0.04	0.000	0.04	0.001	0.04	0.000
0.13	0.000	0.13	0.000	0.13	0.000	0.13	0.000
0.22	0.000	0.23	0.000	0.22	0.000	0.22	0.000
0.31	0.000	0.32	0.009	0.32	0.000	0.32	0.003
0.41	0.014	0.41	0.049	0.41	0.045	0.41	0.105
0.50	0.063	0.51	0.105	0.51	0.271	0.51	0.459
0.59	0.123	0.60	0.146	0.60	0.597	0.60	0.747
0.69	0.158	0.70	0.174	0.69	0.825	0.69	0.879
0.78	0.165	0.79	0.175	0.79	0.935	0.79	0.924
0.87	0.161	0.89	0.168	0.88	0.995	0.88	0.956
0.96	0.140	0.98	0.139	0.97	0.981	0.98	0.902
1.06	0.109	1.07	0.088	1.07	0.780	1.07	0.576
1.15	0.063	1.17	0.047	1.16	0.422	1.16	0.271
1.24	0.033	1.26	0.023	1.25	0.202	1.26	0.116
1.34	0.009	1.36	0.009	1.35	0.090	1.35	0.059
1.43	0.000	1.45	0.002	1.44	0.050	1.44	0.039
1.52	0.000	1.55	0.000	1.54	0.018	1.54	0.012
		1.64	0.000	1.63	0.010	1.63	0.007
				1.72	0.007	1.73	0.007
				1.82	0.004	1.82	0.002